ISSN: 2153-1196 Volume 12, Number 12, October 2021

Scientific Research Publishing

Journal of Modern Physics

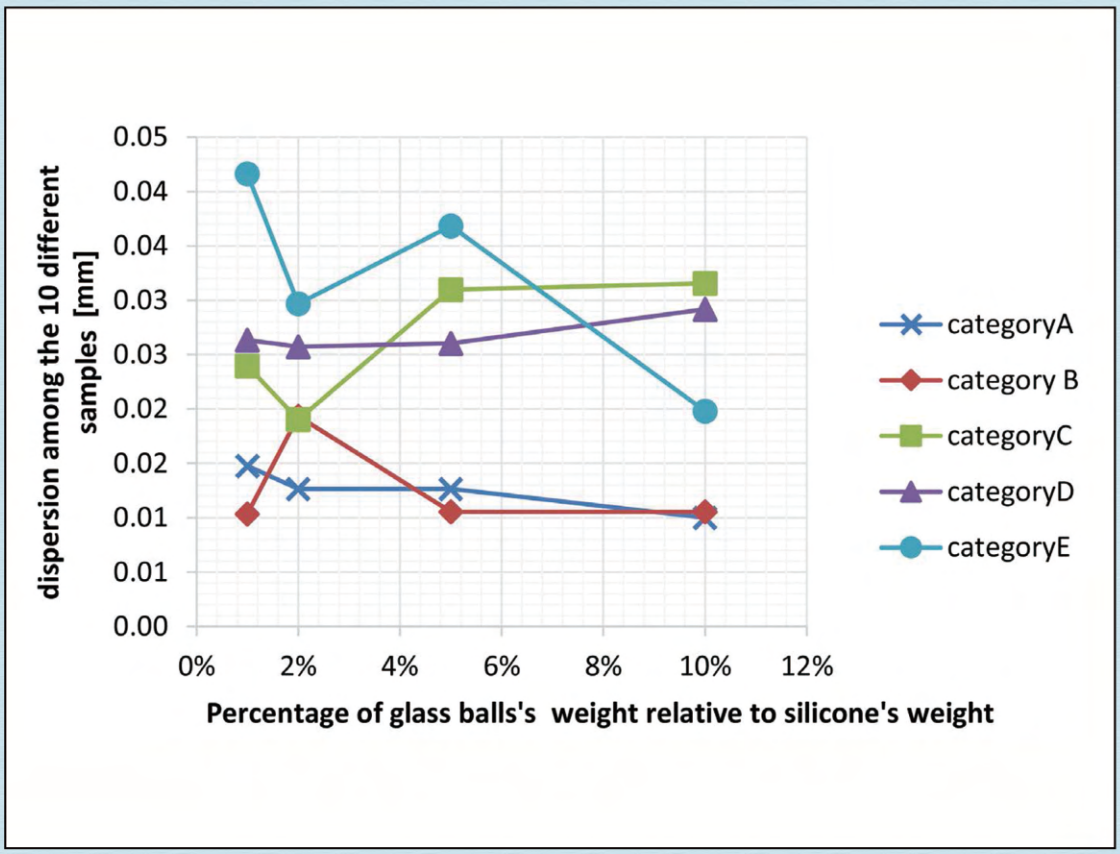

ISSN: 2153-1196
9 772153 119007 12

https://www.scirp.org/journal/jmp

Journal Editorial Board

ISSN: 2153-1196 (Print) ISSN: 2153-120X (Online)
https://www.scirp.org/journal/jmp

Editor-in-Chief

Editorial Board

Scientific Research Publishing

Journal of Modern Physics, 2021, 12, 1607-1728
https://www.scirp.org/journal/jmp
ISSN Online: 2153-120X
ISSN Print: 2153-1196

Table of Contents

Volume 12 Number 12 October 2021

The figure on the front cover is from the article published in Journal of Modern Physics, 2021, Vol. 12, No. 12, pp. 1607-1617 by Intissar Benrhouma, Nabil Ben Hafsia, Bechir Chaouachi, Marta Victoria, Ignacio Anton.

Journal of Modern Physics (JMP)
Journal Information

SUBSCRIPTIONS

The *Journal of Modern Physics* (Online at Scientific Research Publishing, https://www.scirp.org/) is published monthly by Scientific Research Publishing, Inc., USA.

Subscription rates:
Print: $89 per issue.
To subscribe, please contact Journals Subscriptions Department, E-mail: sub@scirp.org

SERVICES

Advertisements
Advertisement Sales Department, E-mail: service@scirp.org

Reprints (minimum quantity 100 copies)
Reprints Co-ordinator, Scientific Research Publishing, Inc., USA.
E-mail: sub@scirp.org

COPYRIGHT

PRODUCTION INFORMATION

For manuscripts that have been accepted for publication, please contact:
E-mail: jmp@scirp.org

Journal of Modern Physics, 2021, 12, 1607-1617
https://www.scirp.org/journal/jmp
ISSN Online: 2153-120X
ISSN Print: 2153-1196

Performance Improving of a Concentrating Photovoltaic System by Using a New Optical Adhesive

Intissar Benrhouma[1], Nabil Ben Hafsia[1], Bechir Chaouachi[1], Marta Victoria[2], Ignacio Anton[2]

[1]Energy, Water, Environment and Process Analysis Laboratory, National Engineering School of Gabes, University of Gabes, Gabes, Tunisia
[2]Instituto de Energía Solar, Universidad Politécnica de Madrid, Ciudad Universitaría, Madrid, Spain
Email: intissar19913@yahoo.fr

How to cite this paper: Benrhouma, I., Hafsia, N.B., Chaouachi, B., Victoria, M. and Anton, I. (2021) Performance Improving of a Concentrating Photovoltaic System by Using a New Optical Adhesive. *Journal of Modern Physics*, **12**, 1607-1617.
https://doi.org/10.4236/jmp.2021.1212095

Received: September 4, 2021
Accepted: October 8, 2021
Published: October 11, 2021

Abstract

The objective of this present study is to manufacture a new silicone-based adhesive which is used for gluing and bonding the second optical elements (SOE) with Concentrating Photovoltaic solar cell (CPV) in order to guarantee a thickness that can provide a good silicone adherence to obtain long term stability and keeping a good solar transmittance performance, too. This new adhesive is made up of a mixture of silicone and transparent glass balls. The experimental part consists of the choice of the best size of glass balls with the suitable proportion of the glass balls weight in the mixture. For this purpose, ten samples were manufactured for every category of glass balls and weight ratio. Glass ball sizes between 100 and 1100 μm, and weight ratios between 1 and 10% were analyzed. For each category of glass balls, four proportions were mixed with the silicone. The thicknesses and transmittance of every sample were measured with appropriate instruments. The experimental results illustrate that the mixture containing balls with sizes inferior to 106 μm, is the best mixture which assures adhesive minimum thickness value necessary for an efficient mechanical bond and preserves also a good transmittance of solar irradiance.

Keywords

Secondary Optical Elements (SOE), Concentrating Photovoltaic Solar Cell (CPV), New Adhesive, Thickness, Transmittance

1. Introduction

Today, concentrator photovoltaic systems (CPV) are used to increase the im-

proving performance of photovoltaic systems (PV) using reflective material lenses, or mirrors to concentrate sunlight on highly efficient solar cells [1]. CPV systems convert solar energy to electric energy by concentrating the incident solar radiation on high efficiency multi-junction (MJ) solar cells. A typical CPV system consists of a solar concentrator, MJ solar cells and a sun tracking system [2].

A concentrated photovoltaic system CPV is composed of a Primary Optical Element POE, a Secondary Optical Element SOE and a solar cell. The role of POE is to concentrate a large area of solar energy into a small solar cell. Furthermore, the SOE is applied to redirect the sun light into the solar cell and to distribute the energy uniformly on the solar cell [3] [4].

Using only a POE in a photovoltaic system, no-uniformity of the concentrated distribution on the solar cell surface is observed, resulting in localized hot spot or even damage of the solar cell [5] [6]. Localized hot spots and poor uniformity will reduce efficiency of the photovoltaic system and service life of the solar cell. Keeping the power production of a photovoltaic system in real operation conditions under influences of wind and vibration is important. Therefore, precise orientation to the sun of the photovoltaic system is required. One of the ways for lowering the effect of the inaccurate orientation on the concentrator system power efficiency and for improving the irradiation uniformity on the solar cell surface is the application of the SOE located before the solar cell [5] [7].

Secondary optical elements are specular or refracting optical elements of various forms. The parameters of SOE used in a CPV unit are usually tailored according to the design parameters of the POE, performance requirements and the size of the solar cell [5]. Using a SOE will achieve high optical efficiency, lower the sensitivity to the sun tracking error, and improve the uniformity of irradiance distribution on a solar cell [7].

Therefore, the SOEs are different from one to the other. The comparison allows us to interpret that each one of SOE has its acceptance angle, its concentration level and its irradiation. Without using SOE, the optical efficiency reaches a value of 80% but with using it, the optical efficiency is enhanced. So, for rising concentration, increasing the acceptance angle and/or equalizing irradiance over the cell, the using of a Secondary Optical Element is necessary [7]. Refractive SOE shows a better performance (for the same concentration, they show a wider acceptance angle), than reflective SOE.

When using SOE in the CPV module we should think about the gluing between the SOE and the solar cell. In fact, silicone or polymer can be manufactured by gluing the SOE with a transparent adhesive onto the solar cell. The adhesive can be a sticky silicone or another transparent polymer. Only a thin layer of adhesive is required that presents an advantage since polymers are the most critical material regarding long term stability [8].

The optical characteristic of a CPV system is very affected by the state of the SOE. Hence, a highly gluing between POE and SOE influences also the optical performance. Maike Wiesenfarth *et al.* manufactured glass-silicone-glass

samples to measure the transmission and investigated the silicone-solar cell interface and silicone-glass interface to identify possible delaminating. Also possible delaminating of the solar cell silicone was investigated by glass-silicone-processed wafer samples and characterized visually. The mechanical stability was investigated with glass cylinders of the same diameter while the optical elements are glued to solar cells. Then, the samples were tested with the substrates held in vertical position in the climate chambers. The complete assemblage is tested with glass-silicone-solar cell samples and characterized before and after testing [8].

A thin layer of silicone is chosen but any increase or decrease in its thickness will affect negatively on the solar cell. With an increasing thickness, the optical efficiency will be lower because it doesn't allow the totality of the irradiance transmission, so a reduction of the PV efficiency. In the other hand, the use of a decreasing thickness could damage the solar cell by the direct contact with the SOE. This direct contact is affected by the silicone loss caused by the temperature increase. The silicone is acting both as an optical coupler to reduce Fresnel losses and as a mechanical bond. To act as mechanical bond it is necessary to use a minimum thickness of silicone. Our objective is to manufacture a mixture between silicone and glass balls to obtain long term stability. The choice of glass balls is due to its optical characteristic; in fact it minimizes the reflection and increasing transmission.

In this work a manufacturing of a new adhesive was investigated. This new adhesive is a mixture of the silicone with the glass balls in order to remain silicone coherent. Several samples were made for different category of glass balls, for each category there were a four percentages that had been studied.

The aim of the present work is to identify a new method to glue the Secondary Optical Element (SOE) to the solar cell and ensure the adequate thickness. The function of using a SOE with a Fresnel lens in a CPV unit is to achieve high optical efficiency, low sensitivity to the sun tracking errors, and improve uniformity of irradiance distribution on the solar cell.

2. Schema of the Studied System

As shown in **Figure 1**, the studied CPV module is composed of the following elements:

- Lens,
- Second optical element,
- Adhesive, that's the layer on which we are going to do the experimental part,
- Solar cell.

3. Experimental Method

The objective of the experimental part is to choose the best size of glass balls, with the suitable proportions of the weight of glass balls compared to that of silicone, from five different types of glass balls (**Table 1** and **Figure 2**).

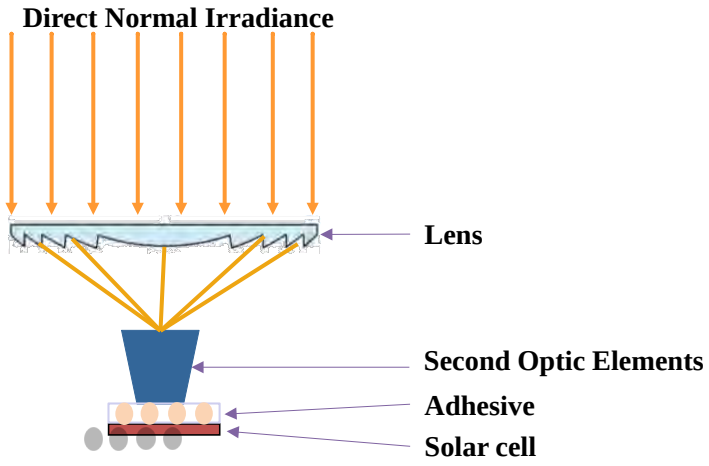

Figure 1. Schema of the studied system.

Figure 2. Different sizes of glass balls using in experience.

Table 1. Different sizes of glass balls using in experience.

Category	Size
A	<106 µm
B	150 - 212 µm
C	212 - 300 µm
D	425 - 600 µm
E	710 - 1180 µm

The proportions of the weight of glass balls compared to that of silicone presented on Table 2.

For all the samples, 2 g of silicone elastomer are mixed with 0.2 g of curing agent to obtain a more coherent silicone. For each type of glass balls, four proportions were mixed with the silicone which was already mixing. 2 g of silicone gives for each type 0.02 g, 0.04 g, 0.1 g and 0.2 g of glass balls.

After mixing, a drop of the resulting mixture is placed between two flat glasses until this mixture finishes. The mixture is done from 4 to 10 samples for each test. First, vacuum is applied to extract air bubbles from the silicone (Figure 3). The silicone is cured in an oven (20 minutes) or at room temperature (48 hours).

Table 2. The weight of glass balls proportions compared to that of silicone.

Proportion	Glass ball weight/silicone weight
1	1%
2	2%
5	5%
10	10%

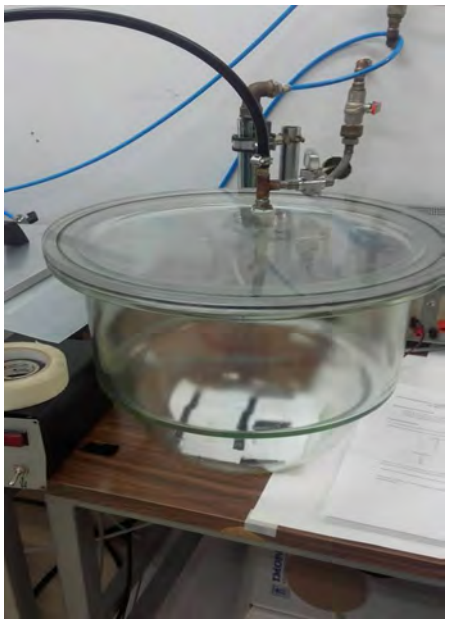

Figure 3. Vacuum for extracting air bubbles.

The different samples thickness measurements is done with the **VERNIER** as shown in **Figure 4** which is a graduated scale placed on the sliding feet, for length and angle measurement. It improves the lecture of the analogical accuracy.

- **Transmittance measurement**

Optical measurements were performed using a visible-near-infrared spectroradiometer (VIS-NIR-1 SPECTRO 320 from Instruments Systems). Instrument measurement accuracy is ±3% and reproducibility is ±0.3% STD. All the optical measurements were performed two times. Transmittances were measured from 250 to 1000 nm. The samples were almost placed in their right position during the UV irradiance exposure and to perform the optical measurements [9].

- **Absorptivity measurement**

Based on the Beer-Lambert law, the optical transmittance of samples $\tau(\lambda)$, is related to its absorption coefficient $\alpha(\lambda)$ and to its optical path-length x as [10]:

$$\tau(\lambda) = \exp\left(-\alpha(\lambda)\cdot x\right)$$

where λ is the wave length. However, the measured transmittance $\tau(\lambda)$ using the spectrophotometer is the total value of the sample layer. Therefore, with only

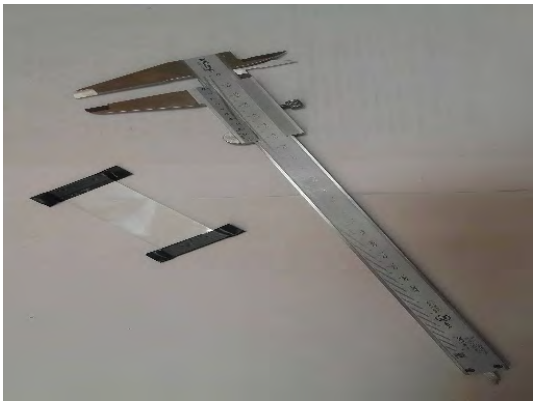

Figure 4. Example of samples with the VERNIER.

silicon samples as the reference, if we obtain two measured transmittance $\tau_i(\lambda)$ (transmittance of samples with different sizes glass balls) and $\tau_{ref}(\lambda)$ (transmittance of samples with only silicon) at two different optical path-lengths x_i corresponding to different sizes glass balls and x_{ref} corresponding to silicon only, the absorption coefficient of the samples $\alpha_i(\lambda)$ can be determined from [10]:

$$\alpha_i(\lambda) = \left[-1/\left(x_i - x_{ref}\right)\right] \ln\left[\tau_i(\lambda)/\tau_{ref}(\lambda)\right] = \left[-1/\Delta x\right] \ln\left[\tau_i(\lambda)/\tau_{ref}(\lambda)\right]$$

4. Results and Discussions

- **Thickness measurements mm**

Figure 5 summarizes thicknesses measured for the different samples. The thickness averages for A, B and C categories are almost equal, for different glass balls' percentage values. Besides, these categories are characterized by a low dispersion (dispersion between glass balls), except C where error is large. For the categories D and E the average values are not the same and their dispersions are large, but we note that for E, error is decreased when the percentage becomes 10%.

Figure 6 shows that the categories A and B which characterized by the smallest balls have the lowest dispersion. Dispersion for C and D categories is higher independently of percentage value. The E category has a higher dispersion but we note also a dispersion decrease when the ratio increases. So, the A and B categories have the best measurement results.

- **Transmittance measurements**

Figure 7(a) and **Figure 7(b)** shows the transmittance values corresponding to 5% and 10% of categories A, B, C, D and E. For the same percentage (5% or 10%) the transmittance values of all categories are around 90%. **Figure 8** also shows that the transmittance remains practically the same when the percentage of glass balls is varied (case of category A).

Figure 9 shows that the transmittance of the samples with glass balls (A) is almost similar to the transmittance of sample with silicone only. The difference between them is very small, and it is only from 290 to 360 nm as shown in **Figure 10**. The difference between glass balls and silicone is not important because for those wavelengths the irradiance value is low.

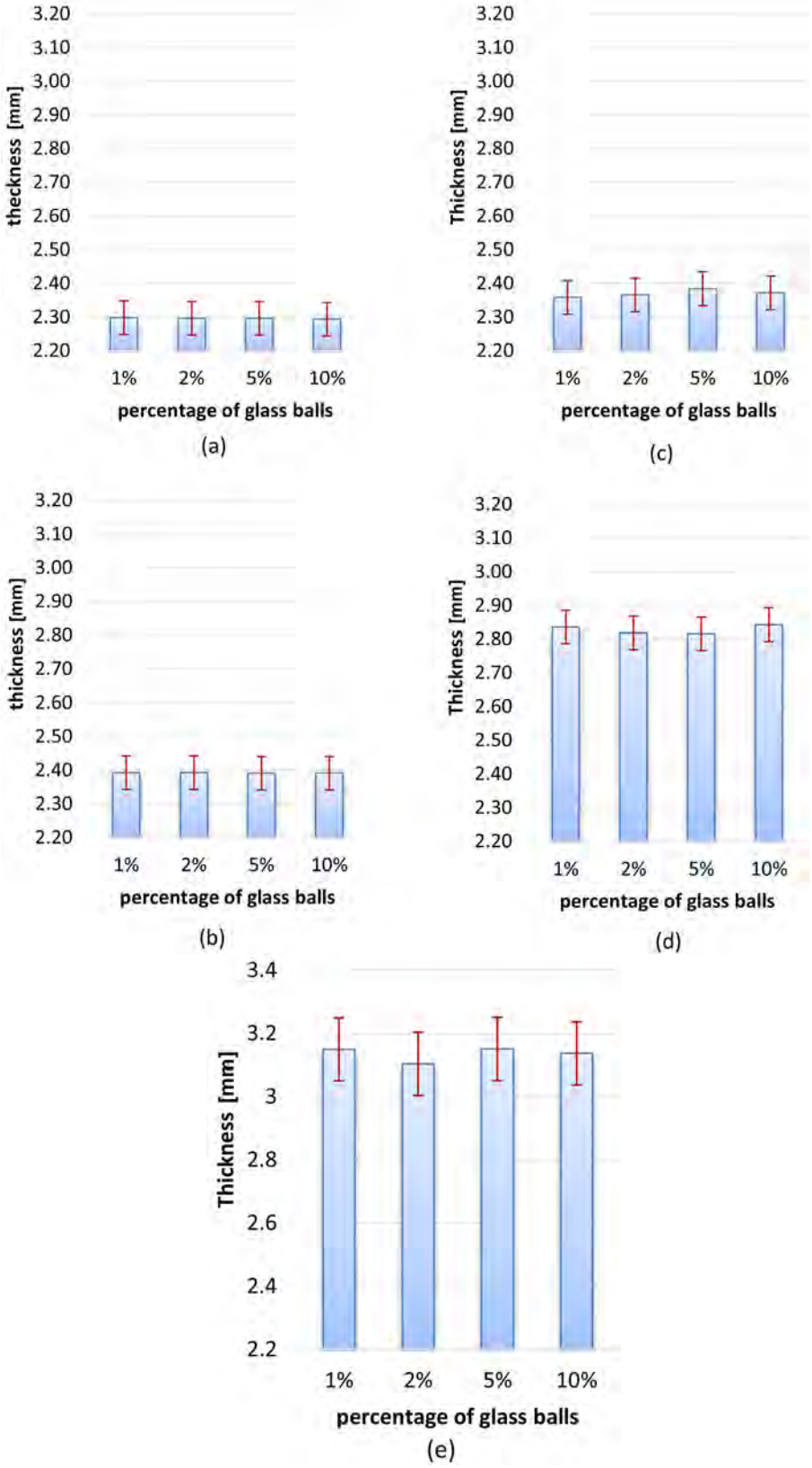

Figure 5. Dimensions with error bars for different categories; (a) A with 1%, 2%, 5% and 10% of glass balls; (b) B with 1%, 2%, 5% and 10% of glass balls; (c) C with 1%, 2%, 5% and 10% of glass balls; (d) D with 1%, 2%, 5% and 10% of glass balls.

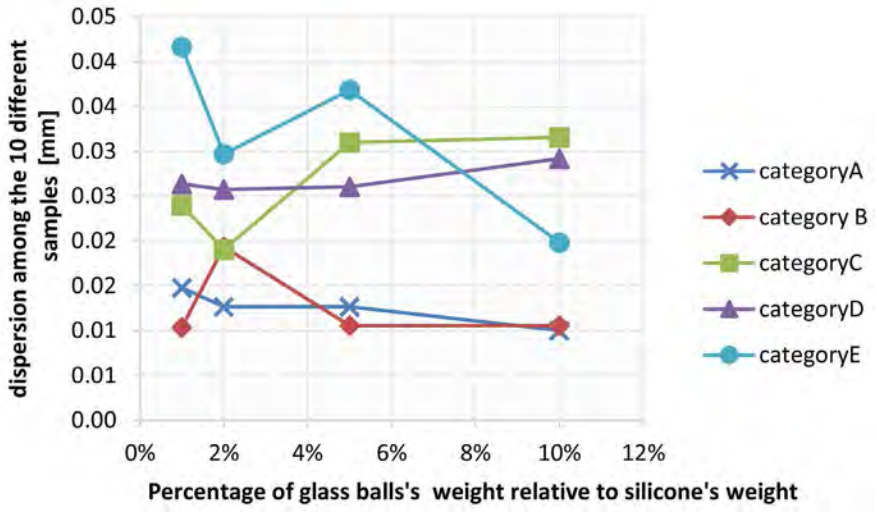

Figure 6. Dispersions for different categories of glass balls.

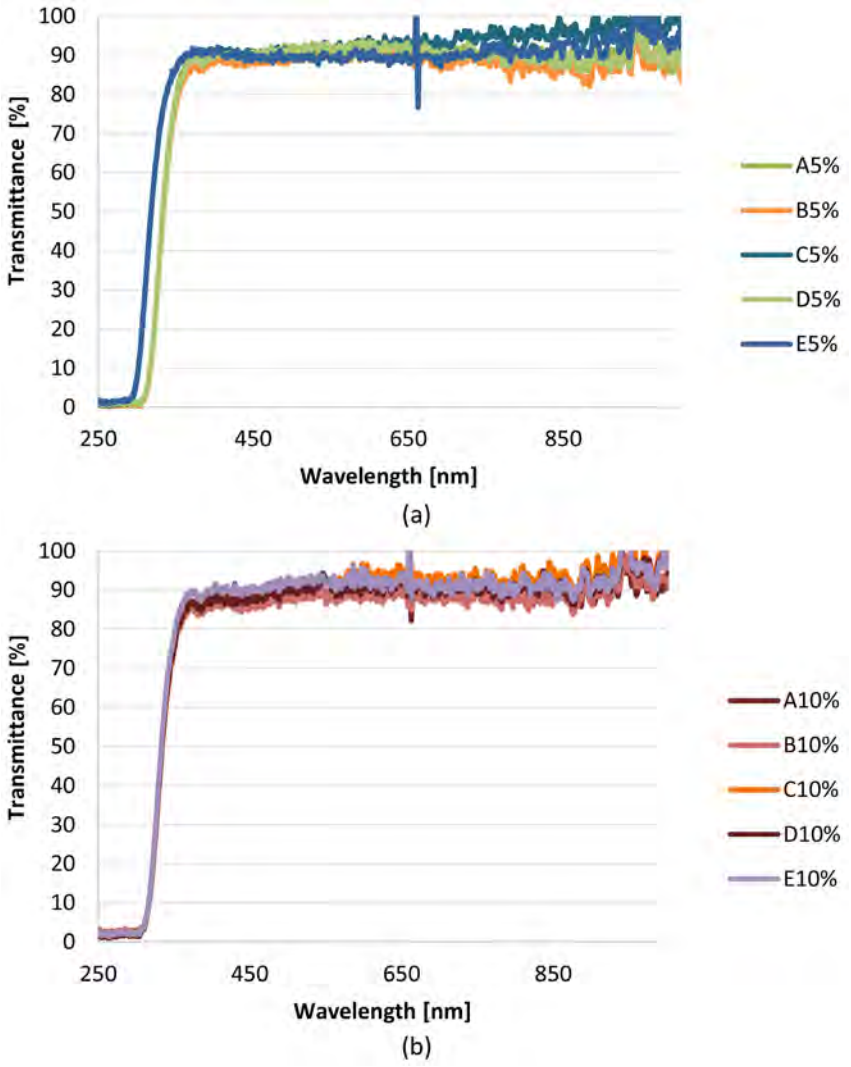

Figure 7. (a) Transmittance corresponding to 5% of categories A, B, C, D and E, (b) Transmittance corresponding to 10% of categories A, B, C, D and E.

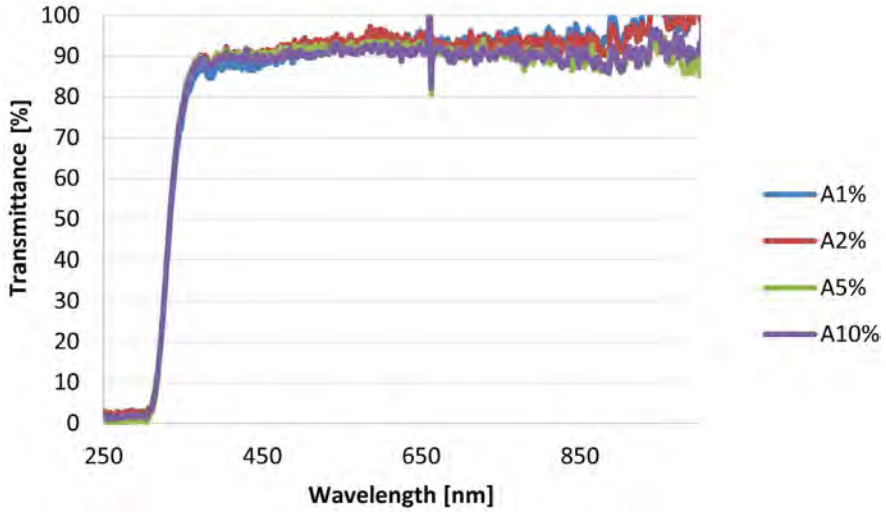

Figure 8. The transmittance corresponding to category A with 1%, 2%, 5% and 10% of glass balls.

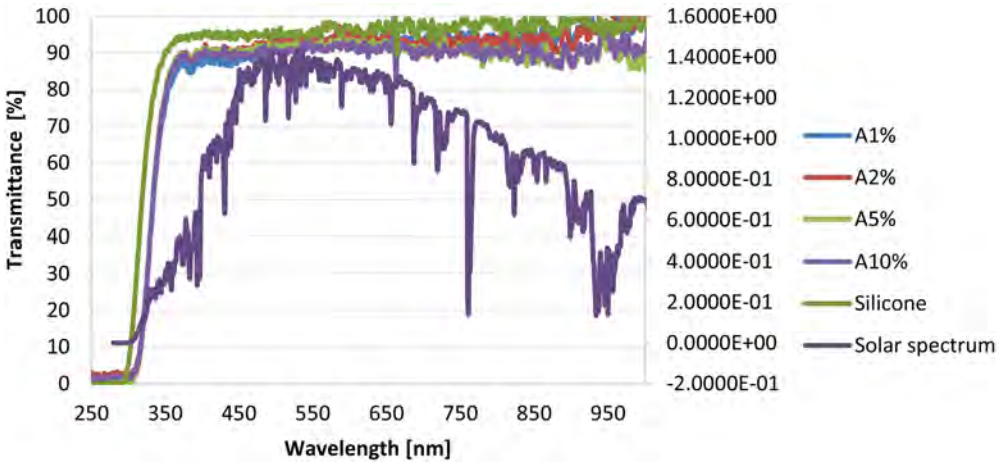

Figure 9. Comparison between the transmittance of the samples with glass balls (A) and the samples with only silicone with the consideration of the irradiance.

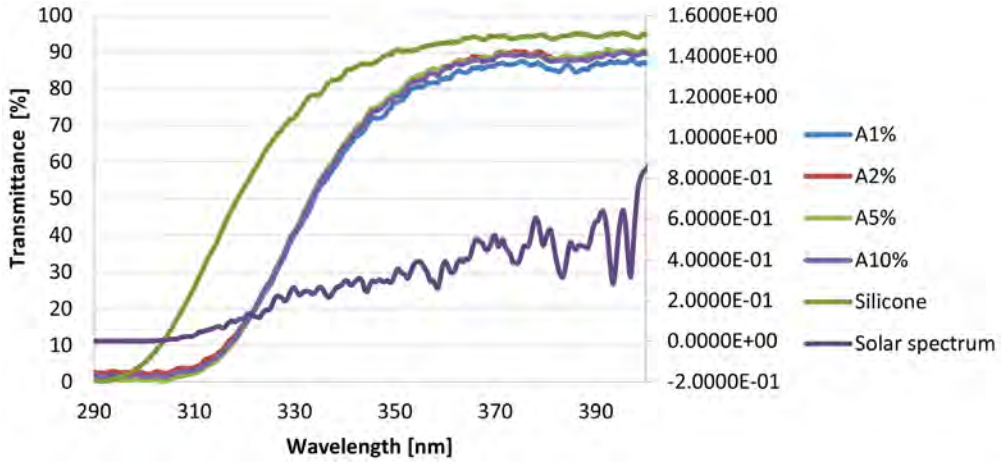

Figure 10. Wavelength interval giving sensitive transmission difference (with glass balls (A) and with only silicone).

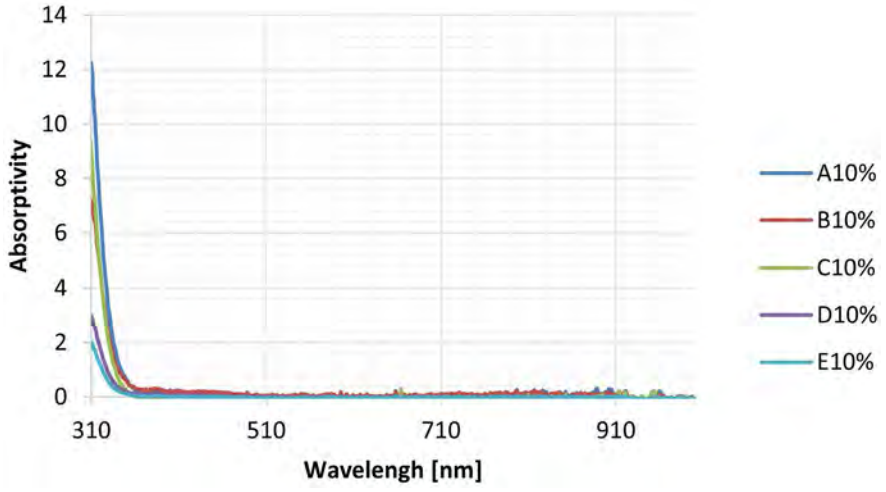

Figure 11. Absorptivity of the samples with different glass balls (A), (B), (C), (D) and (E)

- **Absorptivity measurements**

Figure 11 shows that the absorptivity of the samples with different glass balls is almost similar when wave length is above 360 nm, with a feeble value of the order of 0.05.

A difference is marked for the wavelengths corresponding to the ultra violet (less than 0.4 μm) where the solar irradiation is the lowest especially between (A), (B), (C) categories on one hand and (D) and (E) on the other hand.

5. Conclusions

In this work a new adhesive situated between solar cell and secondary optical elements has been manufactured. This adhesive is identified to silicone and transparent glass mixtures. These mixtures are in different mass proportions of the two compounds and they are classified to five categories according to ball sizes parameter. The experimental study of this adhesive for the different categories shows up essentially that the thickness criterion presents the only parameter allowing to the optimal category choice which is the A category (ball sizes < 106 μm). In fact:

- The adhesive minimum thickness value necessary to act as mechanical bond corresponds to A category where the glass balls size is lowest.
- The transmittance is practically the same for the different categories of the order of 0.9.
- The same thing for the parameter of absortivity is sensibly the same for the different categories of the order of 0.05.

In the continuity of this work we plan to accomplish the experimental part outside the laboratory directly against solar radiation and then compare the results with those found within the laboratory.

As perspectives this study can be extended to look for other mixtures which improve more mechanical cohesion between the secondary optical elements and the solar cell and at the same time keeping a high transmittance of solar irradiations.

Acknowledgements

This work has been carried out for two months at the Solar Energy Institute. The authors acknowledge to this Institute for its invitation and like to thank Dr. Ignacio Antón Hernández and Ms. Marta Victoria Pérez for their support and discussions. Finally, I express thanks to my research laboratory: Energy, Water, Environnemt and Process Analysis for giving me the opportunity to do this internship and I acknowledge the financial support by the University of Gabes.

Conflicts of Interest

The authors declare no conflicts of interest regarding the publication of this paper.

References

[1] Kalogirou, S.A. (2014) Solar Energy Engineering: Processes and Systems. 2nd Edition, Academic Press, Millbrae, CA.

[2] Kali, K., Islam, M., Yasmin, M., Das, S. and Sharker, K. (2019) *Computational Water, Energy, and Environmental Engineering*, **8**, 91-98. https://doi.org/10.4236/cweee.2019.84006

[3] Chen, Y.-C. and Chiang, H.-W. (2015) *Applied Science*, **5**, 770-786. https://doi.org/10.3390/app5040770

[4] Luque, A. and Hegedus, S. (2011) Handbook of Photovoltaic Science and Engineering. 2nd Edition, John Wiley & Sons, United Kingdom. https://doi.org/10.1002/9780470974704

[5] Luque, A. and Andreev, V. (2007) Concentrator Photovoltaic. Springer Verlag, Berlin. https://doi.org/10.1007/978-3-540-68798-6

[6] Andreev, V.M., Grilikhes, V.A., Soluyanov, A.A., Vlasova, E.V. and Shvarts, M.Z. (2008) Optimization of the Secondary Optics for Photovoltaic Units with Fresnel lenses. *Proceedings of the* 23*th European Photovoltaic Solar Energy Conference*, Valencia, 1-5 September 2008, 126-131.

[7] Victoria, M., Domınguez, C., Anton, I. and Sala, G. (2009) *Optics Express*, **17**, 6487-6492. https://doi.org/10.1364/OE.17.006487

[8] Wiesenfarth, M., Dörsam, T., Eltermann, F., Hornung, T., Siefer, G., Steiner, M., van Riesen, S., Neubauer, M., Boos, A., Wanka, S., Gombert, A. and Bett, A.W. (2015) CPV Module with Fresnel Lens Primary Optics and Homogenizing Secondary Optics. 11*th International Conference on Concentrator Photovoltaic Systems, AIP Conference Proceedings*, Volume 1679, Issue 1. https://doi.org/10.1063/1.4931554

[9] Victoria, M., Askins, S., Domınguez, C., Anton, I. and Sala, G. (2013) *Solar Energy Materials & Solar Cells*, **113**, 31-36. https://doi.org/10.1016/j.solmat.2013.01.039

[10] Han, X. Y., Guo, Y.J., Wang, Q. and Phelan, P. (2018) *Solar Energy Materials & Solar Cells*, **174**, 124-131

Journal of Modern Physics, 2021, 12, 1618-1632
https://www.scirp.org/journal/jmp
ISSN Online: 2153-120X
ISSN Print: 2153-1196

Physical Quanta in Quasicrystal Diffraction

Antony J. Bourdillon

UHRL, San Jose, CA, USA
Email: bourdillona@sbcglobal.net

How to cite this paper: Bourdillon, A.J. (2021) Physical Quanta in Quasicrystal Diffraction. *Journal of Modern Physics*, **12**, 1618-1632.
https://doi.org/10.4236/jmp.2021.1212096

Received: August 29, 2021
Accepted: October 16, 2021
Published: October 19, 2021

Abstract

Diffraction in quasicrystals is in irrational and geometric series with icosahedral point group symmetry. None of these features are allowed in Bragg diffraction, so a special theory is required. By means of a hierarchic model, the present work displays exact agreement between an *analytic* metric, with a *numeric* description of diffraction in quasicrystals—one that is founded on quasi-structure-factors that are completely indexed in 3-dimensions. At the quasi-Bragg condition, the steady state wave function of incident radiation is used to show how resonant response, in metrical space and time, enables coherent interaction between the periodic wave packet and hierarchic quasicrystal. The quasi-Bloch wave is invariant about all translations $a\,\tau^m$, where a is the quasi-lattice parameter. This is numerically derived, analyzed, measured, verified and complete. The hierarchic model is mapped in reverse density contrast, and matches the pattern and dimensions of phase-contrast, optimum-defocus images. Four tiers in the hierarchy of icosahedra are confirmed, along with randomization of higher order patterns when the specimen foil is oriented only degrees off the horizontal. This explains why images have been falsely described as having "no translational symmetry".

Keywords

Quasicrystal, Icosahedra, Hierarchic, Resonant Response, Harmonic, Irrational, Geometric Series, Metric, Diffraction Quanta

1. Introduction

The most profound physical effect that is found in a *quasicrystal* (QC), is diffraction in geometric series. The effect is incompatible with Bragg's law for crystals, which is in integral order n. His ordering is due to the physical harmonies that occur at a Bragg condition, between a crystal scattering a periodic probe—whether of photons or electrons—from planes of atoms that are ordered and periodic.

By contrast, the QC was described as a "Metallic phase with long range order and no translational symmetry" [1]. Evidence for long range order is implied by its sharp diffraction. However, there is imaging evidence for hierarchic symmetry, at least in reasonably short range, and this may be called translational. Furthermore, numeric and analytic simulations prove that the probe's quasi-Bloch wave also has, at the quasi-Bragg condition, translational symmetry about $a\,\tau^m$, where a is the measured and calculated quasi-lattice parameter [2]; and where $\tau \equiv \left(1+\sqrt{5}\right)/2$ is the golden section; while the hierarchic order m is integral.

Bragg diffraction is, in momentum space, a quantum effect. It resembles quantized transitions between energy states in the hydrogen atom: we know these states are harmonic, in time and space, because they are solutions to Schrödinger's equation. In this paper, we refresh the argument and add new data, *i.e.* by projecting atoms in the Hierarchical Icosahedral (HI) structure onto the 5-fold $(1\,\tau 0)$ plane. This is done in reverse contrast for the first time and compares closely with transmission electron microscope (TEM) images, including randomization of off-plane cells in the long range.

2. Harmonic Scattering between a Periodic Probe and Hierarchic Quasicrystal

In crystals, elastic scattering is illustrated in Figure 1. Applying Bragg's law, quanta $n\Delta k$ may be generated from a quantum $\Delta k = \hbar\cos(\theta)/\lambda$ where the order n is integral; θ is the Bragg angle; λ the wavelength of the scattered radiation, and $\hbar$ the reduced Planck constant. In case of small angles, as in high energy electron scattering, the interplanar spacing on first order $d_{n=1} \simeq \lambda/2\theta$ is unique and harmonic at any Bragg order n, so that the scattering crystal diffraction is periodic—like the crystal—and harmonic.

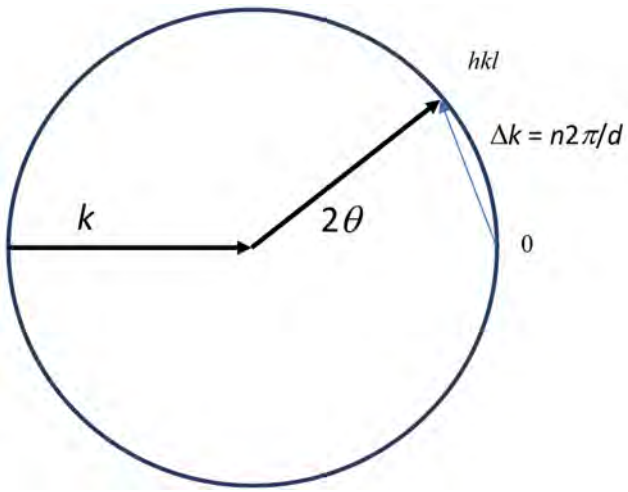

Figure 1. Following Bragg's law, quanta of momentum $n\Delta k$ are transferred for each scattered beam on the periodic Bragg diffraction pattern: the periodic probe and crystal lattice cooperatively harmonize in the well-known way. In high energy electron scattering at the quasi-Bragg condition, the irrational quasi-lattice that is hierarchic and geometric, will be found to cooperate with the beam probe via a quasi-Bloch wave and metric.

The physical basis for this quantization is similar for the quantized eigenvalues of Schrödinger's hydrogen atom in energy space: the eigenstates do not self destruct by interference precisely because their orbits are harmonic as in Bohr's atom. In electron state transitions, energy is transported in wavepackets with $\Delta E = R_H\left(n_f^{-2} - n_i^{-2}\right)$, where n_i and n_f are initial and final state principal quantum numbers, and R_H is the Rydberg unit of energy.

The same theoretic basis is needed for diffraction in QCs that have multiple interplanar spacings, that are not periodic, are not harmonic and that—far from being integral—are actually irrational and in geometric series, τ^m; with $m = -\infty, -1, 0, 1, 2, 3, \cdots$. The quasi-Bragg law is observed [3] [4]:

$$\tau^m \lambda = 2d' \sin\left(\theta'\right) \tag{1}$$

where the quasi-Bragg angle turns out to be $\theta' = \theta / c_s$; with c_s the coherence factor, or metric [5] that will be defined below; and where the quasi-interplanar-spacing is found to be $d' = dc_s$. Every atom scatters from locations on jumbled planes with multiple values of d. We shall see how coherent scattering is won in the QC from this group of properties: the metric, that results from resonant response of the periodic probe to the hierarchic quasi-lattice [6], digitizes its irrational measure, and harmonizes the probe with the QC. The hierarchy is uniquely icosahedral, with cells, clusters and superclusters uniformly aligned by multiple edge sharing at each element.

Quantum mathematics is not enough: to understand digitization and harmony in the scattered wave, we need to briefly recall radiant scatterers in the broader scope of physics. After the Michelson-Morley experiment falsified the ether hypothesis, an attempt was made to salvage it with the Lorentz transformation. This was not as successful as Einstein's foundational relativity: "Physical laws are invariant in all inertial reference frames." A consequence is the Pythagorean equation: $E^2 = \boldsymbol{p}^2 c^2 + m_0^2 c^4$. After quantization by Planck's law for energy E; and by the de Broglie hypothesis for momentum $\boldsymbol{p}$; and with simplification of units $\hbar = c = 1$ for the reduced Planck constant $\hbar$; and for the speed of light c; the rest mass reduces to:

$$m_0^2 = \omega^2 - k^2 = \left(\omega + k\right)\left(\omega - k\right). \tag{2}$$

The brackets govern in turn *particulate* conservation laws, and response that is *wave-like.* The former bracket is real; the latter imaginary. In the diffractive interactions considered here, the response is resonant and harmonic. The particle-wave duality is thus formulated in respective real and imaginary parts of the *normal wave packet* [7]:

$$\varphi = A \cdot \exp\left(\frac{X^2}{2\sigma^2} + X\right)$$

with imaginary:

$$X = i\left(\bar{\omega}t - \bar{k}x\right) \tag{3}$$

where σ depends on initial conditions that determine the coherence of the pack-

et in space and time[1] (rank R^4), and where A^2 is a normalizing constant[2]. The angular frequencies ω and wave vectors k are in fact distributed, but they are represented in Equation (1) by mean values. The intensity $\phi^*\phi$ is a probability density function for a particle, or for a photon having zero mass, $m_0 = 0$. Notice that the response is elastic because its absolute, measurable value is unity: $\left(e^X\right)^* e^X = 1$, everywhere and at all time.

When an electron binds to an atom, the latter's central potential wraps the extended, interacting electron wavepacket into compact harmonic space. This process would be destructive if the wavefunction orbitals were not harmonic in motion, with discreet wavevector and frequency. In quantized quasicrystal diffraction, the scattering is likewise integrated over space and time. Every atom scatters: the integration occurs over multiple, jumbled planes. Scattering at the quasi-Bragg angle is due to discreet integrands and these will be calculated in the next section by the quasi-structure factor (QSF). This factor is independent of scattering angle which is theoretically unknown *a priori*. The QSF is therefore descriptive where Bragg's law is not. However, we will show how the scattering angle is calculated numerically, and exactly matched analytically.

Meanwhile, Equation (2) represents the steady state for the incident radiation and, after a transition involving a change in wave-vector k, it will represent likewise, the steady state of the diffracted wave. When the incident wave strikes the QC, it interacts with its electric field to form quasi-Bloch waves. You can think of these as lattice images observed in crystalline thin foils in the two-beam condition. The waves, as they proceed through the QC, oscillate (by the pendellösung effect) between the two beams (in crystals: [8]; *cf.* in QCs: [2] [9]). In wedge specimens, this oscillation produces images of "thickness fringes". The process requires and ensures harmonic interaction, in both space and time, in the propagation direction as in the transverse. An example will be given in the next section, though the "quasi-lattice image" will not be a true lattice image because of the metric.

Notice that Equations (3) effectively linearize the second order Equation (2) of special relativity, and so do for the free particle what Dirac's equation does for the bound electronic states in atoms. Moreover, the Equations (2) separate the propagation direction from the transverse direction, and this has many consequences including: solutions for negative mass [10][3], phase velocity [7], uncertainty, Newton's second law, electron spin (as induced paramagnetism in phase space, that is consistent with Hundt's rules in atomic structure), intrinsic magnetic radius [11] and fine structure constant, reduction of the wave packet [12] etc. The equations apply in harmonious diffraction by quasicrystals and crystals, as they do in the Schrödinger equation that operates on steady-state, harmonic

[1]Typically, the coherence has transverse components, σ_y, σ_z as well, but these are only implied here for simplicity. Furthermore, when an atom is excited or decays, its central potential wraps the extended, interacting wavepacket into compact harmonic space.

[2]$A^* A = (\int \exp(X^2/\sigma^2) \cdot \mathrm{d}\tau)^{-1}$.

[3]To avoid unphysical singularities when $k = -m_o c$, our antiparticle travels with forward velocity but reverse spin (cf. [6]).

bases. The diffraction orders and quantum numbers respectively describe interaction requirements that are quantized by *necessary constructive interference over space and time.* The formalism in Equation (3) will enable our understanding of the fundamental interaction required in the coherent diffraction in QCs that will be described in what follows.

It is obvious that the diffraction depends on the phase properties of the probe, especially its wavelength; but it also resonates coherently in both space and time. Meanwhile, the metric provides corresponding coherence in spite of the multitude of interplanar spacings that have precise order and symmetry in the HI, as QSFs will prove. The diffraction pattern of i-Al_6Mn has been completely indexed and simulated in three dimensions [4] [13]. Dimensions should not be multiplied without necessity. It is one role of theory to invent short cuts, but quantum math[4] turned the egg upside down and ate the cup. In Aristotle's informal logic, the fallacy is called, *Ignoratio Elenchi*, which is translated: "missing the point".

3. The Metric: Numeric, Analytic and Measured

Since QCs do not obey Bragg's law of diffraction, nothing is known *a priori* about corresponding relationships between θ', λ and d'. However, the *structure factor* (SF) method is independent of θ: we can use the method by applying the known relationship between d' and the index h_{hkl} in cubic structures: $d = a/\sqrt{h^2+k^2+l^2}$. Here a represents the lattice parameter, and subscripts h, k and l represent the 3-dimensional indices in the diffraction pattern [14] [15]. It turns out that all structure-factors in the QC are zero. The implied absence of diffraction should be expected in a solid whose images demonstrate multiple interplanar atomic spacings. However it turns out further, that by introducing a coherence factor c_s, which is specific to the *hierarchic icosahedral* structure, a quasi-Bragg condition is discovered that is as sharp as the Bragg condition commonly observed by rocking crystals. The coherence factor is discovered by simulations in which the factor is numerically scanned while evaluating the *quasi-structure-factor* (QSF), first over the unit cell (order $p = 0$) with atomic scattering factors $f_i = f_{Al}$ or f_{Mn} in Equation (4), and secondly over clusters order p, by iteratively adding cluster centers at $\boldsymbol{r} = \boldsymbol{r}_{cc}$ in Equation (5) [2]:

$$F_{hkl} = \Sigma_i^{Al,Mn} f_i \cos\left(2\pi \cdot c_s \left(\boldsymbol{h}_{hkl} \cdot \boldsymbol{r}_i\right)\right) \tag{4}$$

$$F_{hkl}^{p} = F_{hkl}^{p-1} \cdot \Sigma_{cc} \cos\left(2\pi \cdot c_s \tau^{2p} \left(\boldsymbol{h}_{hkl} \cdot \boldsymbol{r}_{cc}\right)\right) \tag{5}$$

All atoms scatter.

In crystals, the SF is simpler and is represented by Equation (4) with $c_s = 1$. There, the calculation is comparatively easy because the summation is limited to one unit cell which repeats periodically. Symmetry in the unit cell often forces $F_{hkl} = 0$, or to a small range of values. In QCs, by contrast, the QSFs are calculated over all the atoms in a selected order of HI. They contain a spectrum of

[4]Including P.A.M. Dirac's *The Principles of Quantum Mechanics* (1958) Oxford, with such ugly concepts as unstable wavepackets; unexamined internal motion; unphysical electron speed $v = c$; etc.: anomalies falsified by QC diffraction.

amplitudes, whose intensities match measured intensities [4].

The main argument in favor of the hierarchic structural solution is—in physics—overwhelming[5]: uniquely, the solution is in geometric series, fitting the diffraction pattern, and it is consistent with imaging that will be simulated below.

The most substantial result is the discovery of the numeric metric. This will be subsequently proven, firstly by its analytic explanation, and secondly by verified measurement of the lattice parameter. These calculations were initially thought to be ideal; later we will discuss defects, both short range vacancies and interstitials, and also long-range quasi-lattice congruities.

Figure 2 shows one simulation for the (τ00) intensity in a supercluster order 6. Here, c_s is scanned across the quasi-Bragg condition. There is no Bragg diffraction when c_s = 1; diffraction occurs at the quasi-Bragg condition when c_s = 0.894.

The coherence factor is the same for all of the beams in the original data [1] and so is called a metric. What is it? Equation (4) and (5) show that it has the same influence as the lattice parameter or reciprocal lattice parameter. The coherence factor is a virtual breathing strain that switches the quasi-Bragg diffraction on or off, like the rocking curve of a rotating crystal. In consequence, the quasi-Bragg angle in QCs is increased from the corresponding Bragg angle in crystals by about 11%. This difference will become significant in the measurement of the quasi-lattice parameter.

The most remarkable feature of the QSF is its precise value for c_s, as calculated in the HI model (Figure 2)—less than 1/1000th of the quasi-Bragg angle. After analyzing the metric when it is applied to quasi-Bloch waves, the special translational symmetry will become apparent.

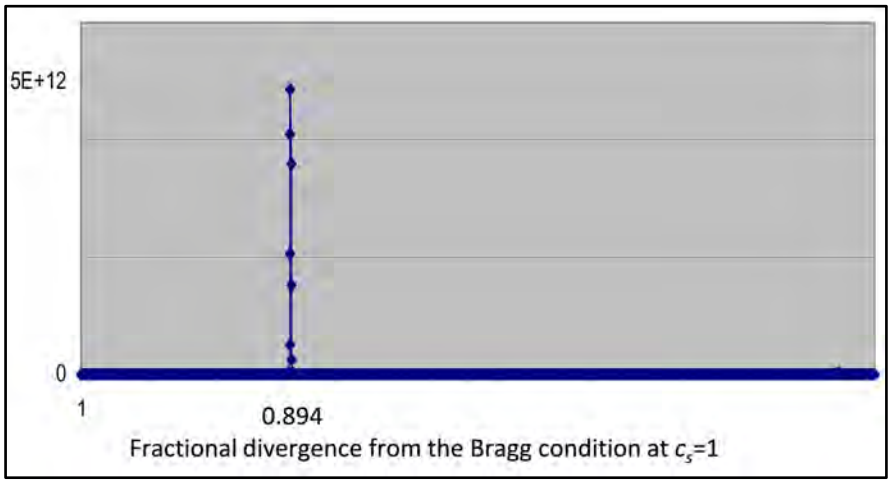

Figure 2. Quasi structure factor for the HI (τ00) diffracted beam, due to a supercluster order 6. On scanning c_s, the QSF is zero at the Bragg condition when c_s = 1; at the quasi-Bragg condition c_s = 0.894. The quasi-Bragg angle is ~11% greater than the corresponding Bragg angle in crystals due to equivalent, except periodic, d. The calculated line width is less than 1/1000th of the corresponding Bragg angle.

[5]In mathematics, all axioms are allowed.

The coherence factor c_s is analyzed as follows. Consider the following mathematical fact that is proved by mathematical induction:

$$\tau^m = F_m(1,\tau) = \partial_{(m,0)} + F_{m+1}(0,1) + F_m(0,1)\tau \tag{6}$$

where $F_m(a,b)$ represents the m^{th} term in the Fibonacci sequence, base (a, b), and $\partial_{(m,0)}$ is the Dirac delta function. From the terms at right, the natural part is separable by approximating $\tau \to 3/2$, and the *metric function* is derived by subtracting out the irrational residue from its corresponding geometric order τ^m:

$$\frac{1}{c_s} = 1 + \frac{\tau^m - F_{m+4}/2}{F_{m+1}} = \frac{1}{0.894} \tag{8}$$

This function turns out to be the exact inverse of the numeric metric that was derived from the QSF. The fact is extremely surprising because the numeric and analytic derivations are independent. The formula is identical for all terms in the series, and in all three spatial dimensions. In QCs, the divergence from the Bragg angle is due to the irrational parts of the indices; this divergence digitizes the separated natural part that provides coherent, harmonic scattering [2], *i.e.* with $c_s = 1$.

Details of the effects of the metric function are illustrated by quasi-Bloch waves. These can be thought of as amplitudes used to construct quasi-lattice images in the 2-beam condition. The quasi-Bloch waves are created in the incident probe by atomic potentials in the hierarchic icosahedral structure. Consider first, a typical Bloch wave in a crystal, like the blue wave in **Figure 3**. The wave is commensurate with the unit cell and with all unit cells, periodically repeating. This wave is not commensurate with the irrational and geometric series intercepts, that mark the central locations of atoms, cells, clusters and super clusters, of whatever order. However, when the blue axis is multiplied by the metric function, the resulting red quasi-Bloch wave becomes commensurate. This is partly due to the rational denominator F_{m+1} in Equation (8). The metric function digitizes and harmonizes the periodic probe when it enters the irrational, geometric, quasi-lattice potential. The function enables coherent diffraction when the probe scatters from the many aperiodic atoms in the hierarchic quasi-lattice. The coherence results from the combined and characteristic translations in the HI. This coherence is calculated in the QSFs (**Figure 2**).

Notice that the probe contains long range order with translational symmetry about all geometric intercepts $a\,\tau^m$, where a is the quasi-lattice parameter. The symmetry occurs also in short range in the quasi-Bloch wave. Only with the analysis provided here, can the parameter be measured.

In QCs, the "lattice parameter" was measured a long time ago, based on the doubtful supposition of Bragg's law of diffraction. The measurement compared the dominant scattering angle in the 5-fold diffraction pattern of i-Al_6Mn with a known scattering angle in a crystalline second phase. The measured value was 0.206 ± 0.005 nm [16] [17]. This corresponds to the indexed beam (τ, 0, 0) and corresponds also with the cell length and intercellular spacing throughout the QC (**Figure 4**), namely $a\,\tau$, where the golden-rectangle cross-section of the unit cell is $\tau \times 1$ in icosahedral units, or $a\,(\tau \times 1)$ in SI.

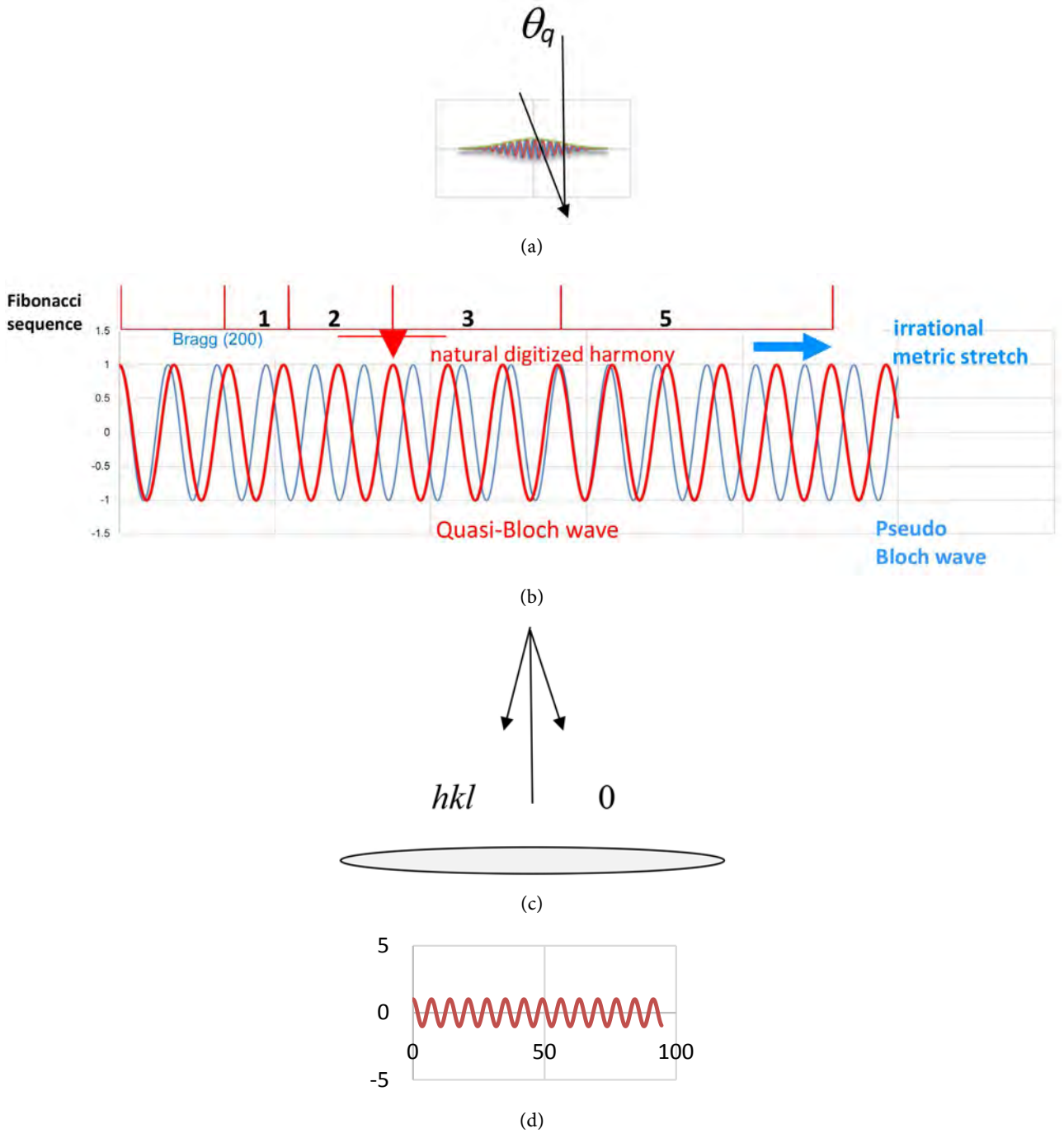

Figure 3. (a) Incident, time-dependent, beam probe (Equation (2)), rank R^4, inclined at quasi-Bragg angle from normal: $\theta_q = \sin^{-1}\left(\lambda\sqrt{h^2+k^2+l^2}\right)\Big/\left(2ac_s\right)$, in electron scattering. (b) Crystalline Bloch waves (blue) are commensurate with their corresponding periodic crystal lattice at the Bragg condition. When this wave is stretched horizontally by the inverse coherence factor $1/c_s$, the quasi-Bloch-wave (red) commensurates with the irrational, geometric and hierarchic, quasi-lattice. Its geometric order is represented by the intercepts on the horizontal line above it. The digitized number of periodic cycles between successive intercepts is in Fibonacci sequence (denominator in Equation (3)), and the diffraction is logarithmically periodic. The natural and irrational parts of the indices are separable: the irrational part is expressed by the metric stretch; the natural part scatters with sharp, coherent diffraction. (c) Diffracted beams emitted beneath foil, including indices. (d) In TEM, beams can be magnetically refocused to produce a quasi-lattice image of the *probe* at the base of the specimen foil. The lattice image is the interference due to the superposition.

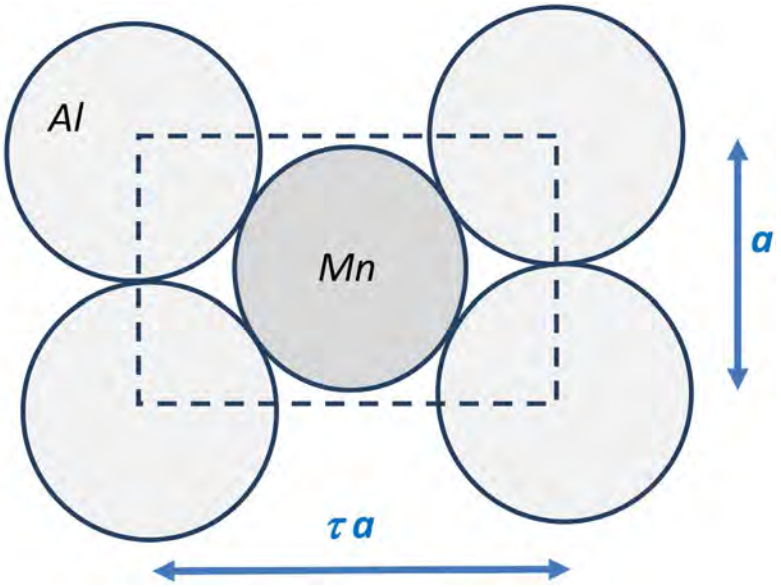

Figure 4. Golden-rectangle cross-section of the icosahedral unit cell in i-Al_6Mn, having side width a (the lattice parameter) and length τa. The unit cell contains 15 identical sections at various orientations. The structure is extremely dense, and depends on atomic diameter ratios $d_{\mathrm{Mn}}/d_{\mathrm{Al}} = \sqrt{1+\tau^2} - 1$.

By using the same formula as applies to cubic crystals to find the interplanar quasi-spacing $d = a/\sqrt{h^2 + k^2 + l^2}$, the correction for the quasi-Bragg law is therefore given $a = 0.205 \times c_s \tau \pm 0.05$ nm. The resulting value is close to the standard value of the diameter of Al in the pure metal. This measurement confirms the structural model and method.

4. Ideals and Defects

The overwhelming advantage of the ideal HI model is the explanation it provides for the observed geometric series diffraction that is apparently unique to QCs. A subsidiary advantage is the explanation for icosahedral symmetry in the diffraction pattern from a structure that repeats, uniquely, as hierarchic. The repetition occurs at the unit cell level and throughout the quasi-lattice. The unit cell is denser than can occur in crystals; but space-filling is taken up beyond the unit. The cell contains a single Mn atom at its center, surrounded by 12 closely packed Al atoms [2]. The extreme density depends on the atomic diameter ratios, $d_{\mathrm{solute}}/d_{\mathrm{solvent}} = \sqrt{1+\tau^2} - 1$. At short range, space occupation is simple enough and is consistent with phase-contrast, optimum-defocus imaging up to the first order of superclusters [18]. At this range, vacancies at cluster centers and interstitial atoms (including tetrahedra or unit cells) at supercluster centers minimally affect the diffraction pattern [5]. However, extracellular holes become an ever-expanding problem in higher orders. Now that the metric is consistently understood in the ideal HI, we return to less conventional ways in which filling may occur in higher orders of the hierarchy.

In crystals, the SF is calculated in the periodically repeating unit cell. The

symmetry of a single unit cell defines the diffraction pattern (whether simple cubic, face-centered cubic (fcc), body centered cubic *etc.*) for the whole crystal, repeating lattice and all. All cells are uniquely aligned because they are face sharing. Meanwhile, no crystal is perfect: interstitials and vacancies are common; as are growth defects such as twinning; and various dislocations that are products of deformation strains. We understand that such defects should be common in HI as they would relieve quasi-lattice stresses, especially those arising from uneven atomic densities near holes but also due to thermal stresses during rapid cooling.

The HI structure proved essential to demonstrating the effects of irrational indices in setting the metric and in establishing harmonic scattering in diffraction. Notice firstly that cell alignment is necessary for the sharp diffraction pattern. This must be due to the *multiple edge sharing* of the icosahedral cells, clusters and superclusters as they indeed occur in the HI. Moreover, since, in crystals, the diffraction pattern symmetry is set by the structure factor of the unit cell, we need to assess, for QCs, the relative importance of the unit cells versus quasi-lattice structures, *i.e.* short range versus long range, as needed to ensure coherence and pattern identity. After describing atomic maps in oriented thin films, we shall consider long range lattice irregularities.

5. Maps onto the 5-Fold Icosahedral (1τ0) Plane

The decoration of the unit cell (in icosahedral units) is as follows:

Mn on the site (0, 0, 0), with

Al on the 12 permutations of $(\pm 1, \pm\tau, 0)$.

On the cluster:

12 unit cells centered on the 12 permutations of $(\pm\tau, \pm\tau^2, 0)$.

On the supercluster, order p:

12 superclusters order $(p-1)$ centered on permutations of $\tau^{2p}(\pm\tau, \pm\tau^2, 0)$.

Our purpose is to simulate the most significant atomic maps that can be observed in the original diatomic quasi-crystal, bearing in mind that our phase-contrast, optimum-defocus shows both limited resolution, and reverse contrast [2] [14] [18]. It is relatively simple to plot every atom: we construct the structure on Cartesian axes and rotate it to make the $(1\,\tau 0)$ horizontal [19]. Then we select a foil thickness as observed in TEM. This thickness might contain the hemisphere of a cluster, for example, or a horizontal slice of the structure. The result has so much structure with unaccounted intensity that it hides the desired pattern [5]. We simplify by plotting only to the low resolution that represents unit cells. We do this by omitting the weakly scattering Al atoms (**Figure 5(a)**). The resulting pattern shows the diameter of the cluster to be 0.9 nm which is close enough to Bursill and Peng's measurement (0.85 nm) based on microscope micron markers and the indefiniteness of their reverse contrast. Our next step is to reverse our simulated contrast by omitting the Al atoms; instead, simulating a cluster of cluster peripheries (**Figure 5(b)**). The peripheries

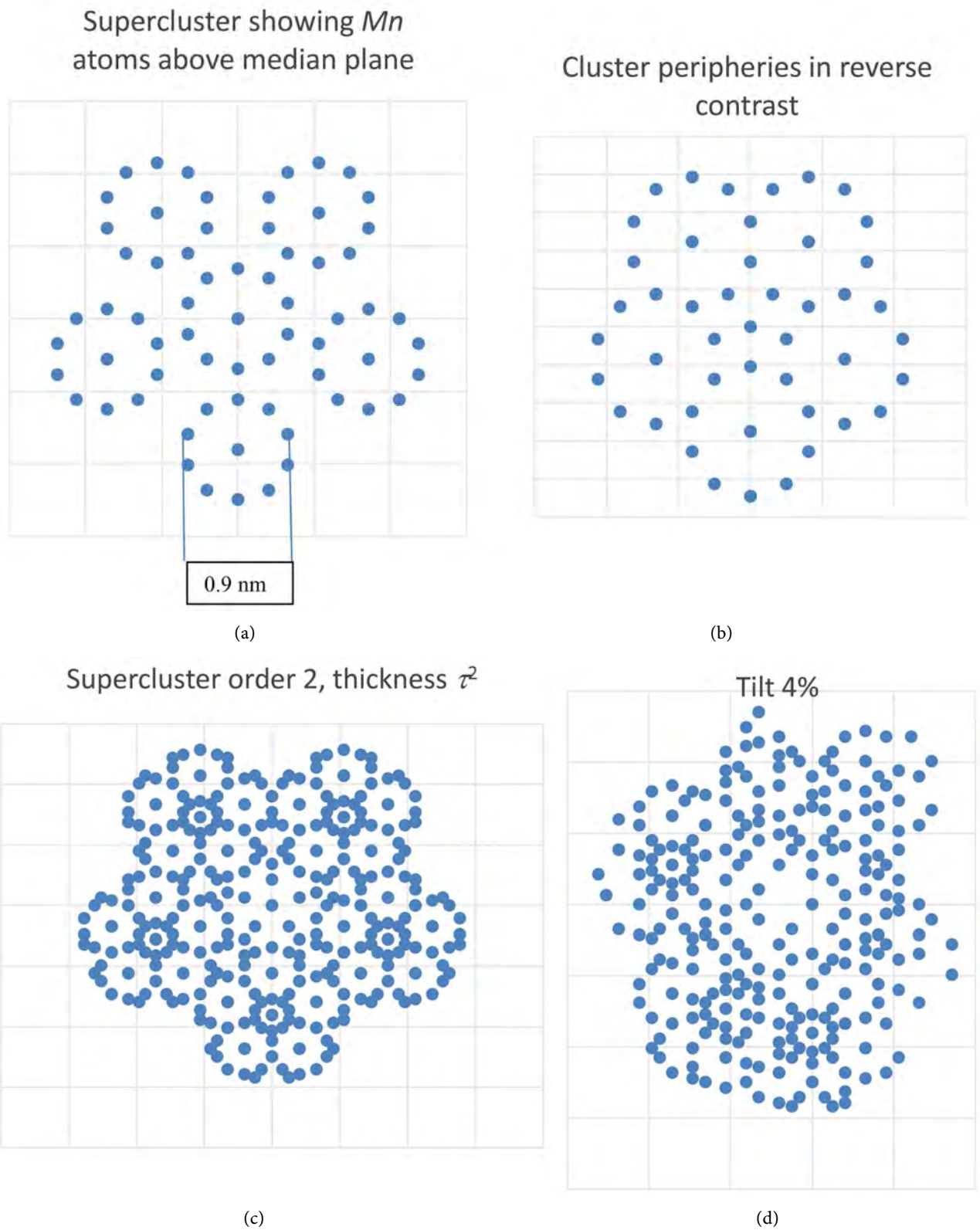

Figure 5. (a) Simulation of an HI supercluster of HI unit cell centers. The sample orientation is (1 τ0) horizontal. The diameter of the circle of cell centers is 0.9 nm. (b) Simulation in reverse contrast that matches the corresponding pattern in Bursill & Peng [18] among others. (c) Simulation of a horizontal supercluster order 2. (d) Simulation of the same supercluster tilted about the vertical axis to a slope of 1:25. Notice that, even with small tilts, the pattern is lost except for apparently random cells and clusters.

occur at a radius τ times greater than atomic separations from corresponding cluster centers. This process yields an excellent simulation of a supercluster in Bursill and Peng's image. In particular, the clusters in reverse contrast touch, *i.e.* at cluster edges [5][6]. Moreover, the dimensions are confirmed along with the hierarchic model up to four tiers of order. The match with Bursill and Peng becomes irresistible, and is generally comparable to other miscroscopic images of quasicrystals.

What about the supercluster order 2? This is shown in reverse contrast in **Figure 5(c)**. As the images expand in area, they become harder to observe because of the precision required in locating a thin foil prepared by either electropolishing or ion milling. For example, an error of only 1:25 in the slope of the polished foil about the vertical axis yields the simulation shown in **Figure 5(d)**. After tilting, the supercluster pattern is, for the most part, lost; though remnants of apparently random cells and clusters are identifiable. It is therefore impractical to expect that large areas of a QC should exhibit superclusters of high order. Nevertheless, hierarchic order is demonstrated in the images, along with their geometric series diffraction.

6. Possibility for Quasi-spherical Cells

In principle, the Hi is infinite in extension. The units are initially and progressively edge-sharing and holey. Defects have been a long-time concern, but given the firm ideal model, progressive solutions are possible.

Previously, we have considered defects in the short range: vacancies, interstitials, disloctions etc. They are natural products of the edge-sharing structure of the HI, but they are not sufficiently dense to noticeably affect the diffraction pattern. Now we consider defects in longer range.

Consider the regular icosahedron as being quasi-spherical. This is justified by its having 15 identical cross-sections (**Figure 4**) at various orientations. Secondly, consider metallic atoms as approximately spherical, so that they may, from a structural viewpoint, be replaced by icosahedra. We may therefore imagine two structures: one an fcc lattice with icosahedral unit cells; and another the icosahedral lattice containing fcc unit cells[7]. In neither case need the cells be edge sharing and space filling. What effect might transformations between the two structures have on the diffraction pattern, can be investigated by QSFs.

Simulated QSFs are shown in **Figure 6**. The specimen sizes are typical for a supercluster order 2. These are compared with each other, and also with the QSF calculated on an HI supercluster order 6, in **Figure 2**. It is clear that for pure fcc Al (**Figure 6(a)**) at the Bragg condition, $c_s = 1$ at the origin, as it must be. In **Figure 2**, $c_s = 0.894$ for i-Al_6Mn, as described above.

[6]The simulation is partly fortuitous: the radius of the cluster is τ times the radus of the unit cell and coincides with the outer edge of cell, *i.e.* including both Mn and the outer lining of Al atoms.

[7]The fcc unit cell is cubic, but its stacking is similar to the unit cell in i-Al_6Mn ([4], p.19).

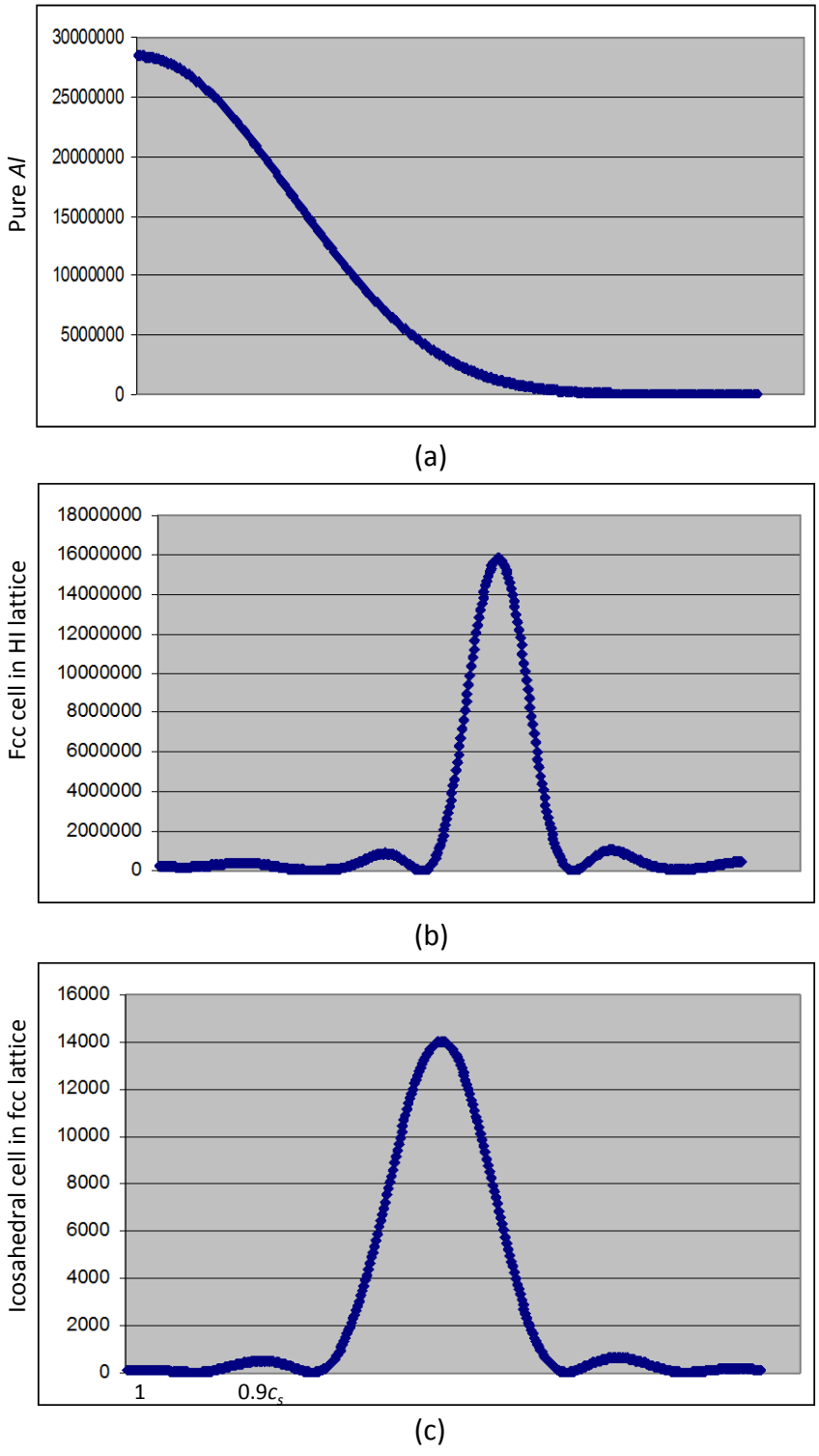

Figure 6. (a) QSFs for a cubic cluster of fcc Al, having about 20,000 atoms, similar to a supercluster order 2. Note $c_s = 1$, *i.e.* Bragg reflection. (b) Computed QSF for (111) diffraction due to an imaginary fcc cell on an icosahedral grid, as in a supercluster order 2. Note $c_s \simeq 0.9$. (c) Computed QSF for (τ, τ, τ) diffraction due to an icosahedral cell on an imaginary cubic grid of side τ. Site population about 20,000 (like a and b). Notice that c_s is similar to configuration in b. [Bourdillon, A.J. (2010) Quasicrystals' 2D Tiles in 3D Superclusters. *UHRL*, San Jose, ISBN 978-0-9789839-2-5 p. 66].

Meanwhile the two imaginary solids in **Figure 6(b)** and **Figure 6(c)** have $c_s \simeq 0.9$. This simulation for the metrics of imaginary structures demonstrates that the QSFs are determined by the lattice as well as the unit cells. (contrast crystals, where SFs are calculated within individual cells and are identical for all cells and for the lattice). The observation implies that, if higher order icosahedra are substituted by cubic structures, or even by quasi-speherical structures, as defects in the quasi lattice, then the diffraction pattern may be approximated by the pattern that is calculated in the ideal HI model. The lattice may then be locally defective, while retaining the principal scattering properties of the ideal HI structure. By this means, a mixture of local quasi-cubic lattice sites with icosahedral quasi-lattice sites of high order might reduce density fluctuations. These would add to conventional vacancies and interstitials as possible defects in the long range. There is no evidence that this occurs, but the data signals that, with regard to long range defects, the geometric series diffraction in QCs is as robust as Bragg diffraction in crystals.

7. Conclusions

Scattering by Hiearchic Icosahedral structures is the most obvious instrument for diffraction of periodic probes into geometric series. The physical process for this fact has been described in detail. It is classical, 3-dimensional, and independent of tiling theory. The quantum requirements for the diffraction in geometric series contain necessary relationships of harmony and digitization. In consequence, resonant quasi-Bloch waves in the scattering probe have translational symmetry at geometric series orders $a\,\tau^m$. The Hierarchic Icosahedral structure is consistent with phase-contrast, optimum-defocus imaging. This is simulated by reverse-contrast mapping of atoms that scatter X-ray or electron probes incident on a thin QC foil. However, owing to the hierarchic translational symmetries, higher orders appear to randomize by specimen tilts of small angles away from horizontal. The difficulty of thin-film specimen preparation with optimized quasicrystollagraphic orientation results in the common conclusion: there is "no translational symmetry"; However this view not only contradicts expectations in "long range order", but is not necessary since hierarchic icosahedra indeed *have* translational symmetry. This occurs consistently, both in the hierarchic structure and in the resonant response.

Finally this solution for both the structure and diffraction differs from the two dominant objectives commonly followed in QC research: Our method is entirely classical and verified [2] [5] [6] [7]: it concentrates on the simplest and original (diatomic) system with minimal complication. The method has successfully identified the principal principles. Those other methods have been admittedly tentative and wishful for forty years. The first is mathematical and in-complete, viz. the mathematics of non-periodic tilings *e.g.* [19]; the second has covered for its shortcomings by spreading the net: the method attempts to find the extent of possible quasicrystals, especially with respect to composition and process *e.g.*

[20]. The net has not uncovered the desired conclusion. Scientific method is empirical; we used to wish, and used to collect data, but our comprehension has since expanded to higher orders.

Conflicts of Interest

The author declares no conflicts of interest regarding the publication of this paper.

References

[1] Shechtman, D., Blech, I., Gratias, D. and Cahn, J.W. (1984) *Physical Review Letters*, **53**, 1951-1953. https://doi.org/10.1103/PhysRevLett.53.1951

[2] Bourdillon, A.J. (2020) *Journal of Modern Physics*, **11**, 581-592. https://doi.org/10.4236/jmp.2020.114038

[3] Bourdillon, A.J. (2011) Logarithmically Periodic Solids. Nova Science, New York.

[4] Bourdillon, A.J. (2012) Metric, Myth and Quasicrystals.

[5] Bourdillon, A.J. (2021) *Journal of Modern Physics*, **12**, 1012-1026. https://doi.org/10.4236/jmp.2021.127063

[6] Bourdillon A.J. (2009) *Solid State Communications*, **149**, 1221-1225. https://doi.org/10.1016/j.ssc.2009.04.032

[7] Bourdillon, A.J. (2017) Dispersion Dynamics in the Hall Effect and Pair Bonding in HiT_c. Nova Science, New York.

[8] Hirsch, P., Howie, A., Nicholson, R.B., Pashley, D.W. and Whelan, M.J. (1977) Electron Microscopy of Thin Crystals. Krieger, New York.

[9] Bourdillon, A.J. (2010) Quasicrystals' 2D Tiles in 3D Superclusters. UHRL, San Jose.

[10] Bourdillon, A.J. (2018) *Journal of Modern Physics*, **9**, 1304-1316. https://doi.org/10.4236/jmp.2018.96079

[11] Bourdillon, A.J. (2018) *Journal of Modern Physics*, **9**, 2295-2307. https://doi.org/10.4236/jmp.2018.913145

[12] Bourdillon, A.J. (2020) *Journal of Modern Physics*, **11**, 1926-1937. https://doi.org/10.4236/jmp.2020.1112121

[13] Bourdillon, A.J. (2013) *Micron*, **51**, 21-25. https://doi.org/10.1016/j.micron.2013.06.004

[14] Bourdillon, A.J. (2009) Quasicrystals and Quasi Drivers.

[15] Bourdillon, A.J. (2020) *Journal of Modern Physics*, **5**, 1079-1084. https://doi.org/10.4236/jmp.2014.512109

[16] Tsai, A.P. (2008) *Science and Technology of Advanced Materials*, **9**, 1-20. https://doi.org/10.1088/1468-6996/9/1/013008

[17] Bourdillon, A.J. (1987) *Philosophical Magazine Letters*, **55**, 21-26. https://doi.org/10.1080/09500838708210435

[18] Bursill, L.A. and Peng, J.L. (1985) *Nature*, **316**, 50-51. https://doi.org/10.1038/316050a0

[19] Grimm, U. and Kramer, P. (2019) Quasicrystals.

[20] Steinhardt, P. (2018) The Second Kind of Impossible: The Extraordinary Quest for a New Form of Matter. Simon & Schuster, New York.

Journal of Modern Physics, 2021, 12, 1633-1655
https://www.scirp.org/journal/jmp
ISSN Online: 2153-120X
ISSN Print: 2153-1196

Mechanism of Quantum Consciousness that Synchronizes Quantum Mechanics with Relativity—Perspective of a New Model of Consciousness

Siva Prasad Kodukula

Independent Researcher, Visakhapatnam, India
Email: sivkod@gmail.com

How to cite this paper: Kodukula, S.P. (2021) Mechanism of Quantum Consciousness that Synchronizes Quantum Mechanics with Relativity—Perspective of a New Model of Consciousness. *Journal of Modern Physics*, **12**, 1633-1655.
https://doi.org/10.4236/jmp.2021.1212097

Received: September 11, 2021
Accepted: October 17, 2021
Published: October 20, 2021

Abstract

Synchronization of quantum mechanics with relativity has been considered differently from the present quantum gravity models. It is originated from the roots of philosophy of physics and the basic concepts of relativity & quantum mechanics. It emphasizes the fact that two conscious observers are necessary to experience one conscious moment. Various concepts of consciousness have been discussed and emphasized the necessity for the introduction of a new model of quantum consciousness. A quantum coordinate system has been introduced to explain the present understanding of the phenomena "observation" and "reality". It has been elaborated that the observation defined by physics is confined to Lorentz space time coordinate system, Minkowski coordinate system and general relativity. But phenomena of observation cannot be completed without considering one more hidden transformation explaining quantum coordinate system which transforms the quantum states into relativistic coordinate system as an interaction between two conscious observers explained by an interactive mechanism of quantum states. A flow chart has been illustrated by a mechanism giving rise to conscious moment and proposed a new model of consciousness. It emphasizes on the fact that "reality" is different from "observation" defined by physics. It affects the relativistic factor of special relativity and suggests a modification for it. If this modified relativistic factor is proved experimentally, the results establish consciousness's mechanism and a remarkable breakthrough in physics of consciousness studies.

Keywords

Quantum Mechanics, Relativity, Double Relativity Effect, Film Theory of

Universe, Consciousness

1. Introduction

Fundamentally quantum mechanics is not synchronizing with General relativity because, at quantum level *i.e.* beyond a limit, General relativity equations cannot explain space time. Quantum mechanics describes discreteness of space time and General Relativity interprets continuous and smooth space time. These two are not in synchronization.

1.1. Present Quantum Mechanics

Wave theory of light has been introduced in 17th century. Double slit experiment proposed in 1803 by Thomas young played an important role in establishing wave theory. In 1900 Planck proposed quantum theory. In 1905 Einstein explained photo electric effect by Planck's quantum theory. Modern quantum mechanics originated after the introduction of de Broglie's equation explaining the wave nature of particle in the years 1923 to 1925.

Later, matrix mechanics was introduced. Schrödinger wave function was introduced in 1926. By 1930 quantum mechanics had been further unified and formalized by David Hilbert, Paul Dirac and Neumann with greater emphasis on measurement, the statistical nature of our knowledge of reality and definition of "observer". Even today, Measurement problem, observables and "observer" plays an important role in the development of quantum theory [1] [2] [3].

Observer and observation has a deeper meaning involving the concept of consciousness [2] [4]. *In this paper it is explained that without observers there is no meaning for the word "Reality" described by physics*. Of course the reality is linked with Relativity also.

1.2. Relativity

Galilean or Newtonian transformations are equations that relate space and time coordinates of two systems moving with constant velocity relative to each other. It is failed to interpret light velocity which was described by Maxwell's equations. They are not invariant in Galilean transformations.

1.3. Lorentz Transformation

According to Lorentz transformation, the observers moving at different velocities may measure different distances such that the velocity of light is the same in all inertial reference frames. This invariance of light velocity has been considered as a postulate of special theory of light.

1.4. Special Relativity

In the year 1905 special theory of relativity has been published. It has elaborated

the conventional notion of an absolute universal time with the notion of a time that is relative to reference frame and its position in space. Rather than an invariant time interval between two events, there is an invariant space time combined with other laws of physics and proposed the mass energy equivalence principle. Special relativity interprets a flat four-dimensional Minkowski space time. It appears to be very similar to the standard Three-dimensional Euclidian space, but there is a difference with respect to time. It has reduced the spatial dimensions in to two, so that we can represent the physics in a three dimensional space. In Newtonian mechanics, quantities that have magnitude and direction are mathematically described as three dimensional vectors in Euclidean space, and in general they are represented by time. In special relativity, this notion is extended by adding the appropriate time like quantity to a space like vector quantity, and we have four dimensional vectors, or "four vectors" in Minkowski space time. The components of vectors are written using tensor notation. In Newtonian gravity, the source is mass. In special relativity, mass turns out to be part of a more general quantity called the energy-momentum tensor which includes both energy and momentum as well as stress pressure and sheer. Using the equivalence principle, this tensor is readily generalized to curved space time.

1.5. General Theory of Relativity

Thus in 1915 General relativity proposed. According to this theory, there is no gravitational force deflecting objects from their natural, straight paths. Instead, gravity tends to changes in the properties of space and time, which in turn changes the straightest-possible paths that objects will naturally follow. The curvature is, in turn, caused by the energy-momentum of matter. As it is constructed using tensors, general relativity exhibits general covariance. It thus satisfies a more stringent general principle of relativity, says that the laws of physics are the same for all observers. In other words, as expressed in the equivalence principle, space-time is Minkowiskian and the laws of physics exhibit Lorentz invariance.

If we consider General relativity as most fundamental and explainable by geometry, quantum theory the basis of understanding matter from elementary particles is unexplainable by space time geometry at quantum level. However, how to reconcile quantum theory with general relativity is still an open question. In order to explain the importance of the problem, few authors conducted a survey and published the results [5].

1.6. Relativistic Quantum Mechanics

Relativistic quantum mechanics is application of special relativity for quantum particles. It is not a theory to reconcile quantum mechanics with general relativity. Dirac equation is resultant of this concept. Based on this concept, super fluid theories have been proposed [6].

According to General Relativity the conventional gravitational wave is:

1) A small fluctuation of curved space time;

2) It has been separated from its source and propagates independently.

These cannot be completely justified in a theory with exact Lorentz symmetry. They are not perfectly described by relativistic theory.

In this paper the conceptual and physical interpretation of quantum coordinates, in to Lorentz or Minkowski's space time have been explained and the space time incorporated in general relativity. Thus mathematical interpretation of space time curvature is possible by the concept of physical transformation of quantum states represented by quantum coordinates to space time coordinate system of reality. This paper has no relation to super fluid relativity. But it is based on a previous calculation of space time diameters for all fundamental forces [7]. All these space time diameters are interpreted as points with zero space in quantum coordinates in order to obey the property of signal required for transformation.

1.7. Synchronization of QM with GR

General relativity equations describe space time curvature. When it is applied to black holes, the physical quantities such as space time divergence at the centre of black holes, when it goes closer to the centre, less than Planck length distance, there is a breakdown of General Relativity (GR) equations. There must be a new theory which goes beyond GR is required and quantum influence plays dominant role. Thus quantum gravity theories originated [8].

1.8. Loop Quantum Gravity (LQG)

The main result of loop quantum gravity is the derivation of a granular structure of space at the Planck length. The quantum state of space time is described in the form of spin networks. Much of the work in "loop quantum gravity" or "quantum geometry" area has been based on Dirac quantization of the constraints, though there have been recent advances in the use of covariant "spin foam" methods [8].

All the above models are based on space time geometries, renormalization [8] [9], space time coordinates defined by Newtonian, Galilean, Lorentz etc. But nowhere it is not mentioned that how does this space time forms. The definition of observer which is a part of these coordinate systems is really in the same system? How are we transforming these systems in to one another without knowing the presence of observer whether it is inside or outside of the system? This probe will lead us to formulate a new approach for synchronizing quantum mechanics with general relativity. "Physics of consciousness" emphasizing on these aspects. Involvement of "consciousness" plays a vital role in the synchronisation of quantum mechanics with general relativity. Present studies on consciousness explains as follows.

1.9. Consciousness

Consciousness is an interdisciplinary concept with quantum mechanics, relativ-

ity, space time structure, and biology. Lots of theories are there to define consciousness. But in this paper, based on earlier work, physics of consciousness especially on "measurement problem", "observer effect", and "wave function collapse" have been considered for further probe in to fundamental physics. Orch-OR [10] is one of the proposals on this subject. According to that, consciousness is associated to Orchestral Reduction process and is related to gravity. Threshold time to form gravitational space time at basic level, has been calculated [7]. This is the first step to synchronise quantum mechanics with relativity since the quantum particle of our four dimensional space time *i.e.* gravity is obeying both quantum mechanics and general relativity principle. This has leaded me to propose new hypotheses of consciousness [11]. Some of the experiments in biology [12] are promising for the proof of this direction of thought. Of course, the author expressed it as a proof of Orch-OR theory. The same can be applied further to new hypothesis of consciousness [11] also and the model elaborated in the present paper regarding the physics part of that biological model of consciousness.

1.10. New Hypothesis of Consciousness

Analysis on some of the concepts involved in Orch-OR proposal such as threshold time, quantum de-coherence, entanglement, system and the environment with which system interacts etc and the process connecting all these phenomena raised so many alternative solutions for connecting concepts and alternative proposals for integration of them. Thus a new hypothesis explaining the model for "consciousness and information processing" has been proposed [11]. Now, in the present paper, a new model of consciousness has been proposed to interpret "consciousness" in terms of physics. It is completely different from the existing models but similar to Orch-OR proposal.

All the above theories tried to explain this synchronization on the basis of General relativity. But special relativity plays a vital role in this synchronization. Special relativity is a simple explanation to transformations from Newtonian, Galilean to Lorentz. Finally Lorentzian manifold has been transformed in to minkowiski space time manifold which is the basis for general relativity. Quantum mechanics is a parallel development and was not based on these transformations. So general relativity is not in synchronization with quantum mechanics. Loop quantum gravity theories tried to synchronize general relativity with quantum mechanics directly from general relativity. Even though they considered the synchronization through Lorentzian manifold, it has not considered the fact of observation and its transformation which is basically connected to consciousness. If we consider the involvement of consciousness in all these transformations, Newtonian, Galilean and Lorentz transformations, we can understand that one transformation is missing. This transformation has been interpreted by quantum coordinate system. Mechanism of consciousness plays an important role in this synchronization. Of course, without double relativity ef-

fect [13] [14] [15] it is not at all possible to get an overall view of quantum coordinates.

Explaining all these transformations along with the mechanism of consciousness again one by one, we can find a new way of interpretation for this synchronization. This interpretation will definitely transform the classical or relativistic concepts and quantities in to quantum mechanical system.

2. Theory & Discussion

Established theoretical background of physics explains the space time notions and the representation of its coordinate systems from Newtonian mechanics to General Relativity. Their transformations also have been well established. Now we are introducing a new coordinate system termed as "Quantum Coordinates" in this sequential order. Before introduction of this coordinates, the sequential order is Newtonian, Galilean, Lorentz, Minkowski and General Relativity. Sequential order means without the previous one, the next one is not possible. After introduction of Quantum coordinates, the sequential order will be changed to Newtonian, Galilean, Lorentz, Quantum and Minkowski or General Relativity. Let us see the interpretation of quantum coordinates in transformations.

2.1. Quantum Coordinate System

A quantum coordinate system is also like Minkowski or general relativity coordinate system. In that, space will be X coordinate and time will be Y coordinate. **Figure 1** shows the quantum coordinate system in terms of relativistic coordinates and its interpretation with respect to relativistic coordinates.

But the difference is in quantum coordinates; all points will have zero space. Time only will exist. But in the interpretation of coordinate system, space axis will be existed. Means, even though, space exists, it is considered as zero only. In conventional coordinate system a point will have both time and space where as time only will exist in quantum coordinate system. But the space will be shown as information. All the points will have different time and different information but with space zero. So instead of space axis there exists information axis when comparing with conventional relativistic coordinate system. As per space time equivalence principle, space converts in to time [16]. At the same time, it (time) is nothing but information [11]. So finally, a point will contain time only and as per its position in the coordinate system, it will have time and information. Its space is zero. This time and information describes that point. Since space is zero, it can not contain any object like mass. In the transformation of this coordinate system to space time coordinates, it will be in synchronization with general relativity with space time coordinates and the general relativity equations will be applied. **Figure 2** illustrates the observers view of an object through quantum phenomena represented by quantum coordinates.

2.2. Transformation of Quantum Coordinate System

For any Lorentz coordinate system, if time changes and space remains constant

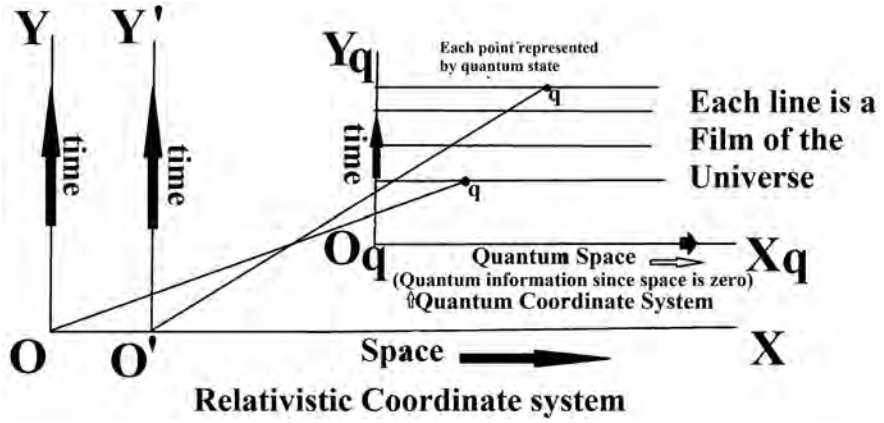

Figure 1. Quantum coordinate system and its interpretation with respect to relativistic coordinate system. Each point represents quantum state and each line represents film of the universe so that the universal film is a superposition of quantum states.

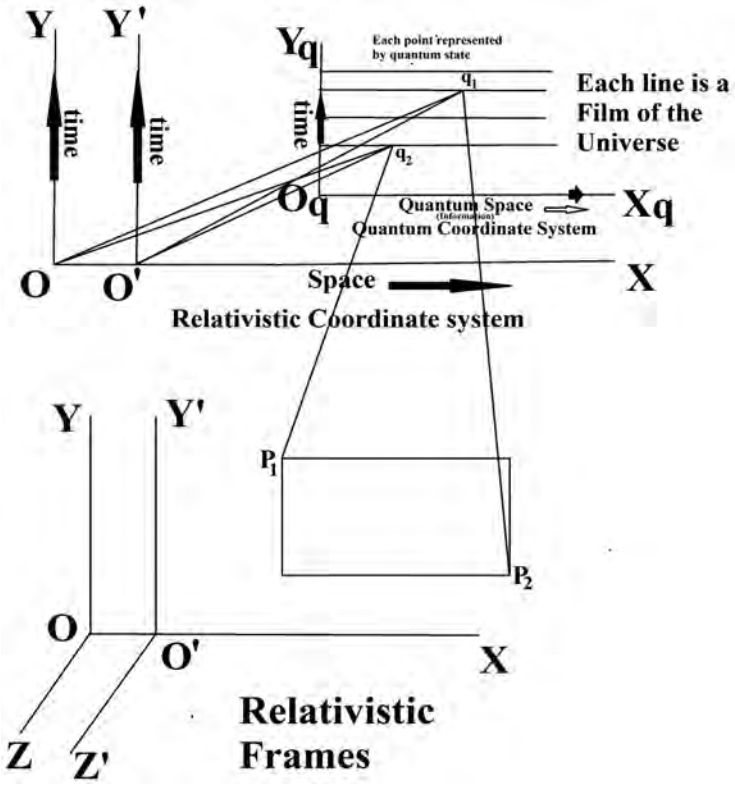

Figure 2. Observer's view of an object through quantum phenomena represented by quantum coordinates. Observer is confined to conventional relativistic frames of reference.

or space changes and time remains constant for a particular frame of reference with velocity, means that frame (or particle) is with a constant velocity relative to all inertial frames of reference. For example, if we observe a particle with velocity "v", it will cover a distance within a duration of time and at the same time if the observing system moves with velocity, then the relative velocity will be different. But if it is not changed, then change in velocity is zero. If change in veloc-

ity is zero, change in either of space or time will be zero. Let us suppose the case that time exists and the space (covered distance) is zero as explained above, then its velocity is constant for all inertial frames of reference. Such particles will not exist in this Lorenz coordinate system. Only velocity exists. Any particle in this world occupies space and can be considered as "combination of particles". So "constant velocity relative to each other" has no meaning for that "combination of particles or mass" and such particles will not exist in this conventional space time coordinate system (or Lorentz coordinate system).

Long back author explained the same phenomena by "double relativity effect" and NC particles [13] [14]. Now in this, it is applied for profound understanding of the relation between quantum states and their interpretation in transformation of relativistic frames.

2.3. Double Relativity Effect

Double Relativity effect is an effect attributable to absolute velocities. While observing a particle with constant velocity relative to all inertial frames of reference (Light particle or a travelling photon is an example for it). In this, special relativity will be applied twice in a single observation at the same time [13] [14] [15].

Here, the velocity considered in the first stage is absolute velocity and will be effected by a phenomena called "double relativity effect". Thus the absolute velocity will be changed to observed velocity. Double relativity effect elaborates that the Absolute velocity and observed velocity is related by equation $v_o = v_a\gamma$ where $\gamma = \dfrac{1}{\sqrt{1-\left(\dfrac{v_a}{c}\right)^2}}$.

Any velocity in this universe must pass through infinitely series of points in relativistic space time coordinates. These points are imaginary only. But when object changes through these points in the course of its velocity, the double relativity effect will be applied to that object at that point in coordinate system. So observed velocity is $v_o = v_a\gamma$.

2.3.1. Role of Observer

The paper [17] explains the role of observer and consciousness on special relativity. In this paper, it is elaborated how does an observer considers the object by the application of absolute velocities concept and how films of the universe changes with time does. Film theory' of the universe has been applied and much more elaborated in the paper [11]

2.3.2. Film of the Universe

A film of the universe is an inertial frame of reference containing same time interval all over the film as per the film theory of the universe [11] [13].

Further when it is applied to Universe, It is postulated that whole universe is existed with points containing absolute velocity [16]. This velocity is constant for all inertial frames of reference and an absolute velocity "v" exist at distance d

from an observer and related by equation $v = Hd$. At the same time it will have a velocity $vd = K$. The resultant is the observed velocity. Here "H" is Hubble's constant and "K" is Siva's constant.

The same concept is applicable to space time and showed that all the fundamental forces are made up of space times but relatively with different space time densities [7]. Interaction between these fundamental fields with separate space times giving raise to new particles. Space time conversion in to matter is also explained [16]. Here it is connected to Quantum physics and emphasizes the fact that "signal in a space time is nothing but the least diameter of space time in that field". Space time diameters for all fundamental forces have been calculated in the previous works [7].

Now let us see how these concepts can be interpreted by quantum mechanics.

2.4. Application to Quantum Mechanics

The physical meaning of quantum state has been explained as per film theory of the universe. [11] [17]. As per film theory of the universe, a film is an inertial frame of reference in which every point shows the same clock. But as per absolute velocities and double relativity effect, the points in space time relativistic coordinates will have different Inertial Frames of references (IFRs) and every point is a representation of universal film with a specific time. At the same time there will not exist passage or flow of time with in it. Once the change of film happens, time flows within the film as well as film to film.

Thus in a space time (Minkowski) all the points will have different quantum states and each quantum state is without flow of time. So in that coordinate systems there exist points with constant time but vary with space. All these points describes the position of the point (contains information) in this universe. It describes an object at that point. But due to the fact that it is quantum point, it will not contain space. The combination of all these points provides positions of all points as a single film of the universe. Here the word "Combination" means "superposition". Thus "super position" of all these quantum states termed as a universal film describing a point in quantum space time or quantum coordinate system.

But we can not observe this quantum point since there will not be flow of time until unless goes from one film to another. So it is imaginary only.

This is the point where we have gone much profoundly than the quantum state interpreted mathematically as state vectors [18] and the wave function involved in Schrodinger wave equation [19]. In these mathematical descriptions, flow of time has been included. It is a hidden secret of nature. But when we consider the physical meaning of quantum states at the most fundamental level, a quantum state is a universal film in which time exists but flow of time will not be there. It is a standstill picture of space (further it is explained as information and time in quantum coordinates). Flow of time exists only when a film changes in to another film (in theory it is described by a mechanism of consciousness).

Even Schrödinger wave equation (time dependent or independent) is also inclusive of flow of time. Obviously, since it is a wave, it must be a part of passage of time. But when it is divided further in to films where time will not exist (only space exist), the quantum state described by mathematics has no meaning. Means, even if it is a pure state, it is a mixture of two more states (which are termed as films). There is a hidden theory in between these purest states that involves origin of time and consciousness. This paper tried to provide that insight as a new model of consciousness

Observation and the Reality

Figure 3 represents the transformation to make time to flow. When time flows, imaginary quantum states will be super positioned and form a reality within the film and at the same time film also will be changed. Since it is working with a mechanism to form an internal superposition, film has to be changed. Thus it continues and shows any point in this space time coordinates with a specific special distance (non zero). Thus all the points of object observed as a reality of that object. Figure 3 illustrates that the super positioned quantum states at point q_s in quantum coordinate system will be transformed as a real point p_r in conventional relativistic frame.

Thus interpretation of observation or measurement of quantum states which

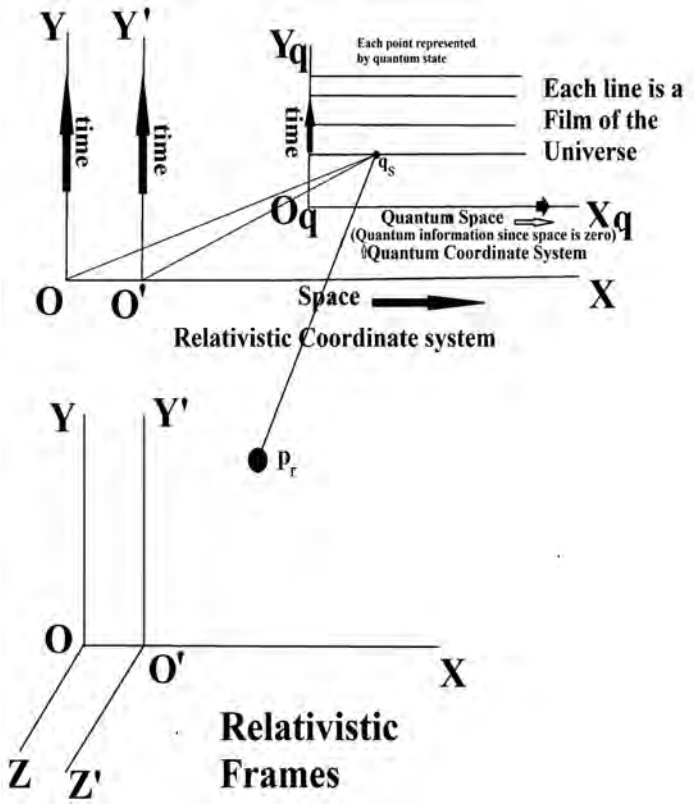

Figure 3. Transformation of quantum coordinate system to relativistic coordinate system in the process of observation. The point q_s in quantum coordinate system will be transformed as the point p_r in conventional relativistic frame as reality.

are not real (imaginary only). The reality exists in transformation through the additional coordinate system called as "quantum coordinate system".

3. Perspective of a New Model of Consciousness

The physics of consciousness has been explained in "new hypothesis on consciousness" [11] elaborately. Actually it is not a hypothesis. It is an analysis of few fundamental queries of philosophy of physics like "why light velocity is constant for all inertial frames of reference?", "how space time originated?", "what is physical entity that makes difference between a living thing and a non living thing?" etc. It has concluded a preliminary model of consciousness integrating all the aspects explained in above sections of this article. It was similar to Orch-OR Theory. But it has refuted the idea of quantum states described by mathematical support. Especially it is contradicting Orch-OR in emphasizing the fact that physical interpretation of quantum state and superposition of states is not relevant at the most fundamental level where time plays an important role. Now in this paper, it was substantiated by introducing quantum coordinate system that was hidden in the conventional transformations. The model has not been questioned much on biological or neurological aspects of the Orch-OR theory. But this paper says that no models or experiments on consciousness can sustain without considering these basics at quantum level.

Let us review the mechanism behind this new model of consciousness (**Figure 4**).

3.1. Mechanism behind This Model

Quantum mechanics interprets a point as space zero (time only will exist) [7].

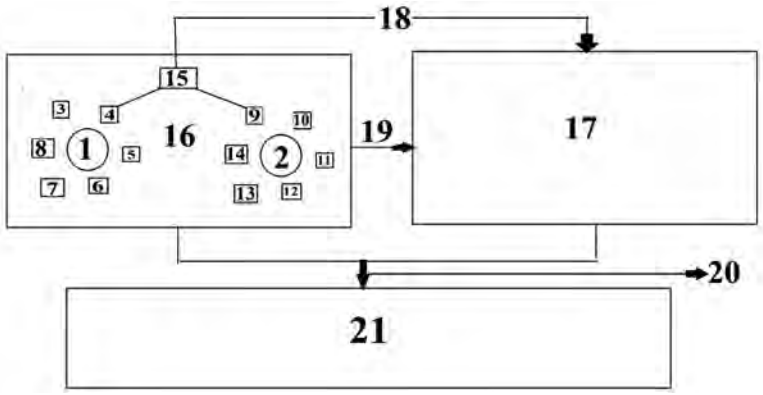

Figure 4. 1 & 2 are separate conscious observers; 3 to 8 are Quantum states associated to observer 1; 9 to 14 are quantum states associated to observer 2; 15 is Super positioned state of one state from observer with one state of observer 2 for example super positioned state of 4 & 9; 16 is Film containing observers 1 & 2; 17 is the change in film 16 as a part of this mechanism; 18 is the Process of mechanism that is to be completed for film change from 16 to 17 (It is the process of super position of 10^{42} quantum states of one observer with one quantum state of another observer); 19 is the Process of mechanism of film change from 16 to 17. It is a consequential and simultaneous process of 18; 20 is the Process indicating Superposition of films 16 & 17; 21 is the Final result, the reality.

A specific time will exist for a specific point. If we interpret this in a quantum coordinate system, specific time will exist for all points on a line parallel to axis denoting space. Thus all the points can be shown with different space on the same line. Line parallel to space coordinate will have different space for each point on that line. But different space does not have a meaning because, according to quantum coordinates there will not exist distance or space. So even though there exist space, it is considered as zero space only. So instead of space coordinates, we can call it as information coordinates. On any parallel line, time will be constant but information will change (in other terms, space changes and the time also changes accordingly). So in order to keep time constant, the excess time will change in to space as per space time equivalence principle. Since space is zero, it will be denoted by change in information). "Zero space" between points means that all these points with different information are super positioned at a specific point. Thus that point is a superposition of all information nothing but superposition of all quantum states.

After overall view of this mechanism, the statement or the postulate that time is information [11] has to be modified as "the quantum of space time is information" according to space time equivalence principle, space and time can be convertible to each other. So to keep time as constant the space has to be converted in to information (information means, it may contain mass like quantities or observables associated to that quantum state). But when we transform it to relativistic coordinates, there will not be zero space point. Whatever small the point is, it contains some diameter. So the super positioned quantum states will be divided to a space and the point will be observed with some diameter. In other words any object can be observed with some length coordinate.

For example, in quantum coordinates, photon is a space zero super positioned quantum state. But in relativistic transformation, it will have space. Since relativity considered it as maximum velocity, as per its basic principle, its space must be zero. Since it is relativistic, it is the space between two divided quantum states. Conscious observer observes it again as super positioned quantum states. This is the final observation called as reality than the observation defined by physics without involvement of consciousness. This is the reality.

In quantum coordinate system "time" and "information" exists and in relativistic system both space and time exist. Means, time converts in to space. Here we have seen that in space time conversion, mass or charge also will be originated. Space time conversion phenomena elaborate it [16].

3.2. Application of Double Relativity Effect to Consciousness

There exists only one signal which is the maximum velocity and whose velocity is constant for all inertial frames in each space time. All fundamental forces will have their own space times and space time diameter can also be calculated [7]. This signal is a point in quantum coordinates with space zero but contains time and information. It will be mathematically represented as quantum state. Since it

is a signal, its velocity is an absolute velocity (velocity is constant for all inertial frames of reference. For example, photon with velocity "c" for our four dimensional universe). Observed velocity is the velocity which can be represented by Lorentz coordinates. As per "double relativity effect", the relation between observed velocity v_o and absolute velocity v_a is $v_o = v_a\gamma$. So the observed velocity "c" will have an absolute velocity as $\frac{c}{\sqrt{2}}$ and $\gamma = \sqrt{2}$ since "c" is the observed velocity follows the equation $v_a\gamma = c$. But without involvement of conscious mechanism as per Figure 2 and Figure 4, one cannot find the reality of the observed velocity. Thus, this observed velocity can be changed as reality as in Figure 5.

Figure 5 explains three instances of observation.

3.2.1. Instance-1

Figure 5(a) shows the phenomena of observation in relativistic coordinates due to "double relativity effect". In that v_a is absolute velocity and v_o is observed velocity and are related by equation

$$v_o = v_a\gamma \tag{1}$$

where

$$\gamma = \frac{1}{\sqrt{1-\left(\frac{v_a}{c}\right)^2}} \tag{2}$$

Figure 5(a) illustrates the "double relativity equation" "$v_o = v_a\gamma$". And the relativistic factor "γ" for conventional relativistic (Galilean or Lorentz coordinates) coordinate system.

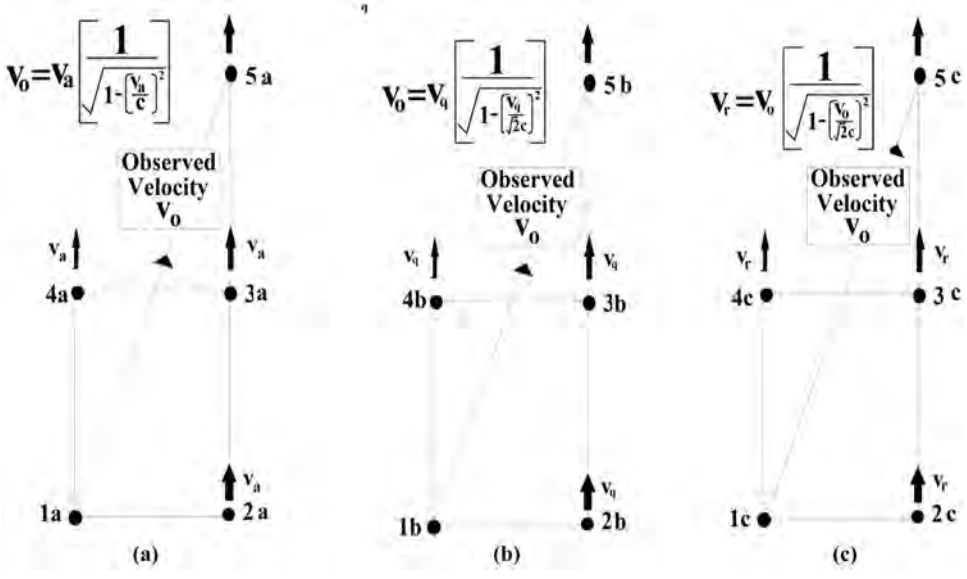

Figure 5. The reality is the consequence of double relativity effect and consciousness on the process of observation. (a) Observation in relativistic coordinates; (b) Observation in Quantum coordinates; (c) Final reality in the process of observation.

3.2.2. Instance-2

The same observation in quantum coordinates has been shown in **Figure 5(b)**. As explained above (Section 2.1) quantum coordinates contains points in space time coordinates with time coordinate only and the space coordinate is always zero. Its quantum particle is "bio force" particle [7] [15] and signal velocity is $\sqrt{2}c$. Thus the same special relativity principle is applied and all the velocities are comparable to that velocity. Here absolute velocity and observed velocity are also related by $v_o = v_a\gamma$ but here $\gamma = \dfrac{1}{\sqrt{1-\left(\dfrac{v_a}{c\sqrt{2}}\right)^2}}$ it represents consciousness frame of super relativity [15]. **Figure 5(b)** shows the quantum coordinates. So the absolute velocity v_a can be replaced with v_q. The same has been explained in **Figure 6** now we can rewrite the quantum relativistic factor $\gamma_q = \dfrac{1}{\sqrt{1-\left(\dfrac{v_q}{c\sqrt{2}}\right)^2}}$

$$\therefore v_o = v_q\gamma_q \tag{3}$$

where

$$\gamma_q = \frac{1}{\sqrt{1-\left(\dfrac{v_q}{c\sqrt{2}}\right)^2}} \tag{4}$$

Figure 5(b) illustrates the "double relativity equation" $v_o = v_q\gamma_q$ and relativistic factor γ_q for quantum coordinate system.

These two instances (instances 1 & 2) are not relevant when we use consciousness mechanism's affect on observation. So the observed velocity in **Figure 5(c)** is a combination of these two instances and the special relativity should not be violated. So the same "double relativity effect" explains it as v_o is observed velocity and it is the reality, where $\gamma_r = \dfrac{1}{\sqrt{1-\left(\dfrac{v_o}{c\sqrt{2}}\right)^2}}$.

$$\therefore v_r = v_o\gamma_r \tag{5}$$

where

$$\gamma_r = \frac{1}{\sqrt{1-\left(\dfrac{v_o}{c\sqrt{2}}\right)^2}} \tag{6}$$

Thus γ_r satisfy both the instances.

Figure 5(c) illustrates the "double relativity equation" "$v_o = v_q\gamma_q$" and relativistic factor "γ_q" as absolute reality due to the affect of consciousness on observation.

This has been elaborated in **Figure 6**. It shows a quantum point with respect to coordinates and its position inside that point. The reality is combination of both.

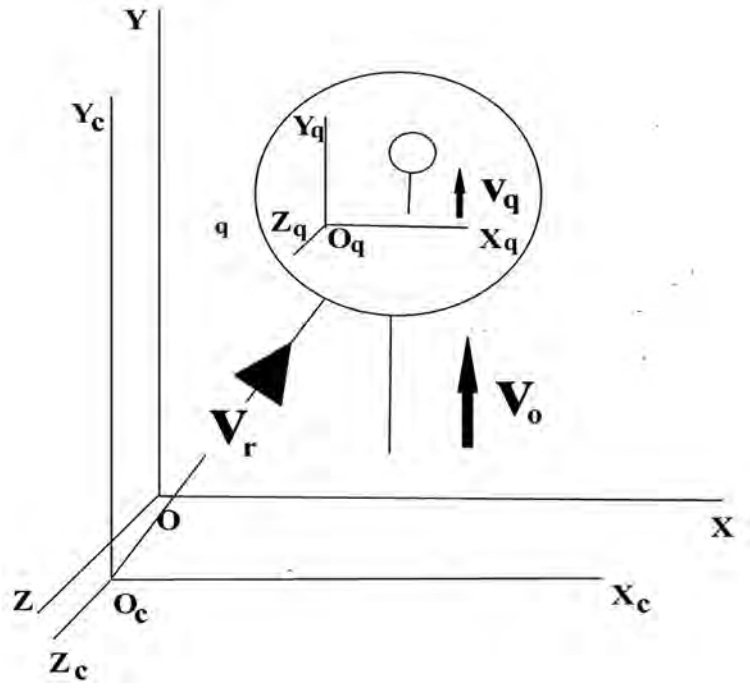

Figure 6. Role of consciousness in relativistic interpretation of quantum point.

With respect to XYZ frame the circle is a point and the space inside is zero. This coordinate system is conventional Lorentz coordinate system obeying special theory of relativity. The velocity shown is v_o. The signal velocity is "c" as it follows special relativity. The same point with respect to the coordinate system $X_qY_qZ_q$ inside circle *i.e.* quantum coordinate system, for which space coordinate is zero for all points. Only time coordinate exist. And the velocity is v_q and follows the equation $v_o = v_q\gamma_q$ where γ_q is according to equation (4). Conscious observer will be in different frame $X_cY_cZ_c$. With reference to conscious observer at origin O_c, the velocity is v_r and follows Equations (5) & (6).

Finally, we can say frame of observation will be affected due to "consciousness" and the frame will be considered as different from observers frame of reference defined in conventional relativistic (Galilean or Lorentz coordinates). Due to "double relativity effect" and "affect of consciousness on observation" the signal velocity expected to become $c\sqrt{2}$ and the relativistic factor will be changed accordingly.

Calculation of this $\sqrt{2}$ is also an important aspect of consciousness which was elaborated in [15]. Now we can emphasize it in simple way.

Simply the logic behind this is.

If the relativity factor for "double relativity effect" and "special relativity" is same, the equation can be written as

$$\gamma = \frac{1}{\sqrt{1-\left(\frac{v_a}{c}\right)^2}}$$

In double relativity effect $v_o = v_a\gamma$ so "c" will be $c\gamma$ since "c" is also absolute velocity. So equation can be written as $\gamma = \frac{1}{\sqrt{1-\left(\frac{v_o}{c}\right)^2}}$. Here signal velocity is $c\gamma$ and observed velocity remains v_o. Therefore we can rewrite the equation as $\gamma = \frac{1}{\sqrt{1-\left(\frac{v_o}{c\gamma}\right)^2}}$.

If we solve it, γ will be $\sqrt{2}$. Now the signal velocity is $c\sqrt{2}$ and the Equations (5) & (6) are applicable.

It is illustrated by **Figure 5(c)** as the reality of observation. Thus the final reality is an overall affect of "double relativity effect" on "consciousness" and observation. **Figure 5** illustrated it. It is not possible to observe these velocities without involvement of consciousness. So the result is a proof for consciousness also.

Finally, in the process of observation, fist the quantum coordinates have to be changed to Lorentz. So double relativity effect must be used. Then these points are compatible with Lorentz coordinates. It is called observation and velocity is observed velocity. This will undergo the process of consciousness mechanism and become reality. So again relativity must be applied with respect to conscious observer. The signal velocity is $c\sqrt{2}$. All velocities must be compared to it. And velocity is observed velocity and follows Equation (5). So this is the final reality for which relativistic factor γ_r follows the Equation (6). This factor is different from Lorentz relativistic factor. Here velocity $v_o \le c\sqrt{2}$. Velocity v_r is the real velocity which is γ_r times than the observed velocity "v_o". Observed velocity is limited to Lorenz coordinates. Real velocity is due to the effect of consciousness on observed velocity. So the consequences like relativistic kinetic energy etc are also different. This result will supersede relevant conclusions of the paper [17] and proposes a profound understanding of the problem. This can be observed by any particle physics laboratory. Specifically these affects can be observed on the observed velocities between $c\sqrt{2}$ to c.

It is not possible to observe these velocities without involvement of consciousness. So the result is a proof for consciousness also.

4. New Perspective on Synchronization of General Relativity with Quantum Mechanics

4.1. Involvement of Concept of Time

Einstein-Hilbert action is a similar approach as a least action principle in which least action is treated as a point in space time and the equation shows a graviton if it converges. Till now it has considered from the point of general relativity. So there are suspicious views of scientists on this approach [20]. Perturbation in basically fixed point is fine at larger distances but quantum mechanically the gravitational interaction is irrelevant [9]. Not only that, the point they considered as least action is not space zero mass zero. In this Cartesian system it must

have some space. Zero space cannot be considered in this system whereas space zero can be considered in quantum system. But when it converts in to space in this coordinate system, it will have space time diameter with a least diameter that converges due to Hilbert action.

4.2. Relevance of Time Operator in Quantum Mechanics

It seems relevant to mention an idea [21] regarding interpretation of "time operator" while discussing these issues. The mathematical methodology the author adopted is good and helpful to develop the conceptual interpretations described in this paper. Otherwise, the author can utilize the theoretical background to interpret the most basic level of quantum state with respect to the involvement of "time operator" proposed by him. The present paper demands the necessity of a Schrödinger equation without a "time operator" or with a zero value. Thus the present paper may lead to an exact and most relevant time independent Schrödinger wave equation to reveal some of the secrets of this nature.

4.3. Relevant to Other Interpretations

Other interpretations like Random discontinuous motion (RDM) interpretation of Quantum Mechanics [22] [23] or "particle interference" rather than wave interference to describe wave function collapse [24] etc. are also must be originated from the conceptual conclusions of the present paper. It elaborates the evolution of time and its involvement in superposition of two time independent quantum states to form space time which is the root cause for the formation of particle or wave.

5. Comparison with Other Models of Consciousness

This model is different from other theories of consciousness in

1) Observation is not for object only. Object is a part of the universal film as a whole at a particular time.

2) Minimum two observers are required to generate one conscious movement of any observer.

5.1. Observer Effect and Necessity of Conscious Observer

On double slit, observer's effect changes the reality. It raised a question on the necessity of conscious observer. Most of the scientists ruled out the point that observer must be conscious [4] [25]. But, as per this paper, observer means conscious observer only. Detector is also part of conscious observer. Instead of detector if we provide conscious observer, that is also not sufficient to accept the affect of conscious observer on observation. The model of consciousness presented in this paper and its mechanism emphasizes on the fact that there must be two conscious observers to observe the physical entities existed in this universe. The transformations of the interactions between quantum states involved in this observation and super position of these states considered as reality which

is more than a simple observation. The change in these interactions with time only will provide wave function and its collapse which turns a particle in to wave and vice versa. So this experiment explains only the measurement problem. It is not connected to consciousness and observation. Two conscious observers must exist to get conscious experience of the effect of observation or reality.

5.2. Refute of the Idea That Consciousness Is Everywhere in This Universe

Few authors are denying the idea that consciousness is attributable to living things only. They are saying that consciousness belongs to whole universe [4] [25] [26] of course there is an argument against it [27] which says that wave function collapsed somewhere and all in one. My paper is supporting that idea and contradicts that consciousness is everywhere. And clearly says that consciousness is for living things only. Because, detector is also part of observation and the conscious observer only can find detector. This can easily understand by double slit experiment. If we provide a detector in between slit and the beam generator, the wave function will be collapsed. If we switch of it, it will not be collapsed. Means, the universal films of observer is a super position of quantum states of the objects signal generator, double slit screen and the detector in the process of signal generation to the screen via slit. It will be collapsed and behaves like a particle if detector is on. If it is switched off, the screen shows interference pattern because the detector finds the reality in to one "eigen state" just like conscious observer. If it is switched off, it is not super positioned as explained for conscious observer. Here there is no observation by conscious observer so when detector switches off, interference pattern occurs. If conscious observer is there in the place of detector, the same results will come. That means, the mechanism is same for a detector as well as conscious observer (Detector itself will not exist without conscious observers). Detector itself is a superposition of lot of quantum states or universal films. So if it is divided in to single states, there will not be existence at all. Again conscious observer is required to create the superposition of quantum states of all the objects and the process.

5.3. This Consciousness Model & the Quantum Eraser Delayed Choice Experiment

One of the outcomes of delayed choice quantum eraser physically means that "the future will change past" Big question is how is it possible?

It is possible only when the observer is conscious and it is completely interlinked with total universe instead of a particular object as explained in the paper [11] where universal film is made up of a loop connecting all the conscious observers only. Non living things or objects are created and experienced by these conscious observers connected in this loop. The loops can be connected from one to another depending upon their time frame. The model elaborated in this paper explains that all the detectors are objects only and they are part of the conscious process generated by conscious observer. So here in this experiment

also all the detectors can be viewed as conscious observers.

Here in this experiment, a photon splits in to a pair of entangled photons. One is delayed than the other. As per this model of consciousness, in the observation of delayed pair of photon, the quantum states super positioned at a point in quantum coordinates and the entangled pair with another point. Quantum coordinates denote a point with time and information. So, for these two pairs the time and information is different. But to observe each pair each observer is required and observer's time is different. If time is different, it cannot be in same film. These two observers must be in the same film if the entangled pair is of one particular photon. Then the process will be continued to next film. So as per this model there is no meaning in "past" and "future" in within these two. Only the "present" exists with combined effect. Whatever change comes to one pair will change another. If we come out of the box of this experiment, whole universe is existed like that. Film of total universe is connected to the loop of conscious observer [11] and the loop will change its connection as per its inertial frame of reference, whenever requires and goes to past films or to future films. It is nothing but time travel. This is the explanation for the question "whether the future will change past?"

5.4. Explanation to Grandfather Paradox by This Model

Grandfather paradox is also an important aspect of "physics of time travel" and "freewill" concepts of philosophy. Few authors [28] elaborated the closed loops of time travel within the scope of existing theories.

According to this model of consciousness,

1) Conscious observer is necessary for the existence of reality of the universe. Reality of the materialistic universe is due to interaction of quantum states of two conscious observers. There may exist lot of films in between these interactions.

2) Two conscious observes create one more conscious observer. There exist several connected films in a sequential order which obey cause and effect law of physics. So any of these two conscious observes erased by any reason before creation of the new conscious observer, the interlinked sequential order of the films will be erased and new conscious observer will be erased. There exist lot of other quantum states of this erased conscious observer but they are all imaginary only since reality requires a devise like brain or a centralized network connecting all. There are lot of films in between interaction of two observers to create a conscious observer with such devise. Without such devise, the interactions are not realistic. So to form this erased observer in to reality there must exist interaction which creates this devise otherwise the connective reality will be erased with the new observer.

3) If it is applied to grandfather paradox. If a grandson of a grandfather goes to past and kills his grandfather, he will also be vanished since the connective films after the death of grandfather will be erased from reality. Grandson is also

part of that reality. Now both the devises grandfather and grandson are compatible to each other. So grandson vanished. Compatible means both are in reality. Above model says that only one reality exists. If one more reality with one more devise exist, both cannot be compatible. All other are imaginary only. Thus the time travel will work out within the compatible devises or one reality only. Thus, if devises are not vanished because of each other, time travel is possible by regulating their devise. Only present will exist for that devise and it is the only reality. For others it may be viewed as past and present. Grandson can change all materialistic things in future and present but it cannot change the interaction of conscious observers who are reason for his birth.

4) With reference to new hypothesis [11] consciousness is a circuit or a loop connecting to conscious observers only [Refer fig. 7 Page no.39]. Here in this paper it is substantiated as reality. So one observer may connect to another observer in so many ways. New observers in this circuit can also be created due to interaction of two observers. Thus a new circuit can also be created like branches from original and sub branches to main branches. In this if any of the main branch erases, all the sub branches will also be erased. Thus in grandfather paradox, grandfather is the main branch and sub branches are father and mother. Grand son is sub branch to father and mother. Here if he kill his grandfather, whatever may be other connections of the grandson, all the connected branches to his grandfather will be erased. And the grandson and his all other connections will be erased.

5) But in some theories it is told that grandson is a copy of the original went to past and other alternate of the universe will be started after killing of grandfather. But here it is only one reality and connects only to conscious observers. without conscious observers the universe will not exist.

6) Thus films with zero time and infinite time are not possible .In between so many films will exist. Finally two conscious states are must to create reality. Thus, those two conscious observers are eternal whatever may be their time frame is. Other conscious observers are created from them. Materialistic creation is due to the interaction of these conscious observers only.

7) Devise and regulators are important for consciousness.

8) Two conscious observers created this space time. At that stage they might have a separate device than us. Later they created several conscious observers with different devises.

9) Now we have a devise called brain and it will have a regulator. If we go back to past, when we have not born, the devise will not be there. So everything connected to this devise will be lost. Devise connection is reality, means, through devise only we can see reality.

10) So we cannot go to future where we will not exist (our consciousness will not exist) and cannot go to past where we have not created (born).

11) Devise will have reality. Reality will have past and future. Another devise is required to see beyond us. So for one devise, the universe will not exist but

universe will exist for other devises.

12) Totally universe exists always as it is with quantum information. Its superposition is time.

13) We will see the universe through devise in a streamlined way otherwise that is only haphazardly distributed information and time only. Since there will not be space it is a simple point from where the time emerges.

14) So if we kill our grandfather in past we will not exist. We will be vanished and universe also will not exist simply it is nothing not even a space.

6. Conclusions

1) The word "observation" of physics has been redefined and it is emphasized on the fact that observation is attributed to Lorentz coordinates only. Till now physics says that "observation" and "measurement" in these conventional coordinates are taken granted as reality. But actual reality is different from this observation. Quantum mechanics is not reality. It remains imaginary until unless it converts into relativistic coordinates. Simply applying relativity to quantum mechanics as in the case of "relativistic quantum mechanics" is not relevant. The physical meaning of quantum states is connected to the problem of time and formation of space time. So the involvement of consciousness is unavoidable in observation or measurement. Thus the imaginary quantum states first have to be interpreted in terms of conventional coordinate system. Prior to transforming these quantum states into conventional coordinate system, "double relativity effect" is to be applied. Due to the application of double relativity effect the observation changes and the reality will be different from observation. The ultimate result says that factor Lorentz relativistic factor "γ" has to be modified as $\gamma_r = \frac{1}{\sqrt{1-\left(\frac{v_o}{c\sqrt{2}}\right)^2}}$. So the observables will be modified than the results of special theory of relativity and the results will be different within the range of velocities $c\sqrt{2}$ to "c". This is can be verified in any laboratory.

2) Application of this concept may provide new path to researchers working on velocities more than that of light and the affect of drastic change in momentum on Einstein's field equations towards singularity. The synchronization of quantum mechanics and relativity applied in this paper indicates that General Relativity equations may be applicable to lower diameters comparable to Planck length up to zero space.

3) A new model of consciousness has been proposed by emphasizing the fact that conscious observer plays an important role in observation. It also proposed that there must exist minimum two conscious observers to find the reality. It explains the concept of origin of time and formation of space time and its curvature at the basic level (in other terms its quantum level). Thus it explains the synchronization between quantum mechanics and relativity.

4) Totally it concludes a major change in observation and reality which can be

observed in any lab. Thus if it is proved experimentally, it will be the best proof for this model of consciousness.

Conflicts of Interest

The author declares no conflicts of interest regarding the publication of this paper.

References

[1] Casado, C.M.M. (2008) *Latin-American Journal of Physics Education*, **2**, 152. http://www.journal.lapen.org.mx,p-152

[2] Deutsch, D. (1985) *International Journal of Theoretical Physics*, **24**, 1-41. https://link.springer.com/article/10.1007/BF00670071 https://doi.org/10.1007/BF00670071

[3] Fields, C. (2012) *Information*, **3**, 92-123. https://doi.org/10.3390/info3010092

[4] Yu, S. and Nikoli, D. (2010) Quantum Mechanics Needs No Consciousness (and the Other Way Around). https://arxiv.org/pdf/1009.2404.pdf

[5] Schlosshauer, M., Koer, J. and Zeilinger, A. (2013) A Snapshot of Foundational Attitudes toward Quantum Mechanics. https://arxiv.org/pdf/1301.1069.pdf

[6] Sinha, K.P., Sivaram, C. and Sudarshan, E.C.G. (1976) *Foundations of Physics*, **6**, 65-70. https://link.springer.com/article/10.1007/BF00708664 https://doi.org/10.1007/BF00708664

[7] Kodukula, S.P. (2019) *Journal of Modern Physics*, **10**, 466-476. https://doi.org/10.4236/jmp.2019.104032

[8] Carlip, S. (2001) Quantum Gravity: A Progress Report. https://arxiv.org/pdf/gr-qc/0108040.pdf

[9] Shomer, A. (2007) A Pedagogical Explanation for the Non-Renormalizability of Gravity. https://arxiv.org/pdf/0709.3555.pdf

[10] Hameroff, S. and Penrose, R. (2014) *Physics of Life Reviews*, **11**, 39-78, 41, 48, 49, 59. https://doi.org/10.1016/j.plrev.2013.08.002

[11] Kodukula, S.P. (2019) *International Journal of Physics*, **7**, 31-43. http://pubs.sciepub.com/ijp/7/2/1

[12] Mihelic, F.M. (2019) Experimental Evidence Supportive of the Quantum DNA Model. *Proceedings SPIE, Quantum Information Science, Sensing, and Computation XI*, Vol. 10984, 1098404. https://doi.org/10.1117/12.2517348

[13] Kodukula, S.P. (2009) Double Relativity Effect & Film Theory of the Universe. Lulu.com, Raleigh, 5-6, 7-12, 13-32.

[14] Kodukula, S.P. (2009) Heart of the God with Grand Proof Equation—A Classical Approach to Quantum Theory. Lulu.com, Raleigh.

[15] Kodukula, S.P. (2014) *American Journal of Modern Physics*, **3**, 232-239. http://article.sciencepublishinggroup.com/pdf/10.11648.j.ajmp.20140306.15.pdf https://doi.org/10.11648/j.ajmp.20140306.15

[16] Kodukula, S.P. (2021) *Journal of High Energy Physics, Gravitation and Cosmology*, **7**, 1333-1352. https://doi.org/10.4236/jhepgc.2021.74083

[17] Kodukula, S.P. (2017) *International Journal of Physics*, **5**, 99-109. http://pubs.sciepub.com/ijp/5/4/1

[18] Weinberg, S. (2012) Collapse of the State Vector. https://arxiv.org/pdf/1109.6462.pdf

[19] Schrodinger, E. (1926) *The Physical Review*, **28**, 1049-1070. https://journals.aps.org/pr/pdf/10.1103/PhysRev.28.1049 https://doi.org/10.1103/PhysRev.28.1049

[20] Padmanabhan, T. (2008) *International Journal of Modern Physics D*, **17**, 367-398. https://doi.org/10.1142/S0218271808012085

[21] Routh, A.K. (2019) *Open Access Library Journal*, **6**, e5816. https://doi.org/10.4236/oalib.1105816

[22] Gao, S. (2020) *Foundations of Physics*, **50**, 1541-1553. https://doi.org/10.1007/s10701-020-00390-0

[23] Wechsler, S.D. (2021) *Journal of Quantum Information Science*, **11**, 99-111. https://doi.org/10.4236/jqis.2021.113008

[24] Niehaus, A. (2019) *Journal of Modern Physics*, **10**, 423-431. https://doi.org/10.4236/jmp.2019.104027

[25] De Barros, J.A. and Oas, G. (2017) *Foundations of Physics*, **47**, 1294-1308. https://doi.org/10.1007/s10701-017-0110-7

[26] Tononi, G. and Koch, C. (2015) *Philosophical Transactions of the Royal Society B*, **370**, Article ID: 20140167. https://doi.org/10.1098/rstb.2014.0167

[27] Reason, C.M. (2017) Comment on the Paper Quantum Mechanics Needs No Consciousness by Yu and Nikolic (2011). https://arxiv.org/abs/1707.01346

[28] Lobo, F. and Crawford, P. (2003) Time, Closed Time like Curves and Causality. https://arxiv.org/pdf/gr-qc/0206078.pdf

Journal of Modern Physics, 2021, 12, 1656-1707
https://www.scirp.org/journal/jmp
ISSN Online: 2153-120X
ISSN Print: 2153-1196

A New Physics Would Explain What Looks Like an Irreconcilable Tension between the Values of Hubble Constants and Allows H_0 to Be Calculated Theoretically Several Ways

Claude Mercier

Independent Researcher, Baie-Comeau, Canada
Email: claude.mercier@cima.ca

How to cite this paper: Mercier, C. (2021) A New Physics Would Explain What Looks Like an Irreconcilable Tension between the Values of Hubble Constants and Allows H_0 to Be Calculated Theoretically Several Ways. *Journal of Modern Physics*, **12**, 1656-1707.
https://doi.org/10.4236/jmp.2021.1212098

Received: September 1, 2021
Accepted: October 23, 2021
Published: October 26, 2021

Abstract

Observing galaxies receding from each other, Hubble found the universe's expansion in 1929. His law that gives the receding speed as a function of distance implies a factor called Hubble constant H_0. We want to validate our theoretical value of $H_0 \approx 72.09548580(32)$ km·s^{-1}·MParsec^{-1} with a new cosmological model found in 2019. This model predicts what may look like two possible values of H_0. According to this model, the correct equation of the apparent age of the universe gives ~ 14.14 billion years. In approximation, we get the well-known equation $1/H_0 \approx 13.56$ billion years. When we force these ages to fit the $1/H_0$ formula, it gives two different Hubble constant values of ~69.2 and 72.1 km·s^{-1}·MParsec^{-1}. When we apply a theoretical correction factor of $\eta \approx 1.042516951$ on the first value, both target the second one. We found 42 equations of H_0 linking different physics constants. Some are used to measure H_0 as a function of the average temperature T of the Cosmological Microwave Background and the universal gravitational constant G:

$H_0 \approx 72.06(90)$ km·s^{-1}·MParsec^{-1} from T by Cobra probe & Equation (16)
$H_0 \approx 71.95(50)$ km·s^{-1}·MParsec^{-1} from T by Partridge & Equation (16)
$H_0 \approx 72.086(36)$ km·s^{-1}·MParsec^{-1} from G & Equation (34)
$H_0 \approx 72.105(36)$ km·s^{-1}·MParsec^{-1} from G & Equations (74), (75), or (76).

With 508 published values, $H_0 \approx 72.0957 \pm 0.33$ km·s^{-1}·MParsec^{-1} seems to be the "ideal" statistical result. It validates our model and our theoretical H_0 value which are useful to find various interactions with the different constants. Our model also explains the ambiguity between the different universe's age measurements and seems to unlock a tension between two H_0 values.

Keywords

Hubble Constant H_0, Hubble Tension, Age of the Universe

1. Introduction

In astrophysics, the Hubble constant H_0 [1] is a parameter to analyze the universe. Nevertheless, it is also one of the lesser-known values.

In 1916, Einstein found the general relativity laws [2]. His equations expect that the universe is either expanding or in a Big Crunch. He could have been the first to predict the universe's expansion, but influenced by the popular idea, Einstein forced his model to be static with a cosmological constant Λ. In 1922, Friedmann showed from relativity that the universe expands at a calculable rate [3]. In 1927, Georges Lemaitre published independent research [4], giving what is now known as Hubble's law. In 1929, Hubble discovered the universe's expansion [1]. Equation (1) gives Hubble's law, with v being the receding speed in km·s^{-1}, D being the distance between the observed object and the observer, and H_0 being the Hubble constant. He measured about $H_0 \approx 500$ km·s^{-1}·MParsec^{-1}. His high value was due to a wrong calibration of the cepheids used to evaluate distances. Hubble's law was correct, but H_0 was remaining to be found with accuracy.

$$v = DH_0 \tag{1}$$

Physicists get H_0 based on far cosmic objects (Cepheids, supernovae, red giants, etc.) or local measurements (CMB, universal gravitational constant G, etc.). Including error margins of published values (see the software in **Annex A**), H_0 is between 19 to 174 km·s^{-1}·MParsec^{-1}. However, two values are often measured ~69.2 and ~72.1 km·s^{-1}·MParsec^{-1}. An irreconcilable tension between some H_0 values shows up [5]. Even with good accuracies, their error margins do not always overlap. It may let us think that only one of these values is right. No one considered it possible that both values may be in some way correct.

In 2019, we wrote an article [6] explaining what may look like two values for H_0. We calculated the universe age, obtained a result of complex type, and an apparent age of the universe of ~14.4 billion years. The complete equation may be approximated by $1/H_0$, giving ~13.56 billion years. We notice that there is a difference of ~4.25% between the approximated and the non-approximated values.

Cosmologists use $1/H_0$ to calculate the universe's age. Thus, if we could measure the apparent age of the universe with no approximation, we would conclude wrongly that the Hubble constant is 4.25% lower than it should be.

We hypothesize that two values of H_0 are somehow obtained from an approximated and non-approximated equation of the apparent age of the universe. The confusion leads to a tension between two values when there should be only one.

We summarize our cosmological model [6] to get H_0 as a function of a, c, and r_c. We found ways to measure H_0 locally by using the Cosmological Microwave Background (CMB) temperature T and by using the universal gravitational constant G [6] [7]. Based on our model, we found a theoretical equation to calculate H_0 from CODATA values (Committee of Data for Science and Technology) [8].

$$H_0 = \frac{c\alpha^{19}\sqrt{\beta}}{r_e} \approx 72.09548580(32)\times 10^{53}\ \mathrm{km\cdot s^{-1}\cdot MParsec^{-1}} \quad (2)$$

where $\beta = 3-\sqrt{5} \approx 0.76$

We want to validate this theoretical value of H_0 and highlight the tension between two measured values of H_0. We list the results of the most recent measures of H_0 and build a graph showing someway the popularity of each H_0 value range.

We list 42 H_0 equations. Certain overcome the difficulties to do experimental measurements. We use one of them as a third measurement of H_0. Our cosmological model shows that H_0 and the speed of light are not constant.

2. Physics Parameters

A compact form of notation is used to display tolerances (*i.e.*, 2.734(10) K means 2.734 ± 0.010 K). The CODATA 2014 [8] is used to compare the results of our new equations with the articles published in 2019 and 2020.

Light speed in a vacuum	$c = 299792458\ \mathrm{m\cdot s^{-1}}$
Permeability of free space	$\mu_0 \approx 4\pi\times 10^{-7}\ \mathrm{NA^{-2}}$
Permittivity of free space	$\varepsilon_0 \approx 8.854187817\times 10^{-12}\ \mathrm{F\cdot m^{-1}}$
Universal gravitational constant	$G \approx 6.67408(31)\times 10^{-11}\ \mathrm{m^3\cdot kg^{-1}\cdot s^{-2}}$
Electron rest mass	$m_e \approx 9.10938356(11)\times 10^{-31}\ \mathrm{kg}$
Classical electron radius	$r_e \approx 2.8179403227(19)\times 10^{-15}\ \mathrm{m}$
Electron charge	$q_e \approx -1.6021766208(98)\times 10^{-19}\ \mathrm{C}$
Planck length	$L_p \approx 1.616229(38)\times 10^{-35}\ \mathrm{m}$
Planck time	$t_p \approx 5.39116(13)\times 10^{-44}\ \mathrm{s}$
Planck mass	$m_p \approx 2.176470(51)\times 10^{-8}\ \mathrm{kg}$
Planck constant	$h \approx 6.626070040(81)\times 10^{-34}\ \mathrm{J\cdot s}$
Fine-structure constant	$\alpha \approx 7.2973525664(17)\times 10^{-3}$
Boltzmann constant	$k_b \approx 1.38064852(79)\times 10^{-23}\ \mathrm{J\cdot K^{-1}}$
Rydberg constant	$R_\infty \approx 10973731.568508(65)\ \mathrm{m^{-1}}$

3. Summary of our Theory

Our theory is based on a cosmological model officially shown in 2019 [6], but it summarizes papers we wrote at www.pragtec.com/physique since 2011. First, we outline some main milestones as we did in 2020 [7].

3.1. Our Cosmological Model

We hypothesize that there was one expanding sphere containing all matter at the Big Bang. There was no light. After ~360000 years [9], electrons became free to move because of a lower density universe, and the light appeared and began to travel through space, creating a 4-D expanding sphere called the "luminous universe". As the matter cannot travel as fast as light [10], it created a smaller 4-D expanding sphere, the "material universe", imbricated in the "luminous universe".

Einstein found that the presence of a massive object reduces the speed of light v_L [11]. Schwarzschild calculated v_L in a context of a weak gravitational field Φ using general relativity [12]. With $|\Phi| << c^2$ around a spherical mass, Equation (3) gives v_L as a function of c and a local refractive index n_0 (function of G [13]).

$$v_L(r) = \frac{c}{n_0} \text{ where } n_0 = \sqrt{\frac{1-2\Phi/c^2}{1+2\Phi/c^2}} \text{ and } \Phi = \frac{-Gm}{r} \le 0 \tag{3}$$

From an observer on Earth, c seems constant. However, the knowledge of a precise value of c dates only from 19 century [14]. In 1929, Edwin Hubble found that the universe is expanding [1]. As the apparent universe radius increases, the density of this latest must decrease over time, causing the refractive index of the vacuum to drop. As a result, it causes light to accelerate slowly.

In Equation (3), c is the local speed limit for light in a vacuum in our universe area. Admitting that light accelerates while the universe expands, it will tend towards another asymptotical speed limit k affected by a local refractive index n. For now, k is unknown. Let us build Equation (4), which is analog to Equation (3) for the universe [2]. Our universe parcel is at a distance r_u from the universe's apparent mass center m_u. The local speed of light c results from Equation (4).

$$c = \frac{k}{n} \text{ where } n = \sqrt{\frac{1-2\Theta/k^2}{1+2\Theta/k^2}} \text{ and } \Theta = \frac{-Gm_u}{r_u} \le 0 \tag{4}$$

Similarly to r_u, the R_u value is the apparent radius of curvature of the luminous universe [6] [15] (also called Hubble radius [16]). It is a function of c and H_0. It is "apparent" since Equation (5) assumes c constant for a time equal to the universe's age. Now, its speed is c, but it is not constant in our model [6]. It was lower in the past and will increase while the universe expands. The H_0 value represents the expansion rate of the material universe in km·s^{-1}·MParsec^{-1} [1]. It is the local derivative of the velocity of matter v_m with respect to the element of distance dr.

$$H_0 = \left.\frac{\mathrm{d}v_m}{\mathrm{d}r}\right|_{r=r_u} = \frac{\beta c}{r_u} = \frac{\beta c}{\beta R_u} \Rightarrow R_u = \frac{c}{H_0} \tag{5}$$

Locally, at a distance $r = r_u$, matter recedes radially from the center of mass of the universe at a rate β times slower than the speed of light c.

$$r_u = \beta R_u = \frac{\beta c}{H_0} \tag{6}$$

The apparent mass m_u of the universe is given by Equation (7) [15] [17]:

$$m_u = \frac{c^3}{GH_0} = \frac{R_u c^2}{G} \tag{7}$$

Our universe parcel is at a distance r_u from the center of the mass m_u. It travels at a speed v_m relative to this latest. The ratio β is the asymptotical speed of light k in a vacuum (when R_u tends towards infinity) influenced by a refractive

index n that is itself influenced by a gravitational potential Θ.

$$v_m = \frac{\beta k}{n} \text{ where } n = \sqrt{\frac{1-2\Theta/k^2}{1+2\Theta/k^2}} \text{ and } \Theta = \frac{-Gm_u}{r_u} \tag{8}$$

Hubble measured H_0 from the global movement of galaxies at our location [1], at r_u. They have their own movement. As the universe expands, they are generally moving away from each other. The derivative of the material universe speed v_m according to the element of distance dr evaluated at $r = r_u$ is H_0 [6].

$$H_0 = \left.\frac{\mathrm{d}v_m}{\mathrm{d}r}\right|_{r=r_u} = \frac{k\beta y}{r_u}\left(\frac{1}{(1+y)\sqrt{1-y^2}}\right) \text{ where } y = \frac{2Gm_u}{k^2 r_u} \tag{9}$$

Solving Equations (4) to (7), and (9) gives Equations (10) to (14) [6]. The expending speed ratio β between the material and the luminous universes is geometric. It is also the ratio between r_u and R_u. It is unique to our model and essential to depict many constants and make links between the infinitely large and small in the Dirac hypothesis on large numbers [18] [19].

$$k = c\sqrt{2+\sqrt{5}} \approx 6.17\times10^8 \text{ m}\cdot\text{s}^{-1} \tag{10}$$

$$\beta = 3-\sqrt{5} \approx 0.764 \tag{11}$$

$$R_u \approx 1.28\times10^{26} \text{ m} \tag{12}$$

$$r_u \approx 9.80\times10^{25} \text{ m} \tag{13}$$

$$m_u \approx 1.73\times10^{53} \text{ kg} \tag{14}$$

3.2. Our First Method to Measure H_0 as a Function of T (from CMB)

The accuracies of m_u, r_u, and R_u widely depend on H_0 which could be between 19 and 174 km·s^{-1}·MParsec^{-1} (listed in the software in **Annex A**). Therefore, a better method of measuring H_0 is required to know m_u, r_u, and R_u more accurately.

We calculated the CMB temperature T as a function of H_0 and G [6]. This equation considers the universe as an ideal black body since it would absorb any incident radiation coming from outside, and it does not reflect or transmit any form of energy outside of the luminous universe (since it expands at the speed of light).

$$T = \frac{\beta}{k_b}\left(\frac{15\alpha^2 h^3 c^5 H_0^2}{8\pi^6 G}\right)^{1/4} \tag{15}$$

Let us isolate H_0 from Equation (15). The accuracy mainly depends on the CMB temperature T. Using $T \approx 2.736(17)$ K (from Cobra probe [20]), we get.

$$H_0(T) = \frac{\pi^3 T^2 k_b^2}{\beta^2 \alpha}\sqrt{\frac{8G}{15c^5 h^3}} \approx 72.06(90) \text{ km}\cdot\text{s}^{-1}\cdot\text{MParsec}^{-1} \tag{16}$$

with Partridge $T \approx 2.734(10)$ K, and $H_0 \approx 71.95(50)$ km·s^{-1}·MParsec^{-1} [21]. As the least accurate value is T, Equation (16) measures H_0 from the CMB temperature. These values lead to new links and are in our software in **Annex A**.

3.3. Dirac Hypothesis about Large Numbers

Dirac found (inaccurately) that large numbers come into a few orders of magnitude with same dimensions quantities ratios [18] [19]. All ratios come from N, via certain factors [22]. It represents the maximum number of photons in the universe. We get the highest number when the associated mass m_{ph} of a photon is the smallest. This happens when the energy of the photons is at its lowest and with a wavelength of the same length as the circumference of the luminous universe (*i.e.*, $2\pi R_u$) [6]. Let us calculate m_{ph} by equating its corpuscular and wave energies.

$$m_{ph}c^2 = \frac{hc}{2\pi R_u} \quad \Rightarrow \quad m_{ph} = \frac{h}{2\pi R_u c} \approx 2.74\times10^{-69} \text{ kg} \tag{17}$$

We get N by dividing the apparent mass m_u of the universe (Equation (7)) by the mass m_{ph} associated with a photon of $2\pi R_u$ wavelength (Equation (17)).

$$N = \frac{m_u}{m_{ph}} = \frac{2\pi c^5}{hGH_0^2} \approx 6.3018(62)\times10^{121} \tag{18}$$

If we try to make a precise evaluation of N by using the Equations (6), (7), (16), and (17), we obtain Equation (19) which is dependent mainly on T. We evaluate the result by using the CODATA 2014 [8] and the average CMB temperature from Cobra probe [20]. Finally, we note that N is dimensionless as α.

$$N = \frac{15h^2\alpha^2\beta^4c^{10}}{4\pi^5G^2k_b^4T^4} \approx 6.31(15)\times10^{121} \tag{19}$$

Assuming α used as a scale factor applied a few times, we postulate Equation (20). It seems impossible to get this equation from standard physics [2].

$$\text{POSTULATE \#1:} \qquad N = 1/\alpha^{57} \approx 6.303419702(84)\times10^{121} \tag{20}$$

In the next formulas, Planck temperature is $T_p \approx 1.42 \times 10^{32}$ K. This is the highest temperature reached at the Big Bang. It happens when we put the entire mass m_u in a point-like pellet of Planck length radius L_p. Planck charge is given by $q_p \approx 1.88 \times 10^{-18}$ C.

"Large" numbers are obtained with N exponent a fraction, such as $N^{1/2}$, $N^{1/3}$, $N^{1/4}$, … $N^{1/57}$, etc. We get these in different ways by using various parameters of the universe [2]. They are always unitless. Some come from Dirac's hypothesis on large numbers [18] [19]. Some links will be used later [6].

$$N^{2/3} = \frac{m_u\alpha}{m_e\beta^{1/2}} = \frac{R_u^2\beta}{r_e^2} = \frac{m_p^4\alpha^4}{m_e^4\beta^2} = \frac{m_e^2\beta}{m_{ph}^2\alpha^2} \approx 1.58\times10^{81} \tag{21}$$

$$N^{1/2} = \frac{m_p}{m_{ph}} = \frac{R_u}{L_p} = \frac{1}{t_pH_0} = \frac{2\pi T_pk_b}{hH_0} = \frac{-1}{q_e}\sqrt{\frac{4\pi m_uR_u\alpha}{\mu_0}} \approx 7.94\times10^{60} \tag{22}$$

$$N^{1/3} = \frac{m_ur_e\alpha}{m_eR_u\beta} = \frac{m_e\sqrt{\beta}}{m_{ph}\alpha} = \frac{R_u\sqrt{\beta}}{r_e} = \frac{\alpha q_e^2}{4\pi\varepsilon_0G\beta m_e^2} \approx 3.99\times10^{40} \tag{23}$$

$$N^{1/4} = \frac{T_p}{T}\left(\frac{15\beta^4\alpha^2}{\pi^3}\right)^{1/4} = \frac{k_bT}{m_{ph}c^2}\left(\frac{\pi^3}{15\beta^4\alpha^2}\right)^{1/4} \approx 2.82\times10^{30} \tag{24}$$

$$N^{1/6} = \frac{r_e}{L_p\sqrt{\beta}} = \frac{m_p\alpha}{m_e\sqrt{\beta}} = \frac{\alpha^3}{4\pi R_\infty L_p\sqrt{\beta}} = \frac{2\pi r_e k_b T_p}{hc\sqrt{\beta}} \approx 1.99\times10^{20} \quad (25)$$

$$N^{1/16} = \left(\frac{4\pi cR_\infty\sqrt{\beta}}{H_0}\right)^{57/256} = \left(\frac{\beta T_p}{T}\right)^{1/4}\left(\frac{15\alpha^2}{\pi^3}\right)^{1/16} \approx 4.10\times10^{7} \quad (26)$$

$$N^{1/19} = \frac{1}{4\pi R_\infty r_e} = \left(\frac{\beta m_e^2}{m_{ph}^2}\right)^{1/12} = 16\pi^2\beta L_p R_u R_\infty^2\sqrt{\alpha} \approx 2.57\times10^{6} \quad (27)$$

$$N^{1/57} = \frac{q_p^2}{q_e^2} = \left(\frac{m_p^2}{m_e^2\beta}\right)^{1/21} = \left(\frac{q_e^2}{4\pi\beta\varepsilon_0 G m_e^2}\right)^{1/20} = \frac{1}{\alpha} \approx 137 \quad (28)$$

In a non-published document [22], we show over 150 links that give N with various parameters. The universe is well-linked between the infinitely large and the infinitely small. Almost everything changes while the universe is expanding.

3.4. Precise Calculation of H_0

Unlike Equation (16), we look for an equation that does not use G and T to get H_0 since they do not have good accuracies. Usually, G intervenes in the calculations of gravitational force and energy. Without any details (see [6] [7]), let us calculate the electrical energy E_e between two electrons separated by a space equal to the classical electron radius r_e. The electrical energy E_e is not linked to the distance since we get $E_e = m_e c^2$. We evaluate the gravitational energy for the same conditions, finding $E_g = Gm_e^2/r_e$. If these experiments are done at the luminous universe periphery, we get an electrical energy $E_e' = E_e$ and a gravitational energy $E_g' = E_g/\beta$. The ratio between E_e' and E_g' gives Equation (29).

$$\frac{E_e'}{E_g'} = \frac{m_e c^2}{\left(\frac{Gm_e^2\beta}{r_e}\right)} = \frac{c^2 r_e}{Gm_e\beta} \approx 5.45\times10^{42} \quad (29)$$

As in Equation (20), we realize that the fine-structure constant α plays a role in determining orders of magnitude. By adjusting the exponent of the fine-structure constant α, we obtain a result identical to Equation (29).

$$\frac{1}{\alpha^{20}} \approx 5.45\times10^{42} \quad (30)$$

Equations (29) and (30) seam equal. By isolating G, we get an equation that becomes postulate #2. We cannot deduce this equation from standard physics.

$$\text{POSTULATE \#2:}\quad G = \frac{c^2 r_e \alpha^{20}}{m_e\beta} \approx 6.673229809(86)\times10^{-11}\ \mathrm{m^3\cdot kg^{-1}\cdot s^{-2}} \quad (31)$$

$$\text{w here } \beta = 3-\sqrt{5}$$

We associate the wave energy with the energy of the electron mass m_e.

$$m_e c^2 = \frac{hc\alpha}{2\pi r_e} \quad (32)$$

with Equations (20), (31), and (32), we get Equation (33).

$$H_0 = \frac{c\alpha^{19}\sqrt{\beta}}{r_e} \approx 72.09548580(32)\ \text{km}\cdot\text{s}^{-1}\cdot\text{MParsec}^{-1} \tag{33}$$

This value is like Soltis with 72.1 ± 2.0 km·s^{-1}·MParsec^{-1}, Murtinelli's with $72.1^{+2.1}_{-1.8}$ km·s^{-1}·MParsec^{-1}, and Salvatelli's with $72.1^{+3.2}_{-2.3}$ km·s^{-1}·MParsec^{-1} (see the list of value in our software in **Annex A**). Our theoretical value seems to make sense.

3.5. Our Second Method to Measure H_0 as a Function of G

We want to find a second way to measure H_0 as a function of G. We must use accurate parameters, such as α and the characteristics of the electron (m_e and r_e). We look for an equation dependent on G without any rational exponent that reduces the sensitivity. We can use Equations (31) and (33). From each of them, we isolate r_e, and we make both equal to get H_0. Since G is the least precise value, Equation (34) evaluates H_0 as a function of G. We used CODATA 2014 values.

$$H_0 = \frac{c^3\alpha^{39}}{Gm_e\sqrt{\beta}} \approx 72.086(36)\ \text{km}\cdot\text{s}^{-1}\cdot\text{MParsec}^{-1} \tag{34}$$

This result is about 25 times more precise than Equation (16) that uses the average CMB temperature T. We included this result in our software in **Annex A**.

4. Hubble Constant versus the Age of the Universe

We calculate the universe's age with our cosmological model to understand what seems to be two potential values of H_0. We measure H_0 by observing cosmological objects. Universe's age Δt_u is of complex type and results from the integral of the inverse of the expanding speed of the material universe v_m with the element of distance dr evaluated between the universe's center of mass (at $r = 0$) and the apparent material universe radius of curvature at our location r_u.

$$\Delta t_u = \int_{r=0}^{r=r_u} \frac{1}{v_m(r)}\,\mathrm{d}r = \Delta t_{hu} + \Delta t_{0h} \tag{35}$$

The Δt_{hu} is the time elapsed between the horizon ($r = r_h$) and here ($r = r_u$):

$$\Delta t_{hu} = \int_{r=r_h}^{r=r_u} \frac{1}{v_m(r)}\,\mathrm{d}r \quad (\text{Real type result}) \tag{36}$$

The Δt_{0h} is the elapsed time between $r = 0$ and the horizon $r = r_h$:

$$\Delta t_{0h} = \int_{r=0}^{r=r_h} \frac{1}{v_m(r)}\,\mathrm{d}r \quad (\text{Imaginary type result}) \tag{37}$$

At the universe horizon $r = r_h$, the speed of light is zero. We cannot see beyond the horizon. The delay Δt_{hu} is the time elapsed between the horizon h and our actual position r_u in the universe. The delay Δt_{0h} is the time elapsed between the center of mass of the universe and the horizon r_h (given by Equation (38)).

$$r_h = \frac{2Gm_u}{k^2} \tag{38}$$

Performing the integral calculation of Equation (35), we get Equation (39).

$$\int \frac{1}{v_m(r)} \mathrm{d}r = \frac{\left(z(r) + 2G \cdot m_u \ln\left(2\left[k^2 r + z(r)\right]\right)\right)}{\beta k^3} \quad \text{where } z(r) = \sqrt{k^4 r^2 - 4G^2 m_u^2} \tag{39}$$

We can decompose the age of the universe Δt_u into two parts, Δt_{hu} and Δt_{0h}. The value Δt_{hu} represents the time elapsed between $r = r_h$ (at the horizon) and our actual position $r = r_u$ in the universe. The value Δt_{0h} gives the time elapsed between $r = 0$ (at the Big Bang) and $r = r_h$ (at the horizon).

$$\Delta t_u = \Delta t_{hu} + \Delta t_{0h} \approx (9.50 + 10.47i) \times 10^9 \text{ years} \quad \text{where } i = \sqrt{-1} \tag{40}$$

The imaginary time Δt_{0h} means that it elapses independently of our time. We cannot see an event between $r = 0$ and $r = r_h$, and an observer located between $r = 0$ and r_h could not see us. The Δt_{hu} equation is:

$$\Delta t_{hu} = \frac{1}{H_0}\left(\frac{\left(\omega + 2\ln\left[\omega + \beta\left(2+\sqrt{5}\right)\right] - \ln(4)\right)^2}{\sqrt{22+10\sqrt{5}}}\right) \approx \frac{7}{10H_0} \quad \text{where } \omega = \sqrt{\beta^2\left(9+4\sqrt{5}\right)-4} \tag{41}$$

The precise equation for Δt_{0h} is:

$$\Delta t_{0h} = \frac{-(2+\pi)}{H_0\sqrt{22+10\sqrt{5}}} i \approx \frac{-77}{100H_0} i \tag{42}$$

The modulus of the complex age Δt_u gives the universe's apparent age T_u.

$$T_u = |\Delta t_u| = |\Delta_{hu} + \Delta t_{0h}| = \sqrt{(\Delta t_{hu})^2 + (\Delta t_{0h} i)^2} \approx 14.14 \times 10^9 \text{ years} \tag{43}$$

$$T_u = \frac{1}{H_0} \underbrace{\sqrt{\left(\frac{\left(\omega + 2\ln\left[\omega + \beta\left(2+\sqrt{5}\right)\right] - \ln(4)\right)^2}{\sqrt{22+10\sqrt{5}}}\right)^2 + \left(\left[\frac{-(2+\pi)}{\sqrt{22+10\sqrt{5}}}\right] i\right)^2}}_{\eta \approx 1 \text{ (with about 4.25 \% of error)}} \tag{44}$$

As the square root over the accolade is approximatively equal to 1, we get:

$$T_u \approx \frac{1}{H_0} \approx 13.56 \times 10^9 \text{ years} \tag{45}$$

The value of the correction factor between Equations (43) and (45) is η.

$$\eta = H_0 T_u = H_0 \sqrt{(\Delta t_{hu})^2 + (\Delta t_{0h} i)^2} \approx 1.042516951 \tag{46}$$

This η explains why scientists currently measure two values of H_0. Scientists can only size the apparent age of the universe with different techniques. They cannot measure the real part and the imaginary part of the universe's age.

There is no "local" or "far" value of H_0. There is only one H_0. Some techniques give H_0 directly, and others need a correction factor. There is no need for any correction factor when H_0 is calculated from Equation (33), measured with the

CMB temperature with Equation (16), or with the universal gravitational constant G with Equation (34). Other techniques may get similar results than Equation (43), and if we impose that value to fit with Equation (45), we get H_0'.

$$H_0' = \frac{1}{|\Delta t_u|} \approx \frac{1}{14.14\times10^9 \text{ years}} \approx \frac{H_0}{\eta} \approx 69.2 \text{ km}\cdot\text{s}^{-1}\cdot\text{MParsec}^{-1} \quad (47)$$

However, Equation (45) gives the actual H_0 value:

$$H_0 \approx \frac{1}{13.56\times10^9 \text{ years}} \approx 72.1 \text{ km}\cdot\text{s}^{-1}\cdot\text{MParsec}^{-1} \quad (48)$$

If scientists could measure the real part of the universe's age and associate this value with $1/H_0$, they would obtain the following value.

$$H_0 \approx \frac{1}{9.50\times10^9 \text{ years}} \approx 102.94 \text{ km}\cdot\text{s}^{-1}\cdot\text{MParsec}^{-1} \quad (49)$$

If scientists could measure the imaginary part somehow, the association of this value with $1/H_0$ (like in Equation (45)) would give the following H_0 value.

$$H_0 \approx \frac{1}{10.47\times10^9 \text{ years}} \approx 93.39 \text{ km}\cdot\text{s}^{-1}\cdot\text{MParsec}^{-1} \quad (50)$$

with different types of experiments to measure the apparent age of the universe, scientists usually get either ~H_0 ≈ 69.2 or ~72.1 km·s^{-1}·Mparsec^{-1}. We assume that all calibration factors are used. New techniques could require other unknown corrective factors that have nothing to do with the related phenomenon.

The articles rarely give enough details to check if the process used needs η. Scientists must verify if the η factor is required for their approach.

5. Other Experimental Measurements of Hubble Constant H_0

In 1929, Hubble made the first observational-based measurements with cepheids and got H_0 ≈ 500 km·s^{-1}·MParsec^{-1} [1]. Sadly, even with a correct principle, his value is higher than the typical value due to errors in distance calibrations.

Let us validate our theoretical H_0 with an adequate interpretation of 508 measurements found on the Internet. The ends of their tolerance ranges give 1016 values. To find H_0 that has the highest probability to be measured, we compile the number of crossings with the tolerance ranges for each value of H_0. It generates a curve with two tips (**Figure 1**). The higher it is, the greater the chances are that this value of H_0 may be part of many tolerance ranges among the collected data.

A simple statistical phenomenon may be described with a Gaussian function. For fitting a wavy curve, it is necessary to make the sum of many Gaussians. A simpler model with fewer degrees of liberty must always be privileged.

A curve fit is done by summing different Gaussians (shown in **Figure 2**). A better gap fitting reduces the risk of finding other results. Thus, we gave a heavier weight (×10) to all data located between 69.2 and 72.1 km·s^{-1}·MParsec^{-1} (from our theory). We tried with and without this approach, and it gives about the same result. As it improves the gap fitting, we kept this approach.

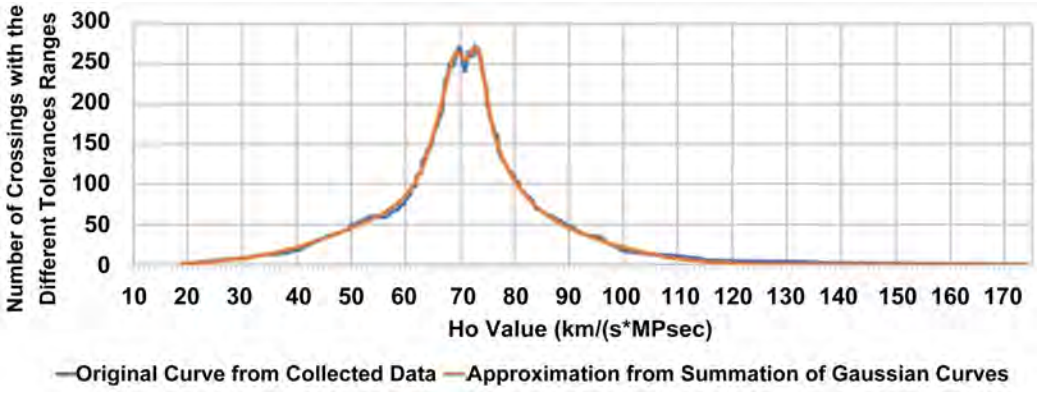

Figure 1. Number of crossings with tolerance ranges as a function of the H_0.

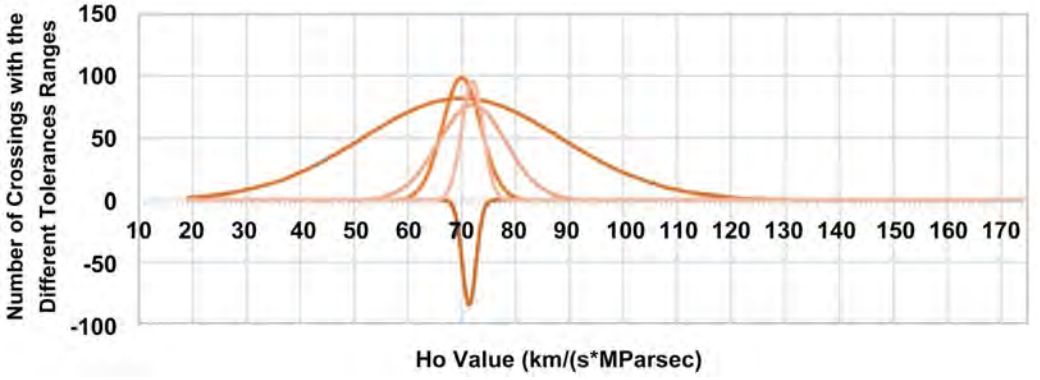

Figure 2. Gaussian curves used to approximate the original curve in **Figure 1**.

Each tip in **Figure 1** is approximated in **Figure 2** with two positive Gaussians. We force these curves to be around two means, even though there are four positive curves. It removes two degrees of liberty. We must add a negative Gaussian to model the gap between the two mean values. We must elaborate on this negative Gaussian. Our theory predicts "two close values" of H_0. On the curve, a deep gap shows up. It is impossible to get such a gap by only adding positives Gaussians which give two little bumps without any gap. To get a real gap, we must add a negative Gaussian. Let us see in **Figure 3** what would look like a curve fit without any negative Gaussian. Since the tips are close, they mix up to build only one tip.

The Gaussian sum in **Figure 3** peaks around $H_0 \approx 71.11$ km·s^{-1}·MParsec^{-1}. The result is not close to our theoretical $H_0 \approx 72.09548580$ km·s^{-1}·MParsec^{-1} (Equation (33)), but it is about what is found if statistics were used through the whole data set, thinking they should see only one tip. Moreover, Jang & Lee showed a similar value of $H_0 \approx 71.17$ km·s^{-1}·MParsec^{-1} (listed in our software in **Annex A**) that supposedly reduces the tension between the values obtained by cepheids (calibrated on SNe Ia) and CMB.

In **Figure 1**, we find two groups around $H_0 \approx 69.7$ and 71.8 km·s^{-1}·MParsec^{-1}. It is known that there is currently a tension between two groups [5]. A significant gap appears between the two tips. The only way to create such a gap is to

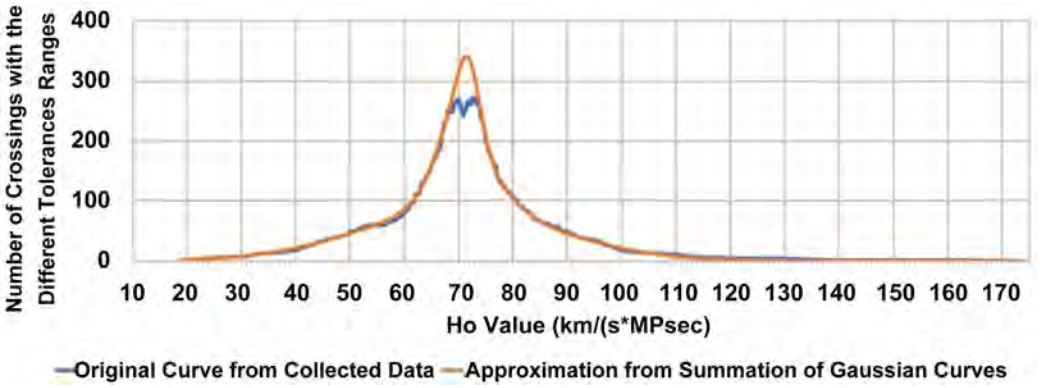

Figure 3. Approximated curve (orange tip) without negative Gaussian curves.

withdraw values nearby a specific value. It would then create a negative Gaussian, such as in Figure 2. It is delicate to debate why some values may have been withdrawn. It could be intentional or not. In the past, it was difficult to see a difference between these groups. Now, the tolerances are small enough to clearly see two groups. With recent growing tensions between these two clans, some may be inclined to shrink or shift some tolerance ranges when it overlaps with neighbor values.

In Figure 4, we apply η to the curves around $H_0 \approx 69.882$ km·s^{-1}·MParsec^{-1}. Then, all curves stand around $H_0 \approx 72.36$ km·s^{-1}·MParsec^{-1}. Then, with the curves of Figure 4, we build the curve in Figure 5. Figure 6 is a zoom of its tip.

We want to know the precise value of H_0 for which the derivative of the Gaussian summation is 0. It corresponds to the highest probability of getting the true H_0 value. Unfortunately, the derivative of a Gaussian summation is not an easy equation to get in a software. We rather use a numerical technic to get it. In Figure 6, we show a zoom of the quadratic curve fit around the tip value. Using the equation, we take the derivative and find its maximum. The quadratic equation has the following form:

$$y(x) = Ax^2 + Bx + C$$

$$\text{At the tip, the slope is : } y'(x) = \frac{\mathrm{d}x}{\mathrm{d}y} = 2Ax + B = 0 \rightarrow x = \frac{-B}{2A} \tag{51}$$

where $x = H_0$, $y =$ number of crossings with different tolerance ranges

$$H_0 = \frac{-B}{2A} \approx \frac{2423.2459592464}{2 \times 16.8057572117} \approx 72.0957088907 \text{ km} \cdot \text{s}^{-1} \cdot \text{MParsec}^{-1} \tag{52}$$

This result is well centered on our theoretical value within 3 parts per million. Our approach considers that both clans are someway right. Indeed, their different approaches and results also highlight a new phenomenon. It gives credit to our theory of the universe's complex age that predicts a few possible fake H_0 values.

We have 508 data. Each has a tolerance range (that may be symmetrical or not) that generates two H_0 values. Therefore, there are a total of $i_{\max} = 1016$ data at the end. The following equation depicts the statistical error e_t:

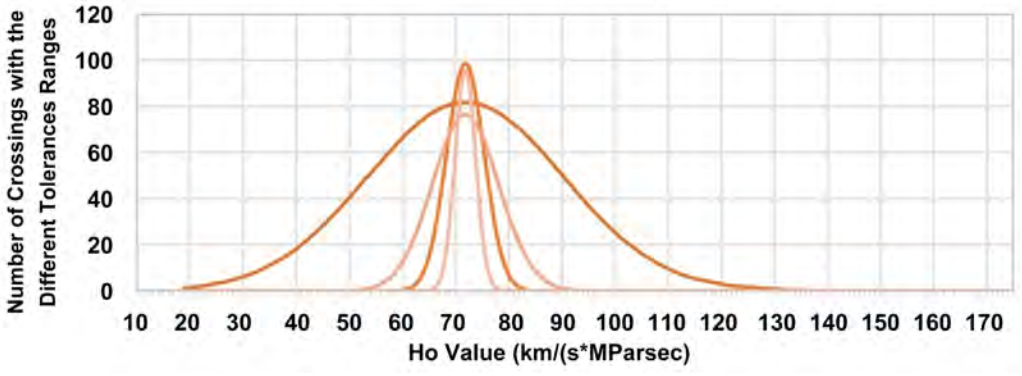

Figure 4. Gaussian curves modified with a correction factor η.

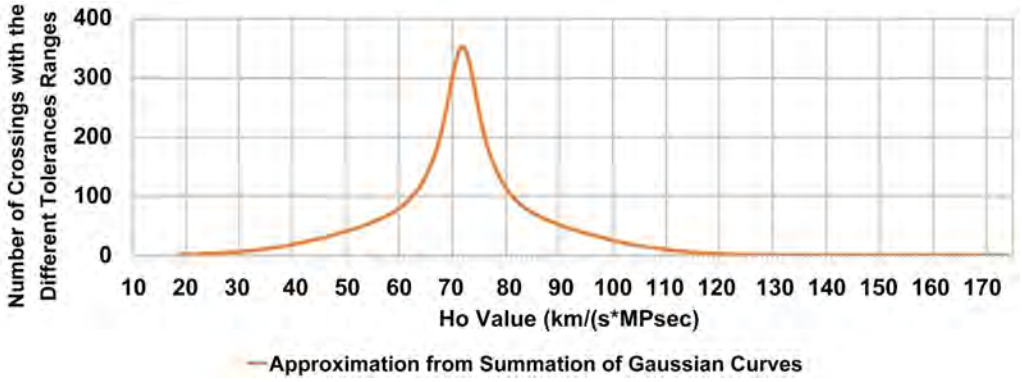

Figure 5. Result of the summation of 4 Gaussian curves from Figure 4.

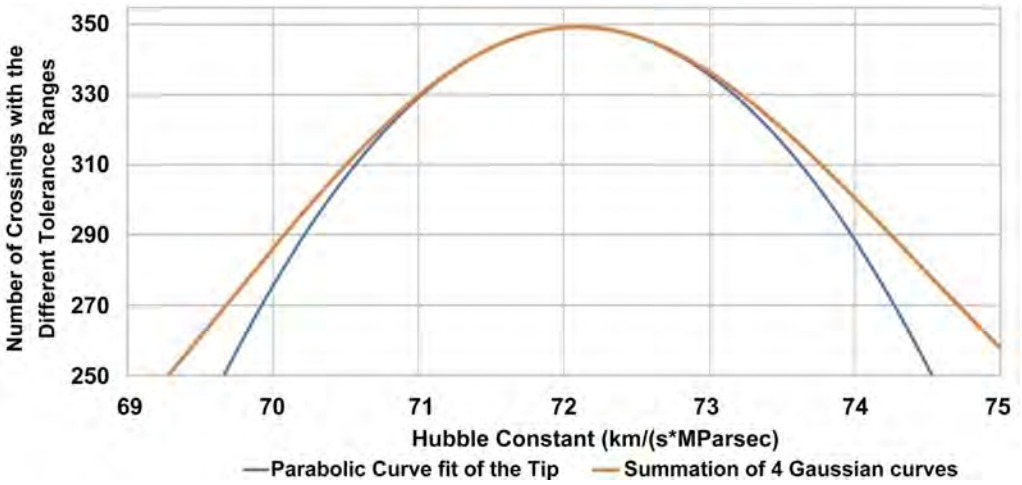

Figure 6. Zoom of the tip shown in Figure 5 + parabolic curve fit.

$$e_t \approx \frac{\sqrt{\sum_{i=1}^{i=i_{\max}} e_i^2}}{i_{\max}} \tag{53}$$

We mention that 16 H_0 values in our software in **Annex A** come from statistics. We kept them since some are mixed up with new valuable data information. So, we modify Equation (53) to remove them to reduce their impact on the total

e_t error. We use the following equation where $n = 2 \times 16 = 32$ (each data generates two H_0 values) is the number of elements to exclude from our sample. The total e_t error reduces with the square root of the number of elements included in our sample.

$$e_t \approx \frac{\sqrt{\sum_{i=1}^{i=i_{\max}} e_i^2}}{i_{\max}} \cdot \left[\frac{\sqrt{i_{\max}}}{\sqrt{i_{\max} - n}} \right] \tag{54}$$

If $n = 0$, we fall back on Equation (53). With $i_{\max} = 1016$, Equation (53) gives $e_t \approx \pm 0.32$ km·s^{-1}·MParsec^{-1}. With $i_{\max} = 1016$ and $n = 32$, Equation (54) rounds up to $e_t \pm 0.33$ km·s^{-1}·MParsec^{-1}. The impact of these n elements has a very little impact.

$$H_0 \approx 72.0957 \pm 0.33 \text{ km} \cdot \text{s}^{-1} \cdot \text{MParsec}^{-1} \tag{55}$$

In **Annex A**, we supply the software used to get this result. All the main steps enumerated in this article are clearly shown. The software uses starting values (found via Excel) to fit the original curve with 5 Gaussian curves (#0 to #4 to use the same numbers as the software). Each Gaussian uses three parameters: μ is the mean value, σ represents the variance, and m is a multiplication factor.

$$f(H_0) \approx \frac{m}{\sigma\sqrt{2\pi}} \text{e}^{\frac{-1}{2}\left(\frac{H_0 - \mu}{\sigma}\right)^2} \tag{56}$$

Here are the values for the 5 Gaussian curves used to fit the original curve:

Gaussian #	μ	σ	m
0	71.271	1.286	−272.7
1	69.882	18.422	3777.7
2		3.554	877.9
3	71.870	6.259	1199.2
4		1.963	470.4

(57)

For Gaussians #1 and #2, we force the software to use the same mean value. We do the same thing for Gaussians #3 and #4. We also note that the mean value of Gaussian #0 is negative. With these values, we stopped iterating when the sum of squares of errors was lower than 22000. We see in **Figure 1** that the obtained approximated curve fits well the original curve. In our software (**Annex A**), the iterations start with values close to what they should be.

The specificity of our approach is to say that the two clans are someway right. However, we must apply a correction factor to one of them. Indirectly, it gives credit to a complex universe age that predicts a few possible fake values of H_0.

After reading this article, scientists should continue their work as they were doing, without applying any correction factor to their raw data. The correction factor should only be used on the final Gaussian curve to analyze data.

6. A Reminder of Different Useful Identities

To avoid repeating everything unnecessarily, we recall different identities that will be used later to determine H_0. Planck units are commonly defined as fol-

lows.

$$\text{Plank mass}: \quad m_p = \sqrt{\frac{hc}{2\pi G}} \approx 2.18\times10^{-8}\ \text{kg} \tag{58}$$

$$\text{Plank time}: \quad t_p = \sqrt{\frac{hG}{2\pi c^5}} = \frac{L_p}{c} \approx 5.91\times10^{-44}\ \text{s} \tag{59}$$

$$\text{Plank length}: \quad L_p = \sqrt{\frac{hG}{2\pi c^3}} = ct_p = 1.61\times10^{-35}\ \text{m} \tag{60}$$

$$\text{Plank Temperature}: \quad T_p = \sqrt{\frac{hc^3}{2\pi G k_b^2}} = \frac{m_p c^2}{k_b} \approx 1.42\times10^{32}\ \text{K} \tag{61}$$

$$\text{Planck charge}: \quad q_p = \sqrt{2ch\varepsilon_0} = \frac{-q_e}{\sqrt{\alpha}} \approx 1.88\times10^{-18}\ \text{C} \tag{62}$$

The fine-structure constant α is linked to Rydberg constant R_∞ and the electron mass m_e by the following equation:

$$R_\infty = \frac{cm_e\alpha^2}{2h} \tag{63}$$

The speed of light c is given as a function of μ_0 and ε_0.

$$c = \frac{1}{\sqrt{\mu_0\varepsilon_0}} \tag{64}$$

Associating the mass-energy of a Planck particle with its wave energy and then, using Equations (31), (32), (64), and (62), we get Planck charge q_P defined several ways and as a function of c, G, and h like the other Plank units.

$$q_p = \sqrt{\frac{2h}{c\mu_0}} = \sqrt{\frac{4\pi m_p L_p}{\mu_0}} = \sqrt{\frac{\beta G h^2}{\pi\mu_0 r_e^2 c^4 \alpha^{19}}} \tag{65}$$

The electron's charge is determined from the mass of the electron m_e, the classical electron radius r_e, and the vacuum permeability μ_0.

$$q_e = \sqrt{\frac{4\pi m_e r_e}{\mu_0}} = -1.60\times10^{-19}\ \text{C} \tag{66}$$

Let us calculate the precise value of the average temperature T of the CMB. We first make equal Equations (16) and (33). Then, we replace G by Equation (31), and we get rid of Plank constant h by its value from Equation (32).

$$T = \frac{m_e c^2}{k_b}\left(\frac{15\beta^6\alpha^{17}}{\pi^3}\right)^{1/4} \approx 2.7367958(16)\ \text{K} \tag{67}$$

This CMB temperature is like Kimura with 2.737 K [23].

7. Different Equations to Calculate H_0

For an academic purpose and to show the interdependence of H_0 with the other "constants", we will enumerate equations using various universe parameters. Some overcome the inherent difficulties in measuring H_0 and show a rounda-

bout way of obtaining an accurate value of it. We also find some others which depend on interesting values, or more precise ones. Using the constants c, k_b, T, m_e, r_e, h, G, μ_0, ε_0, m_u, R_u, R_∞, q_e, q_p, t_p, l_p, T_p, m_p, m_{ph}, and β, we find many equations.

The H_0 parameter is not constant since $1/H_0$ represents an approximation of the apparent universe's age, and H_0 get smaller over time. Since the universe is old, H_0 changes slowly. If the constancy of all the universe's parameters is maintained as it is currently done in metrology, the universe's age and H_0 will seem constant.

Results of 508 different experiences reduce the error by $508^{1/2} \approx 22.5$. It may look like a significant number, but it is nothing besides what has been done to measure the electron characteristics accurately. Particle accelerators use millions of electrons at each experiment, and they repeat these many times to find something new. Computers analyze the collisions' results to make the electron's characteristics more and more accurate. It is why there is no manner to get better results than that of Equation (33), as it is based on well-known characteristics of the electron. We will see further many other equations that give precise results.

Replacing G by Equation (31) in Equation (16), we get Equation (68).

$$H_0 = \pi^3 k_b^2 T^2 \alpha^9 \sqrt{\frac{8r_e}{15m_e c^3 h^3 \beta^5}} \tag{68}$$

Replacing h in Equation (68) by using Equation (32), we get Equation (69).

$$H_0 = k_b^2 T^2 \sqrt{\frac{\pi^3 \alpha^{21}}{15r_e^2 m_e^4 \beta^5 c^6}} \tag{69}$$

Replacing h in Equation (16) by using Equation (32), we get Equation (70).

$$H_0 = \frac{k_b^2 T^2}{\beta^2} \sqrt{\frac{\pi^3 G\alpha}{15r_e^3 m_e^3 c^8}} \tag{70}$$

Replacing T in Equation (70) by using Equation (67), we get Equation (71).

$$H_0 = \beta\alpha^9 \sqrt{\frac{Gm_e}{r_e^3}} \tag{71}$$

Using Equation (32) in Equation (33), we get Equation (72).

$$H_0 = \frac{2\pi m_e c^2 \alpha^{18} \sqrt{\beta}}{h} \tag{72}$$

With Equations (63) and (72), we get the most accurate equation.

$$H_0 = 4\pi c R_\infty \alpha^{16} \sqrt{\beta} \tag{73}$$

Using Equation (31) in Equation (73), we get Equation (74).

$$H_0 = \frac{4\pi G m_e R_\infty \beta^{3/2}}{c r_e \alpha^4} \tag{74}$$

Equation (74) gives H_0 with G_{2014} (from CODATA 2014). The measurement of $H_0(G_{2014}) \approx 72.105(36)$ km·s^{-1}·MParsec^{-1} is our fourth way to measure H_0.

Using Equation (63) in Equation (74), we get Equation (75). This equation is also a good candidate for measuring H_0 as a function of G.

$$H_0 = \frac{8\pi G h R_\infty^2 \beta^{3/2}}{r_e c^2 \alpha^4} \tag{75}$$

Using Equation (32) in Equation (75), we get Equation (76).

$$H_0 = \frac{16\pi^2 G m_e R_\infty^2 \beta^{3/2}}{c\alpha^7} \tag{76}$$

This equation is another good candidate for measuring H_0 as a function of G. The measure still gives the same result as Equation (74).

We will enumerate other equations without making all the rather fastidious demonstrations. However, all these may be found from previous equations.

$$H_0 = \frac{2\pi m_{ph} c^2}{h} \tag{77}$$

$$H_0 = 2c^2 \sqrt{\frac{\pi R_\infty \alpha^{55}}{G m_e}} \tag{78}$$

$$H_0 = \beta \alpha^9 \sqrt{\frac{m_e c}{r_e^3}} \tag{79}$$

$$H_0 = 8\beta \sqrt{G m_e \left(\pi R_\infty\right)^3 \alpha^9} \tag{80}$$

$$H_0 = 8c \sqrt{\beta r_e \left(\pi R_\infty\right)^3 \alpha^{29}} \tag{81}$$

$$H_0 = \sqrt{\frac{2\pi c^5 \alpha^{57}}{hG}} \tag{82}$$

$$H_0 = 2c \sqrt{\frac{\pi \beta R_\infty \alpha^{25}}{r_e}} \tag{83}$$

$$H_0 = \sqrt{\frac{2\pi \beta m_e c^3 \alpha^{37}}{h r_e}} \tag{84}$$

$$H_0 = \frac{2\pi^2}{h} \left(\frac{k_b^4 T^4}{15 m_u \alpha^2 c^2 \beta^4} \right)^{1/3} \tag{85}$$

$$H_0 = \frac{2\pi k_b T_p}{h} \sqrt{\alpha^{57}} \tag{86}$$

$$H_0 = \frac{c\mu_0 q_e^2 \alpha^{19} \sqrt{\beta}}{4\pi m_e r_e^2} \tag{87}$$

$$H_0 = \frac{q_e^2 \alpha^{19} \sqrt{\beta}}{4\pi c \varepsilon_0 m_e r_e^2} \tag{88}$$

$$H_0 = \frac{q_p^2 \alpha^{18} \sqrt{\beta}}{2h\varepsilon_0 r_e} \tag{89}$$

$$H_0 = \frac{c\mu_0 q_p^2 \alpha^{20} \sqrt{\beta}}{4\pi m_e r_e^2} \tag{90}$$

$$H_0 = \frac{q_p^2 \alpha^{20} \sqrt{\beta}}{4\pi c \varepsilon_0 m_e r_e^2} \tag{91}$$

$$H_0 = \frac{c\beta q_p^2 \sqrt{\alpha^{19}}}{4\pi \varepsilon_0 k_b T_p r_e^2} \tag{92}$$

$$H_0 = \frac{c\beta q_e^2 \sqrt{\alpha^{17}}}{4\pi \varepsilon_0 k_b T_p r_e^2} \tag{93}$$

$$H_0 = \frac{c q_e^2 \beta^2}{4\varepsilon_0 k_b T r_e^2} \left(\frac{15\alpha^{97}}{\pi^7} \right)^{1/4} \tag{94}$$

$$H_0 = \frac{2k_b T}{\beta h} \left(\frac{\pi^7 \alpha^{55}}{15} \right)^{1/4} \tag{95}$$

$$H_0 = \frac{k_b T}{\beta r_e m_e c} \left(\frac{\pi^3 \alpha^{59}}{15} \right)^{1/4} \tag{96}$$

$$H_0 = \frac{4\pi k_b T}{\beta c \mu_0 q_e^2} \left(\frac{\pi^3 \alpha^{59}}{15} \right)^{1/4} \tag{97}$$

$$H_0 = \frac{4\pi k_b T}{\beta c \mu_0 q_p^2} \left(\frac{\pi^3 \alpha^{55}}{15} \right)^{1/4} \tag{98}$$

$$H_0 = \frac{G k_b T}{c^3 r_e^2} \left(\frac{\pi^3}{15\alpha^{21}} \right)^{1/4} \tag{99}$$

$$H_0 = \frac{2G m_e k_b T}{h r_e c^2} \left(\frac{\pi^7}{15\alpha^{25}} \right)^{1/4} \tag{100}$$

$$H_0 = \frac{G m_p k_b T}{m_e c^3 r_e^2} \left(\frac{\pi^3 \alpha^{21}}{15\beta^2} \right)^{1/4} \tag{101}$$

$$H_0 = \frac{G m_u k_b T}{m_e c^3 r_e^2} \left(\frac{\pi^3 \alpha^{135}}{15\beta^2} \right)^{1/4} \tag{102}$$

$$H_0 = \frac{G m_e k_b T}{m_p c^3 r_e^2} \left(\frac{\pi^3 \beta^2}{15\alpha^{63}} \right)^{1/4} \tag{103}$$

$$H_0 = \frac{16 c G k_b T \varepsilon_0 m_e^2}{q_e^4} \left(\frac{\pi^{11}}{15\alpha^{21}} \right)^{1/4} \tag{104}$$

$$H_0 = \beta m_e^2 \sqrt{\frac{8\pi^3 G c^3 \alpha^{15}}{h^3}} \tag{105}$$

$$H_0 = \frac{c^3 \alpha^{39}}{G m_e \sqrt{\beta}} \tag{106}$$

The last equation measures H_0 from G since all other constants are accurate. Many equations are excellent candidates for measuring H_0 as a function of G or

T. These equations could represent valuable tools for cosmologists.

This document gives 42 equations of H_0 as a function of various universe parameters. Since H_0 may be defined using different parameters, we suggest that some of the most critical universe parameters are well linked, as much in the infinitely small as in the infinitely large, and H_0 is part of these.

8. Why Is H_0 Not Really a Constant?

We want to explain why Hubble parameter H_0 cannot be constant over time. As simple as it is, the reverse of Hubble parameter H_0 is related to the apparent age of the universe (see Equation (45)). Consequently, the H_0 parameter is changing over time. It is, therefore, by abuse of language that we call H_0 the Hubble "constant". To be more precise, we should say the Hubble "parameter".

When H_0 is expressed in km·s^{-1}·MParsec^{-1}, the ninth digit after the dot changes every year. It goes completely unnoticed. More than that, even if we could achieve this precision in our measurements of H_0, it would still go unnoticed since we forced c to be constant in 1983. In metrology, scientists choose the speed of light as a standard. Even though c changes every year, if we force it to be constant, we willfully readjust all other constants and units (distance, time, and mass) as a function of c to keep it constant. Then, H_0 looks constant as other parameters.

9. Conclusions

This article aimed to show that our theoretical value from Equation (33) (giving $H_0 \approx 72.09548580(32)$ km·s^{-1}·MParsec^{-1}) [6] is the right one, despite a growing tension [5] between values around 69.2 and 72.1 km·s^{-1}·MParsec^{-1}.

With 508 data (from [24] to [310] shown in our software in **Annex A**), a graph showing the actual tension [5] between two values is shown. We decomposed the curve into Gaussians. A negative one is required to explain the large gap between the two H_0 values, and it is due to withdrawn values. So, we restored them by removing that curve. Then, we applied a $\eta \approx 1.042516951$ correction factor (from our theory) to the curves located at $\sim H_0 \approx 69.2$ km·s^{-1}·MParsec^{-1}. Our theory highlights a misunderstanding of the link between $1/H_0$ and the universe's apparent age. With the proper correction factor applied, we get a statistical value of $H_0 \approx 71.85 \pm 0.33$ km·s^{-1}·MParsec^{-1}, which is close to our theoretical value. Our discovery of the η factor may help to reduce the tension between scientists. Someway we show that even if two H_0 values seem to be commonly found with various techniques, both are accurate if a proper correction factor is used.

With a new cosmological model, we get an apparent age of the universe of about 14.14 billion years. The exact formula is approximated from an elaborate integral result by the well-known $1/H_0$ equation that gives 13.56 billion years. Different techniques may lead to either value. It depends if it is an attempt to measure the universe's age locally or far away. There is no "local" or "distant" value of H_0, as some may pretend [46] [47]. Sticking their measurement of the

apparent age of the universe to $1/H_0$, most cosmologists get results that stand around 69.2 or 72.1 km·s^{-1}·MParsec^{-1}. Our hypothesis may explain the actual tension [5] relative to these two values. However, there is only one true H_0 value, and the other one is just misinterpreted as being the Hubble constant without quite being so.

Even if many theoretical equations of H_0 are shown in this article, we highlight that we also found a few interesting ways to measure the H_0 accurately using the CMB temperature T and the value of the universal gravitational constant G from CODATA 2014. These results confirm our theoretical value.

$H_0 \approx 72.06(90)$ km·s^{-1}·MParsec^{-1} and 71.95(50) km·s^{-1}·MParsec^{-1} from T,

$H_0 \approx 72.086(36)$ km·s^{-1}·MParsec^{-1} and 72.105(36) km·s^{-1}·MParsec^{-1} from G.

For an academic purpose, we enumerated 42 equations of H_0 using different parameters. These equations showed that H_0 is intricated with all other "constants". For metrology purposes, the speed of light in a vacuum is forced to be constant to be an unchanging standard. If this situation is considered valid in a metrology context, H_0 should also be considered constant and become part of the CODATA. For the same reasons, H_0 must also be constant in a metrology context and become part of the CODATA. However, if $1/H_0$ represents an approximation of the universe's age, it would also make sense to say that H_0 is changing over time.

Einstein's and Schwarzschild's equations show that massive objects such as the universe influence the speed of light. As the universe expands, its density diminishes, and the local speed of light increases over time.

The fine-structure constant α is unitless and may be described as a ratio where the variation rate at the numerator counterbalances the variation rate at the denominator. Apart from α and β, all "constants" used to describe H_0 in our equations somehow emanate from fundamental units such as the meter, the second, and the kilogram. These units are now defined by the speed of light. As H_0 describes the universe's age and depends on many unit-dependent "constants" based on c, we should consider c and all universe's unit-dependent parameters as changing over time. Forcing c to be constant is necessary for metrology purposes, but it is not in the interest of physicists for explaining phenomena. An accurate value of H_0 has a great interest in deepening our understanding of the universe.

Conflicts of Interest

The author claims that he has no conflict of interest in connection with the publication of this article.

References

[1] Hubble, E. (1929) *Proceedings of the National Academy of Sciences of the United States of America*, **15**, 168-1973. https://doi.org/10.1073/pnas.15.3.168

[2] Einstein, A. (1916) *Annalen der Physik*, **354**, 769-822. https://doi.org/10.1002/andp.19163540702

[3] Friedman, A. (1922) *Zeitschrift für Physics*, **10**, 377-386. https://doi.org/10.1007/BF01332580

[4] Lemaître, G. (1927) *Annales de la Société Scientifique de Bruxelles*, **A47**, 49-59. Partially Translated in English: Lemaître, G. (1931) *Monthly Notices of the Royal Astronomical Society*, **91**, 483-490.

[5] Verde, L., Treu, T. and Riess, A.G. (2019) *Nature Astronomy*, **3**, 891-895. https://doi.org/10.1038/s41550-019-0902-0

[6] Mercier, C. (2019) *Journal of Modern Physics*, **10**, 641-662. https://doi.org/10.4236/jmp.2019.106046

[7] Mercier, C. (2020) *Journal of Modern Physics*, **11**, 1428-1465. https://doi.org/10.4236/jmp.2020.119089

[8] Mohr, P.J., Newell, D.B. and Taylor, B.N. (2016) *Review of Modern Physics*, **88**, Article ID: 035009. https://doi.org/10.1103/RevModPhys.88.035009

[9] Jenkins, A., Villard, R. and Riess, A (2018) Hubblesite. https://stsci-opo.org/STScI-01EVSQXZ976ZY1QKQX17XJ7P5H.pdf

[10] Einstein, A. (1905) *Annalen der Physik*, **322**, 891-921. https://doi.org/10.1002/andp.19053221004

[11] Einstein, A. (1911) *Annalen der Physik*, **340**, 898-908. https://doi.org/10.1002/andp.19113401005

[12] Grøn, Ø. (2016) *American Journal of Physics*, **84**, 537-541. https://doi.org/10.1119/1.4944031

[13] Binney, J. and Merrifield, M. (1998) Galactic Astronomy. Princeton University Press, Princeton, 816 p. https://press.princeton.edu/titles/6358.html

[14] Mulligan, J.F. (1976) *American Journal of Physics*, **44**, 960-969. https://doi.org/10.1119/1.10241

[15] Mercier, C. (2019) *Journal of Modern Physics*, **10**, 980-1001. https://doi.org/10.4236/jmp.2019.108065

[16] Zichichi, A. (2000) *Proceedings of the International School of Subnuclear Physics*, **36**, 1-708.

[17] Carvalho, J.C. (1995) *International Journal of Theoretical Physics*, **34**, 2507-2509. https://doi.org/10.1007/BF00670782

[18] Dirac, P.A.M. (1938) *Proceedings of the Royal Society of London A*: *Mathematical, Physical and Engineering Sciences*, **165**, 199-208. https://doi.org/10.1098/rspa.1938.0053

[19] Dirac, P.A.M. (1974) *Proceedings of the Royal Society of London A*: *Mathematical, Physical and Engineering Sciences*, **338**, 439-446. https://doi.org/10.1098/rspa.1974.0095

[20] Gush, H.P. (1981) *Physical Review Letters*, **47**, 745-748. https://doi.org/10.1103/PhysRevLett.47.745

[21] Partridge, R.B. (1997) An Introduction to the Cosmic Microwave Background Radiation. *From Quantum Fluctuations to Cosmological Structures*: *Proceedings of the* 1*st Moroccan School of Astrophysics*, Casablanca, 1-10 December 1996, 141-184.

[22] Mercier, C. (2016) More than a Hundred Ways to Get the Large Number N. Not Published. http://pragtec.com/physique/index_en.html

[23] Kimura, K., Hashimoto, M., Sakoda, K. and Sakoda, K. (2001) *The Astrophysical Journal*, **561**, L19-L22. https://doi.org/10.1086/324569

[24] Abbott, B.P., *et al.* (2021) *The Astrophysical Journal*, **909**, Article No. 218.

https://doi.org/10.3847/1538-4357/abdcb7

[25] Addison, G.E. (2021) *The Astrophysical Journal*, **912**, Article No. L1. https://doi.org/10.3847/2041-8213/abf56e

[26] Baxter, E.J. and Sherwin, B.D. (2021) *Monthly Notices of the Royal Astronomical Society*, **501**, 1023-1035. https://doi.org/10.1093/mnras/staa3706

[27] Blakeslee, J.P., Jensen, J.B., Ma, C.-P., Milne, P.A. and Greene, J.E. (2021) *The Astrophysical Journal*, **911**, Article No. 65. https://doi.org/10.3847/1538-4357/abe86a

[28] Bonilla, A., Kumar, S. and Nunes, R.C. (2021) *The European Physical Journal C*, **81**, Article No. 127. https://doi.org/10.1140/epjc/s10052-021-08925-z

[29] Dainotti, M.G., *et al.* (2021) *The Astrophysical Journal*, **912**, Article No. 150. https://doi.org/10.3847/1538-4357/abeb73

[30] Denzel, P., Coles, J.P., Saha, P. and Williams, L.L.R. (2021) *Monthly Notices of the Royal Astronomical Society*, **501**, 784-801. https://doi.org/10.1093/mnras/staa3603

[31] Di Valentino, E. (2021) *Monthly Notices of the Royal Astronomical Society*, **502**, 2065-2073. https://doi.org/10.1093/mnras/stab187

[32] Gayathri, V., *et al.* (2021) *The Astrophysical Journal Letters*, **908**, Article No. L34. https://doi.org/10.3847/2041-8213/abe388

[33] Hagstotz, S., Reischke, R. and Lilow R (2021) A New Measurement of the Hubble Constant Using Fast Radio Bursts. arXiv:2104.04538v1, Not Published.

[34] Khetan, N., *et al.* (2021) *Astronomy and Astrophysics*, **647**, Article No. A72. https://doi.org/10.1051/0004-6361/202039196

[35] Mukherjee, S., *et al.* (2021) *Astronomy and Astrophysics*, **646**, Article No. A65. https://doi.org/10.1051/0004-6361/201936724

[36] Park, J.W., *et al.* (2021) *The Astrophysical Journal*, **910**, Article No. 39. https://doi.org/10.3847/1538-4357/abdfc4

[37] Philcox, O.H.E., Sherwin, B.D., Farren, G.S. and Baxter, E.J. (2021) *Physical Review D*, **103**, Article ID: 023538. https://doi.org/10.1103/PhysRevD.103.023538

[38] Qi, J.-Z., Zhao, J.-W., Cao, S., Biesiada, M. and Liu, Y. (2021) *Monthly Notices of the Royal Astronomical Society*, **503**, 2179-2186. https://doi.org/10.1093/mnras/stab638

[39] Riess, *et al.* (2021) *The Astrophysical Journal Letters*, **908**, L6. https://doi.org/10.3847/2041-8213/abdbaf

[40] Soltis, J., Casertano, S. and Riess, A.G. (2021) *The Astrophysical Journal Letters*, **908**, L5. https://doi.org/10.3847/2041-8213/abdbad

[41] Wang, H. and Giannios, D. (2021) *The Astrophysical Journal*, **908**, Article No. 200. https://doi.org/10.3847/1538-4357/abd39c

[42] Zhang, J.-C., Jiao, K. and Zhang, T.-J. (2021) Model-Independent meAsurement of the Hubble Constant and the Absolute Magnitude of Type Ia Supernovae. Not Published. arXiv:2101.05897.

[43] Aghanim, N.A., Forveille, T., Pentericci, L. and Shore, S. (2020) A*stronomy & Astrophysics*, **641**, Article No. E1. https://doi.org/10.1051/0004-6361/202039265

[44] Benevento, G., Hu, W. and Raveri, M. (2020) *Physical Review D*, **101**, Article ID: 103517. https://doi.org/10.1103/PhysRevD.101.103517

[45] Birrer, S., *et al.* (2020) *Astronomy & Astrophysics*, **643**, Article No. A165. https://doi.org/10.1051/0004-6361/202038861

[46] Camarena, D. and Marra, V. (2020) *Physical Review Research*, **2**, Article ID: 013028.

https://doi.org/10.1103/PhysRevResearch.2.013028

[47] Chang, Z. and Zhu, Q.-H. (2020) *Physical Review D*, **101**, Article ID: 084029. https://doi.org/10.1103/PhysRevD.101.084029

[48] Coughlin, M.W., *et al.* (2020) *Nature Communications*, **11**, Article No. 4129. https://doi.org/10.1038/s41467-020-17998-5

[49] D'Agostino, R. and Nunes, R.C. (2020) *Physical Review D*, **101**, Article ID: 103505. https://doi.org/10.1103/PhysRevD.101.103505

[50] Dai, W.M., Ma, Y.-Z. and He, H.-J. (2020) *Physical Review D*, **102**, Article ID: 121302. https://doi.org/10.1103/PhysRevD.102.121302

[51] Dietrich, T., *et al.* (2020) *Science*, **370**, 1450-1453. https://doi.org/10.1126/science.abb4317

[52] Gonzalez, M., Hertzberg, M.P. and Rompineve, F. (2020) *Journal of Cosmology and Astroparticle Physics*, **10**, Article No. 028. https://doi.org/10.1088/1475-7516/2020/10/028

[53] González-Serrena, B., Cuesta, A.J. and Ortiz-Mora, A. (2020) Contributions to the XIV.0 Scientific Meeting (Virtual) of the Spanish Astronomical Society.

[54] Haboury, N. (2020) Measuring the Hubble Constant with Standard Sirens. University of Geneva, Astronomy Department, Geneva, 1-22, Not Published. https://www.researchgate.net/publication/343679057_Measuring_the_Hubble_constant_with_standard_sirens

[55] Harvey, D. (2020) *Monthly Notices of the Royal Astronomical Society*, **498**, 2871-2886. https://doi.org/10.1093/mnras/staa2522

[56] Holanda, R.F.L., Pordeus-da-Silva, G. and Pereira, S.H. (2020) *Journal of Cosmology and Astroparticle Physics*, **9**, Article No. 053. https://doi.org/10.1088/1475-7516/2020/09/053

[57] Howlett, C. and Davis, T.M. (2020) *Monthly Notices of the Royal Astronomical Society*, **492**, 3803-3815. https://doi.org/10.1093/mnras/staa049

[58] De Jaeger, T., Stahl, B.E., Zheng, W., Filippenko, A.V., Riess, A.G. and Galbany, L. (2020) *Monthly Notices of the Royal Astronomical Society*, **496**, 3402–3411. https://doi.org/10.1093/mnras/staa1801

[59] Kim, Y.J., Kang, J., Lee, M.G. and Jang, I.S. (2020) *The Astrophysical Journal*, **905**, Article No. 104. https://doi.org/10.3847/1538-4357/abbd97

[60] Kreisch, C.D., Cyr-Racine, F.-Y. and Doré, O. (2020) *Physical Review D*, **101**, Arrticle ID: 123505. https://doi.org/10.1103/PhysRevD.101.123505

[61] Li, H. and Zhang, X. (2020) *Science Bulletin*, **65**, 1419-1421. https://doi.org/10.1016/j.scib.2020.04.038

[62] Lombriser, L. (2020) *Physics Letters B*, **803**, Arrticle ID: 135303. https://doi.org/10.1016/j.physletb.2020.135303

[63] Millon, M., *et al.* (2020) *Astronomy and Astrophysics*, **639**, Article No. A101. https://doi.org/10.1051/0004-6361/201937351

[64] Mukherjee, S., Ghosh, A., Graham, M.J., Karathanasis, C., *et al.* (2020) First Measurement of the Hubble Parameter from Bright Binary Black Hole GW190521. Not Published (Under Review with MNRAS), arXiv:2009.14199, 1-8.

[65] Nicolaou, C., Lahav, O., Lemos, P., Hartley, W. and Braden, J. (2020) *Monthly Notices of the Royal Astronomical Society*, **495**, 90-97. https://doi.org/10.1093/mnras/staa1120

[66] Niedermann, F. and Sloth, M.S. (2020) *Physical Review D*, **102**, Article ID: 063527.

https://doi.org/10.1103/PhysRevD.102.063527

[67] Palmese, A., *et al.* (2020) *The Astrophysical Journal Letters*, **900**, Article No. L33. https://doi.org/10.3847/2041-8213/abaeff

[68] Pandey, K.L., Karwalb, T. and Dasc, S. (2020) *Journal of Cosmology and Astroparticle Physics*, **7**, Article No. 026. https://doi.org/10.1088/1475-7516/2020/01/026

[69] Pesce, D.W., Braatz, J.A., Reid, M.J., Riess, A.G., *et al.* (2020) *The Astrophysical Journal*, **891**, Article No. L1. https://doi.org/10.3847/2041-8213/ab75f0

[70] Pogosian, L., Zhao, G.-B. and Jedamzik, K. (2020) *The Astrophysical Journal Letters*, **904**, Article No. L17. https://doi.org/10.3847/2041-8213/abc6a8

[71] Guo, R.-Y., Zhang, J.-F. and Zhang, X. (2020) *Science China Physics, Mechanics & Astronomy*, **63**, Article No. 290406. https://doi.org/10.1007/s11433-019-1514-0

[72] Schombert, J., McGaugh, S. and Lelli, F. (2020) *The Astronomical Journal*, **160**, Article No. 71. https://doi.org/10.3847/1538-3881/ab9d88

[73] Shajib, A.J., *et al.* (2020) *Monthly Notices of the Royal Astronomical Society*, **494**, 6072-6102. https://doi.org/10.1093/mnras/staa828

[74] Sharov, G.S. and Sinyakov, E.S. (2020) *Mathematical Modelling and Geometry*, **8**, 1-20. https://doi.org/10.26456/mmg/2020-811

[75] Vasylyev, S.S. and Filippenko, A.V. (2020) *The Astrophysical Journal*, **902**, Article No. 149. https://doi.org/10.3847/1538-4357/abb5f9

[76] Vogl, V. (2020) Cosmological Distances of Type II Supernovae from Radiative Transfer Modeling. Dissertation, Max-Planck-Institut Fur Astrophysik, Garching bei München, 172 p, Not Published. https://mediatum.ub.tum.de/doc/1542626/1542626.pdf

[77] Wei, J.-J. and Melia, F. (2020) *The Astrophysical Journal*, **897**, Article No. 127. https://doi.org/10.3847/1538-4357/ab959b

[78] Wu, W.L.K., Motloch, P., Hu, W. and Raveri, M. (2020) *Physical Review D*, **102**, Article ID: 023510. https://doi.org/10.1103/PhysRevD.102.023510

[79] Yang, T., Birrer, S. and Hu, B. (2020) *Monthly Notices of the Royal Astronomical Society*, **497**, L56-L61. https://doi.org/10.1093/mnrasl/slaa107

[80] Zhang, X. and Huang, Q.-G. (2020) *Science China Physics Mechanical Astronomy*, **63**, Article No. 290402. https://doi.org/10.1007/s11433-019-1504-8

[81] Agrawal, P., Cyr-Racine, F.-Y., Pinner, D. and Randall, L. (2019) Rock 'n' Roll Solutions to the Hubble Tension. Cornell University, Ithaca, arXiv:1904.01016v1, Not Published.

[82] Anderson, R.I. (2019) *Astronomy & Astrophysics*, **631**, Article No. A165. https://doi.org/10.1051/0004-6361/201936585

[83] Birrer, S., Treu, T., Rusu, C.E., Bonvin, V., *et al.* (2019) *Monthly Notices of the Royal Astronomical Society*, **484**, 4726-4753. https://doi.org/10.1093/mnras/stz200

[84] Chang, Z., Huang, Q.-G., Wang, S. and Zhao, Z.-C. (2019) *The European Physical Journal C*, **79**, Article No. 177. https://doi.org/10.1140/epjc/s10052-019-6664-0

[85] Chen, G.C.-F., Fassnacht, C.D., Suyu, S.H., Rusu CE, *et al.* (2019) *Monthly Notices of the Royal Astronomical Society*, **490**, 1743-1773. https://doi.org/10.1093/mnras/stz2547

[86] Collett, T., Montanari, F. and Räsänen, S. (2019) *Physical Review Letters*, **123**, Article ID: 231101. https://doi.org/10.1103/PhysRevLett.123.231101

[87] Cuceu, A., Farr, J., Lemos, P. and Font-Ribera, A. (2019) *Journal of Cosmology and Astroparticle Physics*, **10**, Article No. 044.

https://doi.org/10.1088/1475-7516/2019/10/044

[88] Domínguez, A., *et al.* (2019) *The Astrophysical Journal*, **885**, Article No. 137. https://doi.org/10.3847/1538-4357/ab4a0e

[89] Dutta, K., *et al.* (2019) *Physical Review D*, **100**, Article ID: 075028. https://doi.org/10.1103/PhysRevD.100.075028

[90] Fishbach, M., *et al.* (2019) *The Astrophysical Journal Letters*, **871**, Article No. L13. https://doi.org/10.3847/2041-8213/aaf96e

[91] Freedman, W.L., *et al.* (2019) *The Astrophysical Journal*, **882**, Article No. 34. https://doi.org/10.3847/1538-4357/ab2f73

[92] Guo, R.-Y., Zhang, J.-F. and Zhang, X. (2019) *Journal of Cosmology and Astroparticle Physics*, **2**, Article No. 054. https://doi.org/10.1088/1475-7516/2019/02/054

[93] Hotokezaka, K., *et al.* (2019) *Nature Astronomy*, **3**, 940-944. https://doi.org/10.1038/s41550-019-0820-1

[94] Jee, I., *et al.* (2019) *Science*, **365**, 1134-1138. https://doi.org/10.1126/science.aat7371

[95] Kozmanyan, A., Bourdin, H., Mazzotta, P., Rasia, E. and Sereno, M. (2019) *Astronomy & Astrophysics*, **621**, Article No. A34. https://doi.org/10.1051/0004-6361/201833879

[96] Liao, K., Shafieloo, A., Keeley, R.E. and Linder, E.V. (2019) *The Astrophysical Journal Letters*, **886**, Article No. L23. https://doi.org/10.3847/2041-8213/ab5308

[97] Macaulay, E., *et al.* (2019) *Monthly Notices of the Royal Astronomical Society*, **486**, 2184-2196. https://doi.org/10.1093/mnras/stz978

[98] Martinelli, M. and Tutusaus, I. (2019) *Symmetry*, **11**, Article No. 986. https://doi.org/10.3390/sym11080986

[99] Park, C.-G. and Ratra, B. (2019) *Astrophysics and Space Science*, **364**, Article No. 134. https://doi.org/10.1007/s10509-019-3627-8

[100] Reid, M.J., Pesce, D.W. and Riess, A.G. (2019) *The Astrophysical Journal*, **886**, Article No. L27. https://doi.org/10.3847/2041-8213/ab552d

[101] Riess, A.G., *et al.* (2019) *The Astrophysical Journal*, **876**, Article No. 85. https://doi.org/10.3847/1538-4357/ab1422

[102] Riess, A.G. (2019) *Nature Reviews Physics*, **2**, 10-12. https://doi.org/10.1038/s42254-019-0137-0

[103] Rusu, C.E., *et al.* (2020) *Monthly Notices of the Royal Astronomical Society*, **498**, 1440-1468. https://doi.org/10.1093/mnras/stz3451

[104] Ryan, J., Chen, Y. and Ratra, B. (2019) *Monthly Notices of the Royal Astronomical Society*, **488**, 3844-3856. https://doi.org/10.1093/mnras/stz1966

[105] Saha, S. and Sahoo, S. (2019) *The African Review of Physics*, **14**, 7-9.

[106] Shajib, A.J., Birrer, S., Treu, T., Agnello, A., *et al.* (2019) *Monthly Notices of the Royal Astronomical Society*, **494**, 6072-6102. https://doi.org/10.1093/mnras/staa828

[107] Soares-Santos, M., *et al.* (2019) *The Astrophysical Journal Letters*, **876**, Article No. L7. https://doi.org/10.3847/2041-8213/ab14f1

[108] Taubenberger, S., *et al.* (2019) *Astronomy and Astrophysics*, **628**, Article No. L7. https://doi.org/10.1051/0004-6361/201935980

[109] Tiwari, S., Haney, M. and Boetzel, Y. (2019) A Gravitational-Wave Measurement of the Hubble Constant Following the Second Observing Run of Advanced LIGO and Virgo. University of Zurich, Zurich, Not Published. arXiv.org 1908.06060.

[110] Verde, L., Treu, T. and Riess, A.G. (2019) *Nature Astronomy*, **3**, 891-895.

https://doi.org/10.1038/s41550-019-0902-0

[111] Wong, K.C., *et al.* (2019) *Monthly Notices of the Royal Astronomical Society*, **498**, 1420-1439. https://doi.org/10.1093/mnras/stz3094

[112] Yuan, W., *et al.* (2019) *The Astrophysical Journal*, **886**, Article No. 61. https://doi.org/10.3847/1538-4357/ab4bc9

[113] Zhang, X. and Huang, Q.-G. (2019) *Communications in Theoretical Physics*, **71**, 826-830. https://doi.org/10.1088/0253-6102/71/7/826

[114] Zeng, H. and Yan, D. (2019) *The Astrophysical Journal*, **882**, Article No. 87. https://doi.org/10.3847/1538-4357/ab35e3

[115] Abbott, T.M.C., *et al.* (2018) *Monthly Notices of the Royal Astronomical Society*, **480**, 3879-3888. https://doi.org/10.1093/mnras/sty1939

[116] Benetti, M., Graef, L.L. and Alcaniz, J.S. (2018) *Journal of Cosmology and Astroparticle Physics*, **7**, Article No. 066. https://doi.org/10.1088/1475-7516/2018/07/066

[117] Bolejko, K. (2018) *Physical Review D*, **97**, Article ID: 083515. https://doi.org/10.1103/PhysRevD.97.083515

[118] Braatz, J., *et al.* (2018) *Proceedings of the International Astronomical Union*, **13**, 86-91. https://doi.org/10.1017/S1743921317010249

[119] Cantiello, M., *et al.* (2018) *The Astrophysical Journal Letters*, **854**, Article No. L31. https://doi.org/10.3847/2041-8213/aaad64

[120] Chen, H.-Y., Fishbach, M. and Holz, D.E. (2018) *Nature*, **562**, 545-547. https://doi.org/10.1038/s41586-018-0606-0

[121] Choudhury, S.R. and Choubey, S. (2019) *Journal of Cosmology and Astroparticle Physics*, **9**, Article No. 017. https://doi.org/10.1088/1475-7516/2018/09/017

[122] Dhawan, S., Jha, S.W. and Leibundgut, B. (2018) *Astronomy and Astrophysics*, **609**, Article No. A72. https://doi.org/10.1051/0004-6361/201731501

[123] Di Valentino, E. and Melchiorri, A. (2018) *Physical Review D*, **97**, Article ID: 041301. https://doi.org/10.1103/PhysRevD.97.041301

[124] Gómez-Valent, A. and Amendola, L. (2018) *Journal of Cosmology and Astroparticle Physics*, **4**, Article No. 051. https://doi.org/10.1088/1475-7516/2018/04/051

[125] Grillo, C., *et al.* (2018) *The Astrophysical Journal*, **860**, Article No. 94. https://doi.org/10.3847/1538-4357/aac2c9

[126] Hoeneisen, B. (2018) *International Journal of Astronomy and Astrophysics*, **8**, 386-405. https://doi.org/10.4236/ijaa.2018.84027

[127] Lee, M.G. and Jang, I.S. (2018) The TRGB and the Hubble Constant in 2017: TIPSNU. In: Jensen, J., Michael Rich, R. and de Grijs, R., Eds., *Stellar Populations and the Distance Scale*, Vol. 514, Astronomical Society of the Pacific, San Francisco, 143-150.

[128] Riess, A.G., *et al.* (2018) *The Astrophysical Journal*, **861**, 1-13.

[129] Riess, A.G., *et al.* (2018) *The Astrophysical Journal*, **855**, Article No. 136.

[130] Van Putten, M.H.P.M. (2018) *European Physical Journal Web of Conferences*, **168**, Article No. 08005. https://doi.org/10.1051/epjconf/201816808005

[131] Vitale, S. and Chen, H.-Y. (2018) *Physical Review Letters*, **121**, Article ID: 021303. https://doi.org/10.1103/PhysRevLett.121.021303

[132] Yu, H., Ratra, B. and Wang, F.-Y. (2018) *The Astrophysical Journal*, **856**, Article

No. 3. https://doi.org/10.3847/1538-4357/aab0a2

[133] Zhang, J. (2018) *Publications of the Astronomical Society of the Pacific*, **130**, Article ID: 117002. https://doi.org/10.1088/1538-3873/aae4ca

[134] Abbott, B.P., *et al.* (2017) *Nature*, **551**, 85-88. https://doi.org/10.1038/nature24471

[135] Bethapudi, S. and Desai, S. (2017) *The European Physical Journal Plus*, **132**, Article No. 78. https://doi.org/10.1140/epjp/i2017-11390-3

[136] Bonvin, V., *et al.* (2017) *Monthly Notices of the Royal Astronomical Society*, **465**, 4914-4930. https://doi.org/10.1093/mnras/stw3006

[137] Cardona, W., Kunza, M. and Valeria, P. (2017) *Journal of Cosmology and Astroparticle Physics*, **3**, Article No. 056. https://doi.org/10.1088/1475-7516/2017/03/056

[138] Chen, Y., Kumar, S. and Ratra, B. (2017) *The Astrophysical Journal*, **835**, Article No. 86. https://doi.org/10.3847/1538-4357/835/1/86

[139] Farooq, O., Madiyar, F.R., Crandall, S. and Ratra, B. (2017) *The Astrophysical Journal*, **835**, Article No. 26. https://doi.org/10.3847/1538-4357/835/1/26

[140] Feeney, S.M., Mortlock, D.J. and Dalmasso, N. (2017) *Monthly Notices of the Royal Astronomical Society*, **476**, 3861-3882. https://doi.org/10.1093/mnras/sty418

[141] Grieb, J.N., *et al.* (2017) *Monthly Notices of the Royal Astronomical Society*, **467**, 2085-2112. https://doi.org/10.1093/mnras/stw3384

[142] Guo, R.-Y. and Zhang, X. (2017) *The European Physical Journal C*, **77**, Article No. 882. https://doi.org/10.1140/epjc/s10052-017-5454-9

[143] Hjorth, J., *et al.* (2017) *The Astrophysical Journal Letters*, **848**, Article No. L31. https://doi.org/10.3847/2041-8213/aa9110

[144] Huang, H. and Huang, L. (2017) *International Journal of Modern Physics D*, **26**, Article No. 1740001. https://doi.org/10.1142/S0218271817400016

[145] Jang, I.S. and Lee, M.G. (2017) *The Astrophysical Journal*, **836**, Article No. 74. https://doi.org/10.3847/1538-4357/836/1/74

[146] Pritychenko, B. (2017) *EPJ Web of Conferences*, **146**, Article No. 01006. https://doi.org/10.1051/epjconf/201714601006

[147] Wang, Y., Xu, L. and Zhao, G.-B. (2017) *The Astrophysical Journal*, **849**, Article No. 84. https://doi.org/10.3847/1538-4357/aa8f48

[148] Wei, J.-J. and Wu, X.-F. (2017) *The Astrophysical Journal*, **838**, Article No. 160. https://doi.org/10.3847/1538-4357/aa674b

[149] Wong, K.C., *et al.* (2017) *Monthly Notices of the Royal Astronomical Society*, **465**, 4895-4913. https://doi.org/10.1093/mnras/stw3077

[150] Zhang, B.R. (2017) *Monthly Notices of the Royal Astronomical Society*, **471**, 2254-2285. https://doi.org/10.1093/mnras/stx1600

[151] Ade, P.A.R., *et al.* (2016) *Astronomy & Astrophysics*, **594**, Article No. A13. https://doi.org/10.1051/0004-6361/201525830

[152] Gao, F., *et al.* (2016) *The Astrophysical Journal*, **817**, Article No. 128. https://doi.org/10.3847/0004-637X/817/2/128

[153] Ichiki, K., Yoo, C.-M. and Oguri, M. (2016) *Physical Review D*, **93**, Article ID: 023529. https://doi.org/10.1103/PhysRevD.93.023529

[154] Ludović, V.V., D'Agostino, R. and Vittorio, N. (2016) *Astronomy and Astrophysics*, **595**, Article No. A109. https://doi.org/10.1051/0004-6361/201628217

[155] Moresco, M., *et al.* (2016) *Journal of Cosmology and Astroparticle Physics*, **5**, Arti-

cle No. 014. https://doi.org/10.1088/1475-7516/2016/05/014

[156] Riess, A.G., *et al.* (2016) *The Astrophysical Journal*, **826**, Article No. 56. https://doi.org/10.3847/0004-637X/826/1/56

[157] Tully, R.B., Courtois, H.M. and Sorce, J.G. (2016) *The Astronomical Journal*, **152**, Article No. 50. https://doi.org/10.3847/0004-6256/152/2/50

[158] Cheng, C. and Huang, Q.G. (2015) *Science China Physics, Mechanics & Astronomy*, **58**, Article No. 599801. https://doi.org/10.1007/s11433-015-5684-5

[159] Cuesta, A.J., Verde, L., Riess, A. and Jimenez, R. (2015) *Monthly Notices of the Royal Astronomical Society*, **448**, 3463-3471. https://doi.org/10.1093/mnras/stv261

[160] Jang, I.S. and Lee, M.G. (2015) *The Astrophysical Journal*, **807**, Article No. 133. https://doi.org/10.1088/0004-637X/807/2/133

[161] Kumar, S.R., Stalin, C.S. and Prabhu, T.P. (2015) *Astronomy and Astrophysics*, **580**, Article No. A38. https://doi.org/10.1051/0004-6361/201423977

[162] Kuo, C.Y., Braatz, J.A., Lo, K.Y., Reid, M.J., Suyu, S.H., Pesce, D.W., Condon, J.J., Henkel, C. and Impellizzeri, C.M.V. (2015) *The Astrophysical Journal*, **800**, Article No. 26. https://doi.org/10.1088/0004-637X/800/1/26

[163] Rigault, M. and Schombert, J.M. (2015) *The Astrophysical Journal*, **802**, Article No. 18. https://doi.org/10.1088/0004-637X/802/1/18

[164] Ade, P.A.R., *et al.* (2014) *Astronomy & Astrophysics*, **571**, Article No. A16. https://doi.org/10.1051/0004-6361/201321591

[165] Ben-Dayan, I., Durrer, R., Marozzi, G. and Schwarz, D.J. (2014) *Physical Review Letters*, **112**, Article ID: 221301. https://doi.org/10.1103/PhysRevLett.112.221301

[166] Bennett, C.L., *et al.* (2014) *The Astrophysical Journal*, **794**, Article No. 135. https://doi.org/10.1088/0004-637X/794/2/135

[167] Busti, V.C., Clarkson, C. and Seikel, M. (2014) *Proceedings of the International Astronomical Union*, **10**, 25-27. https://doi.org/10.1017/S1743921314013751

[168] Efstathiou, G. (2014) *Monthly Notices of the Royal Astronomical Society*, **440**, 1138-1152. https://doi.org/10.1093/mnras/stu278

[169] Lima, J.A.S. and Cunha, J.V. (2014) *The Astrophysical Journal Letters*, **781**, Article No. L38. https://doi.org/10.1088/2041-8205/781/2/L38

[170] Bennett, C.L., *et al.* (2013) *The Astrophysical Journal*, **208**, Article No. 20. https://doi.org/10.1088/0067-0049/208/2/20

[171] Braatz, J., *et al.* (2013) *Proceedings of the International Astronomical Union*, **8**, 255-261. https://doi.org/10.1017/S1743921312021515

[172] Farooq, O. and Rathra, B. (2013) *The Astrophysical Journal Letters*, **766**, Article No. L7. https://doi.org/10.1088/2041-8205/766/1/L7

[173] Hinshaw, G., *et al.* (2013) *The Astrophysical Journal Supplement Series*, **208**, Article No. 19. https://doi.org/10.1088/0067-0049/208/2/19

[174] Humphreys, E.M.L., Reid, M.J., Moran, J.M., Greenhill, L.J. and Argon, A.L. (2013) *The Astrophysical Journal*, **775**, Article No. 13. https://doi.org/10.1088/0004-637X/775/1/13

[175] Kuo, C.Y., Braatz, J.A., Reid, M.J., Lo, K.Y., Condon, J.J., Impellizzeri, C.M.V. and Henkel, C. (2013) *The Astrophysical Journal*, **767**, Article No. 155. https://doi.org/10.1088/0004-637X/767/2/155

[176] Pietrzyński, G., *et al.* (2013) *Nature*, **495**, 76-79. https://doi.org/10.1038/nature11878

[177] Reid, M.J., *et al.* (2013) *The Astrophysical Journal*, **767**, Article No. 154. https://doi.org/10.1088/0004-637X/767/2/154

[178] Salvatelli, V., Marchini, A., Lopez-Honorez, L. and Mena, O. (2013) *Physical Review D*, **88**, Article ID: 023531. https://doi.org/10.1103/PhysRevD.88.023531

[179] Scowcroft, V., *et al.* (2013) *Proceedings of the International Astronomical Union*, **8**, 274-281. https://doi.org/10.1017/S1743921312021540

[180] Sereno, M. and Paraficz, D. (2013) *Monthly Notices of the Royal Astronomical Society*, **437**, 600-605. https://doi.org/10.1093/mnras/stt1938

[181] Suyu, S.H., *et al.* (2013) *The Astrophysical Journal*, **766**, Article No. 70. https://doi.org/10.1088/0004-637X/766/2/70

[182] Tully, R.B., *et al.* (2013) *The Astronomical Journal*, **146**, Article No. 86. https://doi.org/10.1088/0004-6256/146/4/86

[183] Xia, J.-Q., Li, H. and Zhang, X. (2013) *Physical Review D*, **88**, Article ID: 063501. https://doi.org/10.1103/PhysRevD.88.063501

[184] Calabrese, E., Archidiacono, M., Melchiorri, A. and Ratra, B. (2012) *Physical Review D*, **86**, Article ID: 043520. https://doi.org/10.1103/PhysRevD.86.043520

[185] Chávez, R., *et al.* (2012) *Monthly Notices of the Royal Astronomical Society*, **425**, L56-L60. https://doi.org/10.1111/j.1745-3933.2012.01299.x

[186] Colless, M., Beutler, F. and Blake, C. (2012) *Proceedings of the International Astronomical Union*, **8**, 319-322. https://doi.org/10.1017/S1743921312021618

[187] Freedman, W.L., *et al.* (2012) *The Astrophysical Journal*, **758**, Article No. 24. https://doi.org/10.1088/0004-637X/758/1/24

[188] Del Pozzo, W. (2012) *Physical Review D*, **86**, Article ID: 043011. https://doi.org/10.1103/PhysRevD.86.043011

[189] Riess, A.G., Fliri, J. and Valls-Gabaud, D. (2012) *The Astrophysical Journal*, **745**, Article No. 156. https://doi.org/10.1088/0004-637X/745/2/156

[190] Wang, M. (2012) *AIP Conference Proceedings*, **1441**, 503-505. https://doi.org/10.1063/1.3700599

[191] Chen, G. and Ratra, B. (2011) *Publications of the Astronomical Society of the Pacific*, **123**, Article No. 1127. https://doi.org/10.1086/662131

[192] Beutler, F., *et al.* (2011) *Monthly Notices of the Royal Astronomical Society*, **416**, 3017-3032. https://doi.org/10.1111/j.1365-2966.2011.19250.x

[193] Jarosik, N., *et al.* (2011) *The Astrophysical Journal Supplement Series*, **192**, Article No. 14. https://doi.org/10.1088/0067-0049/192/2/14

[194] Riess, A.G., *et al.* (2011) *The Astrophysical Journal*, **730**, Article No. 119. https://doi.org/10.1088/0004-637X/730/2/119

[195] Freedman, W.L. and Madore, B.F. (2010) *Annual Review of Astronomy and Astrophysics*, **48**, 673-710. https://doi.org/10.1146/annurev-astro-082708-101829

[196] Paraficz, D. and Hjorth, J. (2010) *The Astrophysical Journal*, **712**, 1378-1384. https://doi.org/10.1088/0004-637X/712/2/1378

[197] Suyu, S.H., *et al.* (2010) *The Astrophysical Journal*, **711**, 201-221. https://doi.org/10.1088/0004-637X/711/1/201

[198] Hinshaw, G., *et al.* (2009) *The Astrophysical Journal Supplement Series*, **180**, 225-245. https://doi.org/10.1088/0067-0049/180/2/225

[199] Komatsu, *et al.* (2009) *The Astrophysical Journal Supplement Series*, **180**, 330-376. https://doi.org/10.1088/0067-0049/180/2/330

[200] Riess, A.G., *et al.* (2009) *The Astrophysical Journal*, **699**, 539-563. https://doi.org/10.1088/0004-637X/699/1/539

[201] Russell, D.G. (2009) *Journal of Astrophysics and Astronomy*, **30**, 93-118. https://doi.org/10.1007/s12036-009-0006-9

[202] Leith, B.M., Ng, S.C.C. and Wiltshir, D.L. (2008) *The Astrophysical Journal*, **672**, L91-L94. https://doi.org/10.1086/527034

[203] Vuissoz, C., *et al.* (2008) *Astronomy & Astrophysics*, **488**, 481-490. https://doi.org/10.1051/0004-6361:200809866

[204] Oguri, M. (2007) *The Astrophysical Journal*, **660**, 1-15. https://doi.org/10.1086/513093

[205] Spergel, D.N., *et al.* (2007) *The Astrophysical Journal Supplement Series*, **170**, 377-408. https://doi.org/10.1086/513700

[206] Bonamente, M., Joy, M.K., La Roque, S.J. and Carlstrom, J.E. (2006) *The Astrophysical Journal*, **647**, 25-54. https://doi.org/10.1086/505291

[207] Hütsi, G. (2006) Cosmic Sound: Measuring the Universe with Baryonic Acoustic Oscillations. Dissertation, Ludwig Maximilian University of Munich, München, 1-148, Not Published. (uni-muenchen.de)

[208] Ngeow, C. and Kanbur, S.M. (2006) *The Astrophysical Journal*, **642**, L29-L32. https://doi.org/10.1086/504478

[209] Sandage, A., *et al.* (2006) *The Astrophysical Journal*, **653**, 843-860. https://doi.org/10.1086/508853

[210] Wang, X., Wang, L., Pain, R., Zhou, X. and Li, Z. (2006) *The Astrophysical Journal*, **645**, 488-505. https://doi.org/10.1086/504312

[211] Gibson, B.K. and Brook, C.B. (2005) *Symposium—International Astronomical Union*, **201**, 200-208. https://doi.org/10.1017/S0074180900216264

[212] Hamuy, M. (2005) The Standard Candle Method for Type II Supernovae and the Hubble Constan. In: Marcaide, J.M and Weiler, K.W., Eds., *Cosmic Explosions*, Vol. 99, Springer, Berlin, Heidelberg, 535-541. https://doi.org/10.1007/3-540-26633-X_71

[213] Magain, P. (2005) Time Delay in Gravitational Lenses: An Alternative Route to the Hubble Constant. *Proceedings of ASP Conference Series*, Vol. 335, Brussels, 19-22 July 2004, 207-214.

[214] Olivares, G., Atrio-Barandela, F. and Pavón, D. (2005) *Physical Review D*, **71**, Article ID: 063523. https://doi.org/10.1103/PhysRevD.71.063523

[215] Riess, A.G. (2005) *The Astrophysical Journal*, **627**, 579-607. https://doi.org/10.1086/430497

[216] Schmidt, R.W., Allen, S.W. and Fabian, A.C. (2004) *Monthly Notices of the Royal Astronomical Society*, **352**, 1413-1420. https://doi.org/10.1111/j.1365-2966.2004.08032.x

[217] Stritzinger, M. and Leibundgut, B. (2004) *Astronomy & Astrophysics*, **431**, 423-431. https://doi.org/10.1051/0004-6361:20041630

[218] Udomprasert, P.S., Mason, B.S., Readhead, A.C.S. and Pearson, T.J. (2004) *The Astrophysical Journal*, **615**, 63-81. https://doi.org/10.1086/423946

[219] Boffi, F.R. and Riess, A.G. (2003) The Type Ia Supernova 1998aq and the Hubble Constant. *ASP Conference Proceedings*, Vol. 303, La Palma, 27-31 May 2002, 101-104.

[220] Dumin, Y.V. (2003) *Advances in Space Research*, **31**, 2461-2466.

https://doi.org/10.1016/S0273-1177(03)00533-7

[221] Jimenez, R., Verde, L., Treu, T. and Stern, D. (2003) *The Astrophysical Journal*, **593**, 622-629. https://doi.org/10.1086/376595

[222] Koopmans, L.V.E., Treu, T., Fassnacht, C.D., Blandford, R.D. and Surpi, G. (2003) *The Astrophysical Journal*, **599**, 70-85. https://doi.org/10.1086/379226

[223] Mei, S., Scodeggio, M., Silva, D.R. and Quinn, P.J. (2003) *Astronomy and Astrophysics*, **399**, 441-448. https://doi.org/10.1051/0004-6361:20021800

[224] Saunders, R., *et al.* (2003) *Monthly Notices of the Royal Astronomical Society*, **341**, 937-940. https://doi.org/10.1046/j.1365-8711.2003.06467.x

[225] Spergel, D.N., *et al.* (2003) *The Astrophysical Journal Supplement Series*, **148**, 175-174. https://doi.org/10.1086/377226

[226] Fassnacht, C.D., Xanthopoulos, E., Koopmans, L.V.E. and Rusin, D. (2002) *The Astrophysical Journal*, **581**, 823-835. https://doi.org/10.1086/344368

[227] Freedman, W.L. (2002) The Status of the Hubble Constant. In: Metcalfe, N. and Shanks, T., Eds., *A New Era in Cosmology. ASP Conference Proceedings*, Vol. 283, Astronomical Society of the Pacific, San Francisco, 249-257.

[228] Grainge, K., *et al.* (2002) *Monthly Notices of the Royal Astronomical Society*, **333**, 318-326. https://doi.org/10.1046/j.1365-8711.2002.05429.x

[229] Kochanek, C.S. (2002) Gravitational Lenses, the Distance Ladder and the Hubble Constant: A New Dark Matter Problem. arXiv:astro-ph/0204043v1.

[230] Tikhonov, N.A. and Galazoutdinova, O.A. (2002) *Astrophysics*, **45**, 253-266. https://doi.org/10.1023/A:1020168130980

[231] Treu, T. and Koopmans, L.V.E. (2002) *Monthly Notices of the Royal Astronomical Society*, **337**, L6-L10. https://doi.org/10.1046/j.1365-8711.2002.06107.x

[232] Freedman, W.L., *et al.* (2001) *The Astrophysical Journal*, **553**, 47-72. https://doi.org/10.1086/320638

[233] Itoh, N. (2001) *The Astronomical Herald*, **94**, 214-220.

[234] Jensen, J.B., *et al.* (2001) *The Astrophysical Journal*, **550**, 503-521. https://doi.org/10.1086/319819

[235] Koopmans, L.V.E. and The CLASS Collaboration (2001) *Publication of Astronomical Society of Australia*, **18**, 179-181. https://doi.org/10.1071/AS01024

[236] Liu, M.C. and Graham, J.R. (2001) *The Astrophysical Journal*, **557**, L31-L34. https://doi.org/10.1086/323174

[237] Mason, B.S., Myers, S.T. and Readhead, A.C.S. (2001) *The Astrophysical Journal*, **555**, L11-L15. https://doi.org/10.1086/321737

[238] Mei, S., Quinn, P.J. and Silva, D.R. (2001) *Astronomy and Astrophysics*, **371**, 779-794. https://doi.org/10.1051/0004-6361:20010427

[239] Tonry, J.L. and High-Z Supernova Search Team (2001) Type Ia Supernovae, the Hubble Constant, the Cosmological Constant and the Age of the Universe. In: von Hippel, T., Simpson, C. and Manset, N., Eds., *Astrophysical Ages and Times Scales*, *ASP Conference Series*, Vol. 245, San Francisc, Astronomical Society of the Pacific, 593-601.

[240] Willick, J.A. and Batra, P. (2001) *The Astrophysical Journal*, **548**, 564-584. https://doi.org/10.1086/319005

[241] Wang, X.-F., Chen, L. and Li, Z.-W. (2001) *Chinese Physics Letters*, **18**, 154-156. https://doi.org/10.1088/0256-307X/18/1/354

[242] Ferrarese, L., *et al.* (2000) *The Astrophysical Journal*, **529**, 745-767. https://doi.org/10.1086/308309

[243] Gibson, B.K., *et al.* (2000) *The Astrophysical Journal*, **529**, 723-744. https://doi.org/10.1086/308306

[244] Mould, J.R., *et al.* (2000) *The Astrophysical Journal*, **529**, 786-794. https://doi.org/10.1086/308304

[245] Sakai, S. (2000) *The Astrophysical Journal*, **529**, 698-722. https://doi.org/10.1086/308305

[246] Tikhonov, N.A., Galazoutdinova, O.A. and Drozdovskii, I.O. (2000) *Astrophysics*, **43**, 367-380. https://doi.org/10.1023/A:1010902305550

[247] Biggs, A.D., Browne, I.W.A., Helbig, P., Koopmans, L.V.E., Wilkinson, P.N. and Perley, R.A. (1999) *Monthly Notices of the Royal Astronomical Society*, **304**, 349-358. https://doi.org/10.1046/j.1365-8711.1999.02309.x

[248] Chae, K.-H. (1999) *The Astrophysical Journal*, **524**, 582-590. https://doi.org/10.1086/307842

[249] Collier, S., Horne, K., Wanders, I. and Peterson, B.M. (1999) *Monthly Notices of the Royal Astronomical Society*, **302**, L24-L28. https://doi.org/10.1046/j.1365-8711.1999.02250.x

[250] Freedman, W.L. and Feng, L.L. (1999) *Proceedings of the National Academy of Sciences of the United States of America*, **96**, 11063-11064. https://doi.org/10.1073/pnas.96.20.11063

[251] Jha, S., *et al.* (1999) *The Astrophysical Journal Supplement Series*, **125**, 73-97. https://doi.org/10.1086/313275

[252] Mason, B.S. (1999) An Improved Measurement of the Hubble Constant Using the Sunyaev-Zeldovich Effect. Dissertations, University of Pennsylvania, Philadelphia, UMI Number: AAI9953569. https://repository.upenn.edu/dissertations/AAI9953569

[253] Mazumdar, A. and Narasimba, D. (1999) *Bulletin of the Astronomical Society of India*, **27**, 267.

[254] Tanvir, N.R. (1999) *Monthly Notices of the Royal Astronomical Society*, **310**, 175-188. https://doi.org/10.1046/j.1365-8711.1999.02954.x

[255] Tripp, R. and Branch, D. (1999) *The Astrophysical Journal*, **525**, 209-214. https://doi.org/10.1086/307883

[256] Branch, D. (1998) *Annual Review of Astronomy and Astrophysics*, **36**, 17-55. https://doi.org/10.1146/annurev.astro.36.1.17

[257] Goicoechea, L.J., Mediavilla, E., Oscoz, A., Serra, M. and Buttrago, J. (1998) *Astrophysics and Space Science*, **261**, 341-344. https://doi.org/10.1023/A:1002042026159

[258] Harris, W.E., *et al.* (1998) *Nature*, **395**, 45-47. https://doi.org/10.1038/25673

[259] Hughes, J.P. and Birkinshaw, M. (1998) *The Astrophysical Journal*, **501**, 1-14. https://doi.org/10.1086/305788

[260] Lauer, T.R., Tonry, J.L., Postman, M., Ajhar, E.A. and Holtzman, J.A. (1998) *The Astrophysical Journal*, **499**, 577-588. https://doi.org/10.1086/305671

[261] Riess, A.G., *et al.* (1998) *The Astronomical Journal*, **116**, 1009-1038. https://doi.org/10.1086/300499

[262] Tamman, G.A. and Labhardt, L. (1998) A Forty-Year Search for the Hubble Constant. In: Riffert, H., Ruder, H., Nollert, H.P. and Hehl, F.W., Eds., *Relativistic Astrophysics*, Vieweg+Teubner Verlag, Wiesbaden, 238-261.

https://doi.org/10.1007/978-3-663-11294-5_15

[263] Tripp, R. (1998) *Astronomy and Astrophysics*, **331**, 815-820.

[264] Giovanelli, R. (1997) The Extragalactic Distance Scale. *Proceedings of the ST ScI May Symposium*, Baltimore, 7-10 May 1996, 113.

[265] Gregg, M.D. (1997) *New Astronomy*, **1**, 363-371. https://doi.org/10.1016/S1384-1076(97)00005-5

[266] Hjorth, J. and Tanvir, N.R. (1997) *The Astrophysical Journal*, **482**, 68-74. https://doi.org/10.1086/304124

[267] Holzapfel, W.L., *et al.* (1997) *The Astrophysical Journal*, **480**, 449-465. https://doi.org/10.1086/303979

[268] Hoyle, F., Burhidge, G. and Narlikar, J.V. (1997) *Monthly Notices of the Royal Astronomical Society*, **286**, 173-182. https://doi.org/10.1093/mnras/286.1.173

[269] Schechter, P.L. (1997) *The Astrophysical Journal*, **475**, L85-L88. https://doi.org/10.1086/310478

[270] Sciama, D.W. (1997) *Monthly Notices of the Royal Astronomical Society*, **289**, 945-947. https://doi.org/10.1093/mnras/289.4.945

[271] Tonry, J.L., Blakeslee, J.P., Ajhar, E.A. and Dressler, A. (1997) *The Astrophysical Journal*, **475**, 399-413. https://doi.org/10.1086/303576

[272] Amendola, L. (1996) *Astronomy and Astrophysics*, **312**, 353-356.

[273] Biesiada, M. (1996) *Monthly Notices of the Royal Astronomical Society*, **283**, 997-982. https://doi.org/10.1093/mnras/283.3.977

[274] Forbes, D.A., Brodie, J.P. and Huchra, J. (1996) *Astronomical Journal*, **112**, 2448-2460. https://doi.org/10.1086/118194

[275] Kobyashi, S., Sasaki, S. and Suto, Y. (1996) *Publications of the Astronomical Society of Japan*, **48**, L107-L111. https://doi.org/10.1093/pasj/48.6.L107

[276] Mallik, D.C.V. (1996) *Current Science*, **71**, 547-552. https://www.jstor.org/stable/24098091

[277] Schaefer, B.E. (1996) *The Astrophysical Journal*, **460**, L19-L23. https://doi.org/10.1086/309963

[278] Grogin, N.A. and Narayan, R. (1995) *The Astrophysical Journal*, **473**, 570-571. https://doi.org/10.1086/178171

[279] Herbig, T., Lawrence, C.R., Readhead, A.C.S. and Gulkis, S. (1995) *The Astrophysical Journal*, **449**, L5-L8. https://doi.org/10.1086/309616

[280] Holzapfel, W.L., *et al.* (1995) *Bulletin of the American Astronomical Society*, **27**, 1413.

[281] Jones, M. (1995) *Astrophysical Letters and Communications*, **32**, 347-353.

[282] Kennicutt Jr., R.C., Freedman, W.L. and Mould, J.R. (1995) *The Astrophysical Journal*, **110**, 1476-1491. https://doi.org/10.1086/117621

[283] Mould, J., *et al.* (1995) *The Astrophysical Journal*, **449**, 413-421.

[284] Nakamura, T.T. and Suto, Y. (1995) *Astrophysical Journal Letters*, **447**, L65-L68. https://doi.org/10.1086/309580

[285] Raphaeli, Y. (1995) *Annual Review of Astronomy and Astrophysics*, **33**, 541-579. https://doi.org/10.1146/annurev.aa.33.090195.002545

[286] Scheafer, B.E. (1995) *The Astrophysical Journal*, **447**, L13-L16.

[287] Tanvir, N.R., Shanks, T., Ferguson, H.C. and Robinson, D.R.T. (1995) *Nature*, **377**, 27-31. https://doi.org/10.1038/377027a0

[288] Whitmore, B.C. and Schweizer, F. (1995) *The Astronomical Journal*, **210**, 960-980 and 1411-1416 (For Graphics).

[289] Birkinshaw, M. and Hughes, J.P. (1994) *The Astrophysical Journal*, **420**, 33-43. https://doi.org/10.1086/173540

[290] Freedman, W., *et al.* (1994) *Nature*, **371**, 757-762. https://doi.org/10.1038/371757a0

[291] Lu, N.Y., Salpeter, E.E. and Hoffman, G.L. (1994) *The Astrophysical Journal*, **426**, 473-485. https://doi.org/10.1086/174083

[292] Schmidt, B.P., *et al.* (1994) *Astrophysical Journal*, **432**, 42-48.

[293] Tully, R.B. (1993) *Proceedings of the National Academy of Sciences of the United States of America*, **90**, 4806-4810. https://doi.org/10.1073/pnas.90.11.4806

[294] Duemmler, R. (1992) *Astronomy and Astrophysics*, **264**, 1-10.

[295] Lauer, T.D. and Postman, M. (1992) *The Astrophysical Journal*, **400**, L47. https://doi.org/10.1086/186646

[296] Leibundgut, B. and Pinto, P. (1992) *The Astrophysical Journal*, **401**, 49-59. https://doi.org/10.1086/172037

[297] Birkinshaw, M., Hughes, J.P. and Arnaud, K.A. (1991) *The Astrophysical Journal*, **379**, 466-481. https://doi.org/10.1086/170522

[298] Tonry, J.L. (1991) *Astrophysical Journal Letters*, **373**, L1. https://doi.org/10.1086/186037

[299] Sandage, A. and Tammann, G.A. (1990) *The Astrophysical Journal*, **365**, 1-12. https://doi.org/10.1086/169453

[300] Visvanathan, N. (1990) *Australian Journal of Physics*, **43**, 189-210. https://doi.org/10.1071/PH900189

[301] Sandage, A. and Tammann, G. (1988) *The Astrophysical Journal*, **328**, 1-3. https://doi.org/10.1086/166263

[302] Dressler, A. (1987) *The Astrophysical Journal*, **317**, 1-10. https://doi.org/10.1086/165251

[303] Tamman, G.A. and Sandage, A. (1985) *The Astrophysical Journal*, **294**, 81-95. https://doi.org/10.1086/163277

[304] Visvanathan, N. (1983) *The Astrophysical Journal*, **275**, 430-444. https://doi.org/10.1086/161544

[305] Hanes, D.A. (1979) *Monthly Notices of the Royal Astronomical Society*, **188**, 901-909. https://doi.org/10.1093/mnras/188.4.901

[306] Bottinelli, L. and Gouguenheim, L. (1976) *Astronomy and Astrophysics*, **51**, 275-306.

[307] Sandage, A. and Tammann, G.A. (1976) *The Astrophysical Journal*, **210**, 7-24. https://doi.org/10.1086/154798

[308] Sandage, A. and Tammann, G.A. (1975) *The Astrophysical Journal*, **197**, 265-280. https://doi.org/10.1086/153510

[309] Sandage, A. and Tammann, G.A. (1974) *The Astrophysical Journal*, **194**, 559-568. https://doi.org/10.1086/153275

[310] Sandage, A. and Tammann, G.A. (1974) *The Astrophysical Journal*, **194**, 223-243. https://doi.org/10.1086/153238

Annex A (C++ Software)

```
// This software finds "the best" experimental value of H0 with a set of 508 data
//Compiled on Dev-C++ 5.11 available for free at:
//              https://sourceforge.net/projects/orwelldevcpp/
#include<stdio.h>
#include<stdbool.h>
#include<math.h>
#define printf __mingw_printf
#define nbH0 508 //Number of measurements of H0 analyzed
#define Pi 3.141592654 //Definition of Pi
double Mean[5],Sigma[5],Multiplier[5];//Caracteristics of Gaussian curves
double A,B,C; //Coefficients of the quadratic equation of the tip
double LMSTip; //Least mean square for the approximation tip curve
double BEH; //Best estimate of H0
double H0[2*nbH0-1],NbCrossings[2*nbH0-1];
double nbCrossings[2*nbH0-1]; //Vector of number of crossings
double Accuracy_ppm; //Accuracy of H0 compared to the theoretical value
double TVH = 72.09548580; //Theoretical value of H0 (in km/(s*MParsec)
unsigned int PosTipIndex; //Index corresponding to the tip of nbCrossing array
int n = 20; //Sample before & after PosTipIndex to build the tip equation

double Sqr(double value) {return value*value;} //***Returns the square value

//***Function that returns the square root value
double Sqrt(double Value) {
   double D; /*Dummy value*/   double V; /*Returned value*/   int i;
/*Counter*/
   V=0;   D=Value;
   for (i=0;i<=50;i++) {   //Gives 50 bits of precision
      D=-D/2;
      if (D<0) while (V*V>Value) V=V+D; else while (V*V<Value) V=V+D;}
   return V;
   }   //End of Sqrt

double Exp(double Value) { return pow(2.718281828,Value);} //***e^Value

//***This procedure creates a table of 2*nbH increasing values
//***of H0[i] with the tolerances T[i] and the signs +/- Variation[i].
void CreateTableOfCrossingH0Ranges(void) {
   double PT[nbH0],NT[nbH0]; //Positive tolerance and negative tolerance
   double Variation[2*nbH0]; //Variation from the tolerance range
   double DH0,DSgn; //Dummy H0 and Sgn used to put H in increasing order
   int DeltaCrossings; //Variation of on the number of crossings
```

```
int i,j,k; //Counters
i=0;
//We enumerate all H0 values and their tolerance range found on Internet
//In brackets, we add the bibliographic references
H0[i]=69;        PT[i]=+16;     NT[i++]=-8; //[24]Abbott et al.
H0[i]=70;        PT[i]=+2.7;    NT[i++]=-2.7; //[25]Addisson
H0[i]=72.4;      PT[i]=+3.9;    NT[i++]=-4.8; //[25]Addisson
H0[i]=73.1;      PT[i]=+3.3;    NT[i++]=-3.9; //[25]Addisson
H0[i]=73.2;      PT[i]=+1.3;    NT[i++]=-1.3; //[25]Addisson
H0[i]=68.7;      PT[i]=+1.3;    NT[i++]=-1.3; //[25]Addisson
H0[i]=73.5;      PT[i]=+5.3;    NT[i++]=-5.3; //[26]Baxter & Sherwin
H0[i]=73.3;      PT[i]=+0.7;    NT[i++]=-0.7; //[27]Blakeslee et al.
H0[i]=73.78;     PT[i]=+0.84;   NT[i++]=-0.84; //[28]Bonilla
H0[i]=73.577;    PT[i]=+0.106;  NT[i++]=-0.106; //[29]Dainotti et al.
H0[i]=73.493;    PT[i]=+0.144;  NT[i++]=-0.144; //[29]Dainotti et al.
H0[i]=73.222;    PT[i]=+0.262;  NT[i++]=-0.262; //[29]Dainotti et al.
H0[i]=73.664;    PT[i]=+0.223;  NT[i++]=-0.223; //[29]Dainotti et al.
H0[i]=73.576;    PT[i]=+0.105;  NT[i++]=-0.105; //[29]Dainotti et al.
H0[i]=73.513;    PT[i]=+0.142;  NT[i++]=-0.142; //[29]Dainotti et al.
H0[i]=73.192;    PT[i]=+0.265;  NT[i++]=-0.265; //[29]Dainotti et al.
H0[i]=73.678;    PT[i]=+0.223;  NT[i++]=-0.223; //[29]Dainotti et al.
H0[i]=71.8;      PT[i]=+3.9;    NT[i++]=-3.3; //[30]Denzel et al.
H0[i]=72.94;     PT[i]=+0.75;   NT[i++]=-0.75; //[31]Di Valentino
H0[i]=72.7;      PT[i]=+1.1;    NT[i++]=-1.1; //[31]Di Valentino
H0[i]=68.8;      PT[i]=+45.7;   NT[i++]=-25.5; //[32]Gayathri et al.
H0[i]=62.3;      PT[i]=+9.1;    NT[i++]=-9.1; //[33]Hagstotz et al.
H0[i]=70.5;      PT[i]=+2.37;   NT[i++]=-2.37; //[34]Kethan et al.
H0[i]=72.86;     PT[i]=+0.036;  NT[i++]=-0.036; //Mercier (this document)
H0[i]=72.105;    PT[i]=+0.036;  NT[i++]=-0.036; //Mercier (this document)
H0[i]=68.3;      PT[i]=+4.6;    NT[i++]=-4.6; //[35]Mukherjee et al.
H0[i]=70;        PT[i]=+0.5;    NT[i++]=-0.5; //[36]Park et al.
H0[i]=65.1;      PT[i]=+3;      NT[i++]=-5.4; //[37]Philcox et al.
H0[i]=65.6;      PT[i]=+3.4;    NT[i++]=-3.5; //[37]Philcox et al.
H0[i]=70.6;      PT[i]=+3.7;    NT[i++]=-5; //[37]Philcox et al.
H0[i]=78.3;      PT[i]=+2.9;    NT[i++]=-2.9; //[38]Qi et al.
H0[i]=73.6;      PT[i]=+1.8;    NT[i++]=-1.6; //[38]Qi et al.
H0[i]=73;        PT[i]=+1.4;    NT[i++]=-1.4; //[39]Riess et al.
H0[i]=73.2;      PT[i]=+1.3;    NT[i++]=-1.3; //[39]Riess et al.
H0[i]=72.1;      PT[i]=+2;      NT[i++]=-2; //[40]Soltis et al.
H0[i]=69.5;      PT[i]=+4;      NT[i++]=-4; //[41]Wang & Giannios
H0[i]=71;        PT[i]=+20;     NT[i++]=-20; //[42]Zhang et al.
H0[i]=67.4;      PT[i]=+0.5;    NT[i++]=-0.5; //[43]Aghanim et al.
H0[i]=67.73;     PT[i]=+0.41;   NT[i++]=-0.41; //[44]Benevento
```

```
H0[i]=68.22;  PT[i]=+0.39;  NT[i++]=-0.39; //[44]Benevento
H0[i]=72.5;   PT[i]=+1.85;  NT[i++]=-1.85; //[44]Benevento
H0[i]=69.17;  PT[i]=+1.09;  NT[i++]=-1.09; //[44]Benevento
H0[i]=74.5;   PT[i]=+5.6;   NT[i++]=-6.1; //[45]Birrer et al.
H0[i]=67.4;   PT[i]=+4.1;   NT[i++]=-3.2; //[45]Birrer et al.
H0[i]=75.35;  PT[i]=+1.68;  NT[i++]=-1.68; //[46]Camarena & Marra
H0[i]=74;     PT[i]=+0.625; NT[i++]=-0.625; //[47]Chang & Zhu
H0[i]=73.8;   PT[i]=+6.3;   NT[i++]=-5.8; //[48]Coughlin et al.
H0[i]=71.2;   PT[i]=+3.2;   NT[i++]=-3.1; //[48]Coughlin et al.
H0[i]=72.4;   PT[i]=+1.4;   NT[i++]=-1.4; //[49]D'Agostino
H0[i]=71.5;   PT[i]=+1.3;   NT[i++]=-1.3; //[49]D'Agostino
H0[i]=71.54;  PT[i]=+1.78;  NT[i++]=-1.78; //[50]Dai WM et al.
H0[i]=73.12;  PT[i]=+1.14;  NT[i++]=-1.14; //[50]Dai WM et al.
H0[i]=66.2;   PT[i]=+4.4;   NT[i++]=-4.2; //[51]Dietrich et al.
H0[i]=69.9;   PT[i]=+0.84;  NT[i++]=-0.86; //[52]Gonzalez et al.
H0[i]=71;     PT[i]=+4;     NT[i++]=-4; //[53]González-Serrena et al.
H0[i]=74.62;  PT[i]=+12.35; NT[i++]=-11.34; //[54]Haboury
H0[i]=71.89;  PT[i]=+11.02; NT[i++]=-10.17; //[54]Haboury
H0[i]=76.44;  PT[i]=+55.76; NT[i++]=-50.17; //[54]Haboury
H0[i]=50.9;   PT[i]=+31.1;  NT[i++]=-31.9; //[54]Haboury
H0[i]=50.81;  PT[i]=+28.19; NT[i++]=-27.81; //[54]Haboury
H0[i]=71;     PT[i]=+2;     NT[i++]=-3; //[55]Harvey
H0[i]=65.9;   PT[i]=+1.5;   NT[i++]=-1.5; //[56]Holanda et al.
H0[i]=65.9;   PT[i]=+4.4;   NT[i++]=-4; //[56]Holanda et al.
H0[i]=64.3;   PT[i]=+4.5;   NT[i++]=-4.4; //[56]Holanda et al.
H0[i]=66.8;   PT[i]=+13.4;  NT[i++]=-9.2; //[57]Howlett & Davis
H0[i]=64.8;   PT[i]=+7.3;   NT[i++]=-7.2; //[57]Howlett & Davis
H0[i]=75.8;   PT[i]=+5.2;   NT[i++]=-4.9; //[58]Jaeger et al.
H0[i]=65.8;   PT[i]=+3.5;   NT[i++]=-3.5; //[59]Kim et al.
H0[i]=72.3;   PT[i]=+1.4;   NT[i++]=-1.4; //[60]Kreisch et al.
H0[i]=71.5;   PT[i]=+11.9;  NT[i++]=-10.6; //[61]Li & Zhang
H0[i]=74.7;   PT[i]=+5.8;   NT[i++]=-5.8; //[62]Lombriser
H0[i]=72.06;  PT[i]=+0.09;  NT[i++]=-0.09; //[7]Mercier
H0[i]=74;     PT[i]=+1.6;   NT[i++]=-1.6; //[63]Millon et al.
H0[i]=74.2;   PT[i]=+1.7;   NT[i++]=-1.8; //[63]Millon et al.
H0[i]=50.4;   PT[i]=+28.1;  NT[i++]=-19.5; //[64]Mukherjee et al.
H0[i]=62.2;   PT[i]=+29.5;  NT[i++]=-19.7; //[64]Mukherjee et al.
H0[i]=43.1;   PT[i]=+24.6;  NT[i++]=-11.4; //[64]Mukherjee et al.
H0[i]=67.6;   PT[i]=+4.3;   NT[i++]=-4.2; //[64]Mukherjee et al.
H0[i]=68.6;   PT[i]=+14;    NT[i++]=-8.5; //[65]Nicolaou et al.
H0[i]=69.6;   PT[i]=+1;     NT[i++]=-1.3; //[66]Niedermann and Sloth
H0[i]=71.4;   PT[i]=+1;     NT[i++]=-1; //[66]Niedermann and Sloth
H0[i]=72;     PT[i]=+12;    NT[i++]=-8.2; //[67]Palmese et al.
```

```
H0[i]=69.03;  PT[i]=+0.87;  NT[i++]=-0.87; //[68]Pandey et al.
H0[i]=70.6;   PT[i]=+1.1;   NT[i++]=-1.1; //[68]Pandey et al.
H0[i]=68.44;  PT[i]=+0.52;  NT[i++]=-0.52; //[68]Pandey et al.
H0[i]=68.1;   PT[i]=+0.58;  NT[i++]=-0.58; //[68]Pandey et al.
H0[i]=73.9;   PT[i]=+3;     NT[i++]=-3; //[69]Pesce et al.
H0[i]=68.6;   PT[i]=+1.8;   NT[i++]=-1.8; //[70]Pogosian et al.
H0[i]=74.03;  PT[i]=+1.42;  NT[i++]=-1.42; //[71]Rui-Yun et al.
H0[i]=75.1;   PT[i]=+2.3;   NT[i++]=-2.3; //[72]Schombert et al.
H0[i]=74.2;   PT[i]=+2.7;   NT[i++]=-3; //[73]Shajib et al.
H0[i]=67.52;  PT[i]=+0.96;  NT[i++]=-0.95; //[74]Sharov & Sinyakov
H0[i]=70.87;  PT[i]=+1.63;  NT[i++]=-1.62; //[74]Sharov & Sinyakov
H0[i]=69;     PT[i]=+29;    NT[i++]=-14; //[75]Vasylyev & Filippenko
H0[i]=67;     PT[i]=+41;    NT[i++]=-26; //[75]Vasylyev & Filippenko
H0[i]=71;     PT[i]=+34;    NT[i++]=-30; //[75]Vasylyev & Filippenko
H0[i]=70;     PT[i]=+29;    NT[i++]=-18; //[75]Vasylyev & Filippenko
H0[i]=72.3;   PT[i]=+2.9;   NT[i++]=-2.8; //[76]Vogl
H0[i]=75.3;   PT[i]=+3;     NT[i++]=-2.9; //[77]Wei & Melia
H0[i]=75.3;   PT[i]=+1.9;   NT[i++]=-1.9; //[77]Wei & Melia
H0[i]=67.9;   PT[i]=+1.1;   NT[i++]=-1.3; //[78]Wu et al.
H0[i]=72;     PT[i]=+2.1;   NT[i++]=-2.5; //[78]Wu et al.
H0[i]=73.65;  PT[i]=+1.95;  NT[i++]=-2.26; //[79]Yang et al.
H0[i]=67.95;  PT[i]=+0.78;  NT[i++]=-1.03; //[80]Zhang & Huang
H0[i]=69.81;  PT[i]=+2.22;  NT[i++]=-2.7; //[80]Zhang & Huang
H0[i]=66.75;  PT[i]=+3.42;  NT[i++]=-4.23; //[80]Zhang & Huang
H0[i]=70.75;  PT[i]=+1.55;  NT[i++]=-1.55; //[81]Agrawal
H0[i]=73.7;   PT[i]=+1.4;   NT[i++]=-1.4; //[82]Anderson
H0[i]=72.5;   PT[i]=+2.1;   NT[i++]=-2.3; //[83]Birrer
H0[i]=67.4;   PT[i]=+0.5;   NT[i++]=-0.5; //[84]Chang et al.
H0[i]=82.8;   PT[i]=+9.4;   NT[i++]=-8.3; //[85]Chen et al.
H0[i]=70.1;   PT[i]=+5.3;   NT[i++]=-4.5; //[85]Chen et al.
H0[i]=77;     PT[i]=+4;     NT[i++]=-4.6; //[85]Chen et al.
H0[i]=75.6;   PT[i]=+3.2;   NT[i++]=-3; //[85]Chen et al.
H0[i]=76.8;   PT[i]=+2.6;   NT[i++]=-2.6; //[85]Chen et al.
H0[i]=75.7;   PT[i]=+4.5;   NT[i++]=-4.4; //[86]Collett
H0[i]=76.8;   PT[i]=+4.2;   NT[i++]=-3.8; //[86]Collett
H0[i]=74.2;   PT[i]=+3;     NT[i++]=-2.9; //[86]Collett
H0[i]=67.6;   PT[i]=+1.1;   NT[i++]=-1.1; //[87]Cuceu et al.
H0[i]=67.4;   PT[i]=+6;     NT[i++]=-6.2; //[88]Domínguez
H0[i]=66.6;   PT[i]=+1.6;   NT[i++]=-1.6; //[88]Domínguez
H0[i]=70.3;   PT[i]=+1.36;  NT[i++]=-1.35; //[89]Dutta et al.
H0[i]=77;     PT[i]=+37;    NT[i++]=-18; //[90]Fishbach et al.
H0[i]=76;     PT[i]=+19;    NT[i++]=-13; //[90]Fishbach et al.
H0[i]=69.8;   PT[i]=+0.8;   NT[i++]=-0.8; //[91]Freedman et al.
```

```
H0[i]=68.09;    PT[i]=+0.45;    NT[i++]=-0.45; //[92]Guo et al.
H0[i]=69.34;    PT[i]=+0.93;    NT[i++]=-0.93; //[92]Guo et al.
H0[i]=69.67;    PT[i]=+0.95;    NT[i++]=-0.94; //[92]Guo et al.
H0[i]=69.36;    PT[i]=+0.82;    NT[i++]=-0.82; //[92]Guo et al.
H0[i]=69.25;    PT[i]=+0.99;    NT[i++]=-0.99; //[92]Guo et al.
H0[i]=74;       PT[i]=+16;      NT[i++]=-8; //[93]Hotokezaka et al.
H0[i]=70.3;     PT[i]=+5.3;     NT[i++]=-5; //[93]Hotokesaka et al.
H0[i]=82.4;     PT[i]=+8.4;     NT[i++]=-8.3; //[94]Jee et al.
H0[i]=67;       PT[i]=+3;       NT[i++]=-3; //[95]Kozmanyan et al.
H0[i]=72.2;     PT[i]=+2.1;     NT[i++]=-2.1; //[96]Liao et al.
H0[i]=73;       PT[i]=+2.8;     NT[i++]=-3; //[96]Liao et al.
H0[i]=67.8;     PT[i]=+1.3;     NT[i++]=-1.3; //[97]MacAulay et al.
H0[i]=67.37;    PT[i]=+0.62;    NT[i++]=-0.62; //[98]Martinelli
H0[i]=68.8;     PT[i]=+1.6;     NT[i++]=-1.6; //[98]Martinelli
H0[i]=73.9;     PT[i]=+2.5;     NT[i++]=-2.5; //[98]Martinelli
H0[i]=67.68;    PT[i]=+0.46;    NT[i++]=-0.46; //[98]Martinelli
H0[i]=68.4;     PT[i]=+1;       NT[i++]=-1; //[98]Martinelli
H0[i]=69.2;     PT[i]=+1.5;     NT[i++]=-1.5; //[98]Martinelli
H0[i]=67.51;    PT[i]=+0.61;    NT[i++]=-0.61; //[98]Martinelli
H0[i]=68.9;     PT[i]=+1.1;     NT[i++]=-1.1; //[98]Martinelli
H0[i]=72.1;     PT[i]=+2.1;     NT[i++]=-1.8; //[98]Martinelli
H0[i]=67.75;    PT[i]=+0.46;    NT[i++]=-0.46; //[98]Martinelli
H0[i]=68.59;    PT[i]=+0.86;    NT[i++]=-0.86; //[98]Martinelli
H0[i]=69.6;     PT[i]=+1.3;     NT[i++]=-1.3; //[98]Martinelli
H0[i]=71.505;   PT[i]=+0.03;    NT[i++]=-0.03; //[2]Mercier
H0[i]=69;       PT[i]=+1.7;     NT[i++]=-1.7; //[99]Park & Ratra
H0[i]=69.8;     PT[i]=+1.8;     NT[i++]=-1.8; //[99]Park & Ratra
H0[i]=68.9;     PT[i]=+1.7;     NT[i++]=-1.7; //[99]Park & Ratra
H0[i]=70.1;     PT[i]=+1.9;     NT[i++]=-1.9; //[99]Park & Ratra
H0[i]=68.5;     PT[i]=+1.8;     NT[i++]=-1.8; //[99]Park & Ratra
H0[i]=69.6;     PT[i]=+1.9;     NT[i++]=-1.9; //[99]Park & Ratra
H0[i]=72;       PT[i]=+1.9;     NT[i++]=-1.9; //[100]Reid
H0[i]=73.5;     PT[i]=+1.4;     NT[i++]=-1.4; //[100]Reid
H0[i]=74.22;    PT[i]=+1.82;    NT[i++]=-1.82; //[101]Riess et al.
H0[i]=74.03;    PT[i]=+1.42;    NT[i++]=-1.42; //[101]Riess et al.
H0[i]=72.8;     PT[i]=+1.1;     NT[i++]=-1.1; //[102]Riess
H0[i]=74.3;     PT[i]=+1;       NT[i++]=-1; //[102]Riess
H0[i]=71.6;     PT[i]=+3.8;     NT[i++]=-4.9; //[103]Rusu et al.
H0[i]=67.99;    PT[i]=+0.91;    NT[i++]=-0.88; //[104]Ryan
H0[i]=68.24;    PT[i]=+2.39;    NT[i++]=-2.33; //[104]Ryan
H0[i]=66.79;    PT[i]=+2.6;     NT[i++]=-2.32; //[104]Ryan
H0[i]=66.8;     PT[i]=+2.5;     NT[i++]=-2.3; //[104]Ryan
H0[i]=66.13;    PT[i]=+1.38;    NT[i++]=-2.09; //[104]Ryan
```

```
H0[i]=67.1;     PT[i]=+2.4;     NT[i++]=-2.3; //[104]Ryan
H0[i]=68.44;    PT[i]=+0.7;     NT[i++]=-0.69; //[104]Ryan
H0[i]=69.32;    PT[i]=+1.42;    NT[i++]=-1.42; //[104]Ryan
H0[i]=68;       PT[i]=+2.27;    NT[i++]=-1.94; //[104]Ryan
H0[i]=66.6;     PT[i]=+2.2;     NT[i++]=-1.9; //[104]Ryan
H0[i]=67.19;    PT[i]=+1;       NT[i++]=-1.6; //[104]Ryan
H0[i]=66.8;     PT[i]=+1.8;     NT[i++]=-1.7; //[104]Ryan
H0[i]=63.13;    PT[i]=+6.48;    NT[i++]=-6.48; //[105]Saha & Sahoo
H0[i]=74.2;     PT[i]=+2.7;     NT[i++]=-3; //[106]Shajib et al.
H0[i]=75;       PT[i]=+40;      NT[i++]=-32; //[107]Soares-Santos
H0[i]=78;       PT[i]=+96;      NT[i++]=-24; //[107]Soares-Santos
H0[i]=73.1;     PT[i]=+0.7;     NT[i++]=-0.7; //[108]Taubenberger et al.
H0[i]=68;       PT[i]=+14;      NT[i++]=-7; //[109]Tiwari et al.
H0[i]=68;       PT[i]=+18;      NT[i++]=-8; //[109]Tiwari et al.
H0[i]=73.9;     PT[i]=+1;       NT[i++]=-1; //[110]Verde et al.
H0[i]=72.5;     PT[i]=+1.2;     NT[i++]=-1.2; //[110]Verde et al.
H0[i]=73.3;     PT[i]=+1.7;     NT[i++]=-1.8; //[111]Wong et al.
H0[i]=72.4;     PT[i]=+2;       NT[i++]=-2; //[112]Yuan et al.
H0[i]=68.36;    PT[i]=+0.53;    NT[i++]=-0.52; //[113]Zhang & Huang
H0[i]=64.9;     PT[i]=+4.6;     NT[i++]=-4.3; //[114]Zeng and Yan
H0[i]=67.4;     PT[i]=+1.1;     NT[i++]=-1.2; //[115]Abbott et al.
H0[i]=69.3;     PT[i]=+0.4;     NT[i++]=-0.6; //[115]Abbott et al.
H0[i]=73.24;    PT[i]=+1.74;    NT[i++]=-1.74; //[116]Benetti et al.
H0[i]=72.5;     PT[i]=+2.1;     NT[i++]=-2.1; //[117]Bolejko
H0[i]=68.1;     PT[i]=+2;       NT[i++]=-2; //[117]Bolejko
H0[i]=76;       PT[i]=+8;       NT[i++]=-8; //[118]Braatz
H0[i]=69.3;     PT[i]=+4.2;     NT[i++]=-4.2; //[118]Braatz
H0[i]=71.9;     PT[i]=+7.1;     NT[i++]=-7.1; //[119]Cantiello et al.
H0[i]=73.24;    PT[i]=+1.74;    NT[i++]=-1.74; //[120]Chen
H0[i]=67.4;     PT[i]=+0.5;     NT[i++]=-0.5; //[120]Chen
H0[i]=73.24;    PT[i]=+1.74;    NT[i++]=-1.74; //[121]Choudhury & Choubey
H0[i]=72.8;     PT[i]=+1.6;     NT[i++]=-1.6; //[122]Dhawan et al.
H0[i]=55;       PT[i]=+7;       NT[i++]=-20; //[123]Di Valentino & Mel-
chiorri
H0[i]=67.06;    PT[i]=+1.68;    NT[i++]=-1.68; //[124]Gomez-Valent
H0[i]=68.9;     PT[i]=+1.96;    NT[i++]=-1.96; //[124]Gomez-Valent
H0[i]=68.45;    PT[i]=+2;       NT[i++]=-2; //[124]Gomez-Valent
H0[i]=73.5;     PT[i]=+4.6;     NT[i++]=-4.7; //[125]Grillo
H0[i]=72.8;     PT[i]=+4.3;     NT[i++]=-4.1; //[125]Grillo
H0[i]=69.8;     PT[i]=+5.3;     NT[i++]=-4.1; //[125]Grillo
H0[i]=70.38;    PT[i]=+0.6;     NT[i++]=-0.6; //[126]Hoeneisen et al.
H0[i]=71.17;    PT[i]=+1.66;    NT[i++]=-1.66; //[127]Lee & Jang
H0[i]=73.52;    PT[i]=+1.62;    NT[i++]=-1.62; //[128]Riess et al.
```

```
H0[i]=73.83;    PT[i]=+1.48;    NT[i++]=-1.48; //[128]Riess et al.
H0[i]=73.48;    PT[i]=+1.66;    NT[i++]=-1.66; //[129]Riess et al.
H0[i]=74.4;     PT[i]=+4.9;     NT[i++]=-4.9; //[130]Van Putten
H0[i]=74.5;     PT[i]=+7.3;     NT[i++]=-7.3; //[130]Van Putten
H0[i]=74.9;     PT[i]=+2.6;     NT[i++]=-2.6; //[130]Van Putten
H0[i]=66.8;     PT[i]=+1.9;     NT[i++]=-1.9; //[130]Van Putten
H0[i]=73.75;    PT[i]=+1.44;    NT[i++]=-1.44; //[130]Van Putten
H0[i]=70;       PT[i]=+12;      NT[i++]=-8; //[131]Vitale
H0[i]=67;       PT[i]=+4;       NT[i++]=-4; //[132]Yu et al.
H0[i]=67.498;   PT[i]=+7.97;    NT[i++]=-3.278; //[133]Zhang
H0[i]=70;       PT[i]=+12;      NT[i++]=-8; //[134]Abbott
H0[i]=72.5;     PT[i]=+2.5;     NT[i++]=-8; //[135]Bethapudi & Desai
H0[i]=71.9;     PT[i]=+2.4;     NT[i++]=-3; //[136]Bonvin et al.
H0[i]=69.2;     PT[i]=+1.4;     NT[i++]=-2.2; //[136]Bonvin et al.
H0[i]=79;       PT[i]=+4.4;     NT[i++]=-4.2; //[136]Bonvin et al.
H0[i]=73.75;    PT[i]=+2.11;    NT[i++]=-2.11; //[137]Cardona
H0[i]=67.81;    PT[i]=+0.92;    NT[i++]=-0.92; //[137]Cardona
H0[i]=66.93;    PT[i]=+0.62;    NT[i++]=-0.62; //[137]Cardona
H0[i]=73.46;    PT[i]=+1.4;     NT[i++]=-1.4; //[137]Cardona
H0[i]=68.3;     PT[i]=+2.7;     NT[i++]=-2.6; //[138]Chen Yun et al.
H0[i]=68.4;     PT[i]=+2.9;     NT[i++]=-3.3; //[138]Chen Yun et al.
H0[i]=65;       PT[i]=+6.6;     NT[i++]=-6.6; //[138]Chen Yun et al.
H0[i]=67.9;     PT[i]=+2.4;     NT[i++]=-2.4; //[138]Chen Yun et al.
H0[i]=68;       PT[i]=+2.8;     NT[i++]=-2.8; //[139]Farooq
H0[i]=73.24;    PT[i]=+1.74;    NT[i++]=-1.74; //[139]Farooq
H0[i]=72.72;    PT[i]=+1.67;    NT[i++]=-1.67; //[140]Feeney et al.
H0[i]=73.15;    PT[i]=+1.78;    NT[i++]=-1.78; //[140]Feeney et al.
H0[i]=67.6;     PT[i]=+0.7;     NT[i++]=-0.6; //[141]Grieb et al.
H0[i]=73;       PT[i]=+1.75;    NT[i++]=-1.75; //[142]Guo & Zhang
H0[i]=73.24;    PT[i]=+1.74;    NT[i++]=-1.74; //[143]Hjorth et al.
H0[i]=69.13;    PT[i]=+0.24;    NT[i++]=-0.24; //[144]Huang and Huang
H0[i]=71.66;    PT[i]=+1.8;     NT[i++]=-1.8; //[145]Jang & Lee
H0[i]=73.72;    PT[i]=+2.03;    NT[i++]=-2.03; //[145]Jang & Lee
H0[i]=71.17;    PT[i]=+1.66;    NT[i++]=-1.66; //[145]Jang & Lee
H0[i]=66.2;     PT[i]=+8.9;     NT[i++]=-8.9; //[146]Pritychenko
H0[i]=67.2;     PT[i]=+6.9;     NT[i++]=-6.9; //[146]Pritychenko
H0[i]=69.13;    PT[i]=+2.34;    NT[i++]=-2.34; //[147]Wang et al.
H0[i]=73.24;    PT[i]=+1.74;    NT[i++]=-1.74; //[148]Wei & Wu
H0[i]=69.6;     PT[i]=+0.7;     NT[i++]=-0.7; //[148]Wei & Wu
H0[i]=73.1;     PT[i]=+5.7;     NT[i++]=-6; //[149]Wong et al.
H0[i]=72.5;     PT[i]=+3.1;     NT[i++]=-3.1; //[150]Zhang et al.
H0[i]=67.8;     PT[i]=+0.9;     NT[i++]=-0.9; //[151]Ade et al.
H0[i]=66;       PT[i]=+6;       NT[i++]=-6; //[152]Gao et al.
```

```
H0[i]=70.1;     PT[i]=+0.34;   NT[i++]=-0.34; //[153]Ichiki et al.
H0[i]=66.5;     PT[i]=+1.8;    NT[i++]=-1.8; //[154]Ludovic et al.
H0[i]=64.2;     PT[i]=+1.9;    NT[i++]=-1.9; //[154]Ludovic et al.
H0[i]=91.8;     PT[i]=+5.3;    NT[i++]=-5.3; //[155]Moresco et al.
H0[i]=72.25;    PT[i]=+2.51;   NT[i++]=-2.51; //[156]Riess et al.
H0[i]=72.04;    PT[i]=+2.67;   NT[i++]=-2.67; //[156]Riess et al.
H0[i]=76.18;    PT[i]=+2.37;   NT[i++]=-2.37; //[156]Riess et al.
H0[i]=74.5;     PT[i]=+3.27;   NT[i++]=-3.27; //[156]Riess et al.
H0[i]=73.24;    PT[i]=+1.74;   NT[i++]=-1.74; //[156]Riess et al.
H0[i]=76.2;     PT[i]=+3.4;    NT[i++]=-3.4; //[157]Tully et al.
H0[i]=75;       PT[i]=+2;      NT[i++]=-2; //[157]Tully et al.
H0[i]=68.17;    PT[i]=+1.55;   NT[i++]=-1.56; //[158]Cheng & Qing Guo
H0[i]=68.11;    PT[i]=+1.69;   NT[i++]=-1.69; //[158]Cheng & Qing Guo
H0[i]=68.11;    PT[i]=+0.86;   NT[i++]=-0.86; //[158]Cheng & Qing Guo
H0[i]=67.7;     PT[i]=+1.1;    NT[i++]=-1.1; //[159]Cuesta et al.
H0[i]=69.8;     PT[i]=+2.6;    NT[i++]=-2.6; //[160]Jang & Lee
H0[i]=72.2;     PT[i]=+3.3;    NT[i++]=-3.3; //[160]Jang & Lee
H0[i]=68.1;     PT[i]=+5.9;    NT[i++]=-5.9; //[161]Kumar et al.
H0[i]=73;       PT[i]=+26;     NT[i++]=-22; //[162]Kuo et al.
H0[i]=70.6;     PT[i]=+2.6;    NT[i++]=-2.6; //[163]Rigault et al.
H0[i]=68.8;     PT[i]=+3.3;    NT[i++]=-3.3; //[163]Rigault et al.
H0[i]=67.3;     PT[i]=+1.2;    NT[i++]=-1.2; //[164]Ade et al.
H0[i]=70.8;     PT[i]=+2.4;    NT[i++]=-2.4; //[165]Ben-Dayan et al.
H0[i]=69.6;     PT[i]=+0.7;    NT[i++]=-0.7; //[166]Bennett et al.
H0[i]=64.9;     PT[i]=+4.2;    NT[i++]=-4.2; //[167]Busti et al.
H0[i]=72.5;     PT[i]=+2.5;    NT[i++]=-2.5; //[168]Efstathiou
H0[i]=70.6;     PT[i]=+3.3;    NT[i++]=-3.3; //[168]Efstathiou
H0[i]=74.1;     PT[i]=+2.2;    NT[i++]=-2.2; //[169]Lima & Cunha
H0[i]=70;       PT[i]=+2.2;    NT[i++]=-2.2; //[170]Bennett et al.
H0[i]=69.32;    PT[i]=+0.8;    NT[i++]=-0.8; //[170]Bennett et al.
H0[i]=68;       PT[i]=+4.8;    NT[i++]=-4.8; //[171]Braatz et al.
H0[i]=68;       PT[i]=+2.8;    NT[i++]=-2.8; //[172]Farooq & Bathra
H0[i]=73.8;     PT[i]=+2.4;    NT[i++]=-2.4; //[172]Farooq & Bathra
H0[i]=69.7;     PT[i]=+2.4;    NT[i++]=-2.4; //[173]Hinshaw et al.
H0[i]=70.4;     PT[i]=+2.5;    NT[i++]=-2.5; //[173]Hinshaw et al.
H0[i]=69.33;    PT[i]=+0.88;   NT[i++]=-0.88; //[173]Hinshaw et al.
H0[i]=70.2;     PT[i]=+1.4;    NT[i++]=-1.4; //[173]Hinshaw et al.
H0[i]=70;       PT[i]=+3;      NT[i++]=-3; //[174]Humphreys et al.
H0[i]=68;       PT[i]=+9;      NT[i++]=-9; //[175]Kuo et al.
H0[i]=49.97;    PT[i]=+0.19;   NT[i++]=-0.19; //[176]Pietrzynski et al.
H0[i]=68.9;     PT[i]=+7.1;    NT[i++]=-7.1; //[177]Reid et al.
H0[i]=72.1;     PT[i]=+3.2;    NT[i++]=-2.3; //[178]Salvatelli et al.
H0[i]=74.1;     PT[i]=+2.1;    NT[i++]=-2.1; //[179]Scowcroft et al.
```

```
H0[i]=69;     PT[i]=+6;     NT[i++]=-6; //[180]Sereno and Pacificz
H0[i]=80;     PT[i]=+5.8;   NT[i++]=-5.7; //[181]Suyu et al.
H0[i]=75.2;   PT[i]=+4.4;   NT[i++]=-4.2; //[181]Suyu et al.
H0[i]=73.1;   PT[i]=+2.4;   NT[i++]=-3.6; //[181]Suyu et al.
H0[i]=74.4;   PT[i]=+3;     NT[i++]=-3; //[182]Tully et al.
H0[i]=71.3;   PT[i]=+2;     NT[i++]=-2; //[183]Xia et al.
H0[i]=73.8;   PT[i]=+2.4;   NT[i++]=-2.4; //[184]Calabrese et al.
H0[i]=68;     PT[i]=+2.8;   NT[i++]=-2.8; //[184]Calabrese et al.
H0[i]=69.7;   PT[i]=+2.5;   NT[i++]=-2.5; //[184]Calabrese et al.
H0[i]=74.3;   PT[i]=+3.1;   NT[i++]=-3.1; //[185]Chavez
H0[i]=67;     PT[i]=+3.2;   NT[i++]=-3.2; //[186]Colless et al.
H0[i]=74.3;   PT[i]=+3;     NT[i++]=-3; //[187]Freedman et al.
H0[i]=70.2;   PT[i]=+0.14;  NT[i++]=-0.14; //[188]Pozzo
H0[i]=75.4;   PT[i]=+2.9;   NT[i++]=-2.9; //[189]Riess et al.
H0[i]=56;     PT[i]=+2;     NT[i++]=-2; //[190]Wang
H0[i]=68;     PT[i]=+5.5;   NT[i++]=-5.5; //[191]Chen & Ratra
H0[i]=67;     PT[i]=+3.2;   NT[i++]=-3.2; //[192]Beutler et al.
H0[i]=71;     PT[i]=+2.5;   NT[i++]=-2.5; //[193]Jarosik et al.
H0[i]=70.4;   PT[i]=+1.3;   NT[i++]=-1.4; //[193]Jarosik et al.
H0[i]=74.8;   PT[i]=+3.1;   NT[i++]=-3.1; //[194]Riess et al.
H0[i]=74.4;   PT[i]=+2.5;   NT[i++]=-2.5; //[194]Riess et al.
H0[i]=73.8;   PT[i]=+2.4;   NT[i++]=-2.4; //[194]Riess et al.
H0[i]=73;     PT[i]=+2;     NT[i++]=-2; //[195]Freedman & Madore
H0[i]=66;     PT[i]=+6;     NT[i++]=-4; //[196]Paraficz et Hjorth
H0[i]=76;     PT[i]=+3;     NT[i++]=-3; //[196]Paraficz et Hjorth
H0[i]=70.6;   PT[i]=+3.1;   NT[i++]=-3.1; //[197]Suyu et al.
H0[i]=69.7;   PT[i]=+4.9;   NT[i++]=-5; //[197]Suyu et al.
H0[i]=70.5;   PT[i]=+1.3;   NT[i++]=-1.3; //[198]Hinshaw et al.
H0[i]=71.9;   PT[i]=+2.6;   NT[i++]=-2.7; //[198]Hinshaw et al.
H0[i]=70.5;   PT[i]=+1.3;   NT[i++]=-1.3; //[199]Komatsu et al.
H0[i]=70.4;   PT[i]=+1.4;   NT[i++]=-1.4; //[199]Komatsu et al.
H0[i]=70.9;   PT[i]=+1.3;   NT[i++]=-1.3; //[199]Komatsu et al.
H0[i]=70.1;   PT[i]=+1.3;   NT[i++]=-1.3; //[199]Komatsu et al.
H0[i]=74.2;   PT[i]=+3.6;   NT[i++]=-3.6; //[200]Riess et al.
H0[i]=84.2;   PT[i]=+6;     NT[i++]=-6; //[201]Russell
H0[i]=83.4;   PT[i]=+8;     NT[i++]=-8; //[201]Russell
H0[i]=88;     PT[i]=+6;     NT[i++]=-6; //[201]Russell
H0[i]=61.7;   PT[i]=+1.2;   NT[i++]=-1.1; //[202]Leith et al.
H0[i]=67;     PT[i]=+13;    NT[i++]=-10; //[203]Vuissoz et al.
H0[i]=63;     PT[i]=+7;     NT[i++]=-3; //[203]Vuissoz et al.
H0[i]=70;     PT[i]=+6;     NT[i++]=-6; //[204]Oguri
H0[i]=68;     PT[i]=+6;     NT[i++]=-6; //[204]Oguri
H0[i]=73.5;   PT[i]=+3.2;   NT[i++]=-3.2; //[205]Spergel et al.
```

H0[i]=73.2; PT[i]=+3.1; NT[i++]=-3.2; //[205]Spergel *et al.*
H0[i]=70.4; PT[i]=+1.5; NT[i++]=-1.6; //[205]Spergel *et al.*
H0[i]=76.9; PT[i]=+3.9; NT[i++]=-3.4; //[206]Bonamente *et al.*
H0[i]=73.7; PT[i]=+4.6; NT[i++]=-3.8; //[206]Bonamente *et al.*
H0[i]=77.6; PT[i]=+4.8; NT[i++]=-4.3; //[206]Bonamente *et al.*
H0[i]=70.8; PT[i]=+1.9; NT[i++]=-1.8; //[207]Hütsi
H0[i]=74.92; PT[i]=+2.28; NT[i++]=-2.28; //[208]Ngeow and Kanbur
H0[i]=74.37; PT[i]=+2.27; NT[i++]=-2.27; //[208]Ngeow and Kanbur
H0[i]=62.3; PT[i]=+1.3; NT[i++]=-1.3; //[209]Sandage *et al.*
H0[i]=60.9; PT[i]=+1.3; NT[i++]=-1.3; //[209]Sandage *et al.*
H0[i]=60.7; PT[i]=+1.5; NT[i++]=-1.5; //[209]Sandage *et al.*
H0[i]=72; PT[i]=+6; NT[i++]=-6; //[210]Wang *et al.*
H0[i]=73.2; PT[i]=+7; NT[i++]=-7; //[211]Gibson & Brook
H0[i]=75; PT[i]=+7; NT[i++]=-7; //[212]Hamuy
H0[i]=65; PT[i]=+12; NT[i++]=-12; //[212]Hamuy
H0[i]=58; PT[i]=+2; NT[i++]=-2; //[213]Magain
H0[i]=58; PT[i]=+2; NT[i++]=-2; //[214]Olivares *et al.*
H0[i]=73; PT[i]=+4; NT[i++]=-4; //[215]Riess
H0[i]=69; PT[i]=+8; NT[i++]=-8; //[216]Schmidt *et al.*
H0[i]=66; PT[i]=+8; NT[i++]=-8; //[217]Stritzinger *et al.*
H0[i]=78; PT[i]=+9; NT[i++]=-9; //[217]Stritzinger *et al.*
H0[i]=67; PT[i]=+30; NT[i++]=-18; //[218]Udomprasert *et al.*
H0[i]=64; PT[i]=+7; NT[i++]=-4; //[219]Boffi & Riess
H0[i]=33; PT[i]=+5; NT[i++]=-5; //[220]Dumin
H0[i]=69; PT[i]=+12; NT[i++]=-12; //[221]Jimenez *et al.*
H0[i]=75; PT[i]=+7; NT[i++]=-6; //[222]Koopmans
H0[i]=70; PT[i]=+7; NT[i++]=-7; //[223]Mei *et al.*
H0[i]=68; PT[i]=+6; NT[i++]=-6; //[223]Mei *et al.*
H0[i]=68; PT[i]=+5; NT[i++]=-5; //[223]Mei *et al.*
H0[i]=71; PT[i]=+4; NT[i++]=-4; //[223]Mei *et al.*
H0[i]=77; PT[i]=+19; NT[i++]=-15; //[224]Saunders *et al.*
H0[i]=85; PT[i]=+20; NT[i++]=-17; //[224]Saunders *et al.*
H0[i]=72; PT[i]=+5; NT[i++]=-5; //[225]Spergel *et al.*
H0[i]=71; PT[i]=+4; NT[i++]=-3; //[225]Spergel *et al.*
H0[i]=63; PT[i]=+2; NT[i++]=-2; //[226]Fassnacht *et al.*
H0[i]=72; PT[i]=+8; NT[i++]=-8; //[227]Freedman
H0[i]=57; PT[i]=+23; NT[i++]=-16; //[228]Grainge *et al.*
H0[i]=48; PT[i]=+7; NT[i++]=-4; //[229]Kochanek
H0[i]=71; PT[i]=+6; NT[i++]=-6; //[229]Kochanek
H0[i]=72; PT[i]=+8; NT[i++]=-8; //[229]Kochanek
H0[i]=62; PT[i]=+7; NT[i++]=-7; //[229]Kochanek
H0[i]=75; PT[i]=+8; NT[i++]=-8; //[230]Tikhonov & Galazoutdinova

```
H0[i]=81;  PT[i]=+5;  NT[i++]=-5; //[230]Tikhonov & Galazoutdinova
H0[i]=59;  PT[i]=+15;  NT[i++]=-10; //[231]Treu & Koopmans
H0[i]=71;  PT[i]=+2;  NT[i++]=-2; //[232]Freedman et al.
H0[i]=71;  PT[i]=+3;  NT[i++]=-3; //[232]Freedman et al.
H0[i]=70;  PT[i]=+5;  NT[i++]=-5; //[232]Freedman et al.
H0[i]=72;  PT[i]=+9;  NT[i++]=-9; //[232]Freedman et al.
H0[i]=82;  PT[i]=+6;  NT[i++]=-6; //[232]Freedman et al.
H0[i]=72;  PT[i]=+8;  NT[i++]=-8; //[232]Freedman et al.
H0[i]=65;  PT[i]=+5;  NT[i++]=-5; //[233]Itoh
H0[i]=76;  PT[i]=+1.3;  NT[i++]=-1.3; //[234]Jensen et al.
H0[i]=72;  PT[i]=+2.3;  NT[i++]=-2.3; //[234]Jensen et al.
H0[i]=65;  PT[i]=+5;  NT[i++]=-5; //[235]Koopmans et al.
H0[i]=71;  PT[i]=+8;  NT[i++]=-8; //[236]Liu & Graham
H0[i]=64;  PT[i]=+14;  NT[i++]=-18; //[237]Mason et al.
H0[i]=66;  PT[i]=+14;  NT[i++]=-11; //[237]Mason et al.
H0[i]=70;  PT[i]=+7;  NT[i++]=-7; //[238]Mei et al.
H0[i]=69;  PT[i]=+4;  NT[i++]=-4; //[239]Tonry
H0[i]=71;  PT[i]=+6;  NT[i++]=-6; //[240]Willick & Puneet
H0[i]=63;  PT[i]=+4.3;  NT[i++]=-4.3; //[241]Xiao-Feng et al.
H0[i]=69;  PT[i]=+4;  NT[i++]=-4; //[242]Ferrarese et al.
H0[i]=68;  PT[i]=+2;  NT[i++]=-2; //[243]Gibson et al.
H0[i]=71;  PT[i]=+6;  NT[i++]=-6; //[244]Mould et al.
H0[i]=68;  PT[i]=+6;  NT[i++]=-6; //[244]Mould et al.
H0[i]=71;  PT[i]=+4;  NT[i++]=-4; //[245]Sakai et al.
H0[i]=77;  PT[i]=+7;  NT[i++]=-7; //[246]Tikhonov et al.
H0[i]=69;  PT[i]=+12;  NT[i++]=-19; //[247]Biggs et al.
H0[i]=69;  PT[i]=+18;  NT[i++]=-12; //[248]Chae KH
H0[i]=74;  PT[i]=+18;  NT[i++]=-17; //[248]Chae KH
H0[i]=42;  PT[i]=+9;  NT[i++]=-9; //[249]Collier et al.
H0[i]=73;  PT[i]=+6;  NT[i++]=-6; //[250]Freedman et al.
H0[i]=64;  PT[i]=+8;  NT[i++]=-6; //[251]Jha et al.
H0[i]=85;  PT[i]=+27;  NT[i++]=-23; //[252]Mason & Myers
H0[i]=61;  PT[i]=+15;  NT[i++]=-14; //[252]Mason & Myers
H0[i]=61;  PT[i]=+23;  NT[i++]=-21; //[252]Mason & Myers
H0[i]=80;  PT[i]=+19;  NT[i++]=-17; //[252]Mason & Myers
H0[i]=68;  PT[i]=+21;  NT[i++]=-19; //[252]Mason & Myers
H0[i]=71;  PT[i]=+5;  NT[i++]=-5; //[252]Mason & Myers
H0[i]=86;  PT[i]=+24;  NT[i++]=-24; //[253]Mazumdar & Narasimba
H0[i]=67;  PT[i]=+7;  NT[i++]=-7; //[254]Tanvir et al.
H0[i]=62.9;  PT[i]=+1.6;  NT[i++]=-1.6; //[255]Tripp & Branch
H0[i]=62;  PT[i]=+2;  NT[i++]=-2; //[255]Tripp & Branch
H0[i]=60;  PT[i]=+10;  NT[i++]=-10; //[256]Branch
```

```
H0[i]=66;    PT[i]=+15;    NT[i++]=-14; //[257]Goicoechea et al.
H0[i]=77;    PT[i]=+8;     NT[i++]=-8; //[258]Harris et al.
H0[i]=47;    PT[i]=+23;    NT[i++]=-15; //[259]Hughes & Birkinshaw
H0[i]=82;    PT[i]=+8;     NT[i++]=-8; //[260]Lauer et al.
H0[i]=89;    PT[i]=+10;    NT[i++]=-10; //[260]Lauer et al.
H0[i]=65.2;  PT[i]=+1.3;   NT[i++]=-1.3; //[261]Riess et al.
H0[i]=63.8;  PT[i]=+1.3;   NT[i++]=-1.3; //[261]Riess et al.
H0[i]=55;    PT[i]=+8;     NT[i++]=-8; //[262]Tammann & Labhardt
H0[i]=60;    PT[i]=+6;     NT[i++]=-6; //[263]Tripp
H0[i]=70;    PT[i]=+5;     NT[i++]=-5; //[264]Giovanelli
H0[i]=76;    PT[i]=+8;     NT[i++]=-8; //[264]Giovanelli
H0[i]=67;    PT[i]=+8;     NT[i++]=-8; //[264]Giovanelli
H0[i]=75;    PT[i]=+6;     NT[i++]=-6; //[265]Gregg
H0[i]=67;    PT[i]=+8;     NT[i++]=-8; //[266]Hjorth & Tanvir
H0[i]=70;    PT[i]=+7;     NT[i++]=-7; //[266]Hjorth & Tanvir
H0[i]=60;    PT[i]=+40;    NT[i++]=-23; //[267]Holzapfel et al.
H0[i]=78;    PT[i]=+34;    NT[i++]=-28; //[267]Holzapfel et al.
H0[i]=78;    PT[i]=+60;    NT[i++]=-40; //[267]Holzapfel et al.
H0[i]=58;    PT[i]=+10;    NT[i++]=-5; //[268]Hoyle et al.
H0[i]=74;    PT[i]=+10;    NT[i++]=-10; //[269]Schechter
H0[i]=52.5;  PT[i]=+2.5;   NT[i++]=-2.5; //[270]Sciama
H0[i]=54.8;  PT[i]=+0.3;   NT[i++]=-0.3; //[270]Sciama
H0[i]=81;    PT[i]=+6;     NT[i++]=-6; //[271]Tonry et al.
H0[i]=69;    PT[i]=+8;     NT[i++]=-8; //[272]Amendola
H0[i]=80;    PT[i]=+17;    NT[i++]=-17; //[272]Amendola
H0[i]=49.5;  PT[i]=+4.5;   NT[i++]=-4.5; //[273]Biesiada
H0[i]=65;    PT[i]=+8;     NT[i++]=-8; //[274]Forbes et al.
H0[i]=103;   PT[i]=+59;    NT[i++]=-28; //[275]Kobayashi
H0[i]=82;    PT[i]=+56;    NT[i++]=-24; //[275]Kobayashi
H0[i]=60;    PT[i]=+24;    NT[i++]=-13; //[275]Kobayashi
H0[i]=51;    PT[i]=+10;    NT[i++]=-7; //[275]Kobayashi
H0[i]=33;    PT[i]=+22;    NT[i++]=-9; //[275]Kobayashi
H0[i]=74;    PT[i]=+26;    NT[i++]=-15; //[275]Kobayashi
H0[i]=63;    PT[i]=+28;    NT[i++]=-15; //[275]Kobayashi
H0[i]=80;    PT[i]=+17;    NT[i++]=-17; //[276]Mallik
H0[i]=87;    PT[i]=+7;     NT[i++]=-7; //[276]Mallik
H0[i]=55;    PT[i]=+3;     NT[i++]=-3; //[277]Schaefer
H0[i]=56;    PT[i]=+3;     NT[i++]=-3; //[277]Schaefer
H0[i]=82.5;  PT[i]=+5.9;   NT[i++]=-3; //[278]Grogin & Narayan
H0[i]=82.5;  PT[i]=+8.7;   NT[i++]=-5.6; //[278]Grogin & Narayan
H0[i]=71;    PT[i]=+30;    NT[i++]=-25; //[279]Herbig
H0[i]=74.6;  PT[i]=+47;    NT[i++]=-33; //[280]Holzapfel et al.
H0[i]=38;    PT[i]=+18;    NT[i++]=-16; //[281]Jones
```

```
H0[i]=80;       PT[i]=+17;     NT[i++]=-17; //[282]Kennicutt Jr et al.
H0[i]=73;       PT[i]=+11;     NT[i++]=-11; //[283]Mould
H0[i]=81;       PT[i]=+11;     NT[i++]=-11; //[283]Mould
H0[i]=84;       PT[i]=+16;     NT[i++]=-16; //[283]Mould
H0[i]=76;       PT[i]=+10;     NT[i++]=-10; //[283]Mould
H0[i]=82;       PT[i]=+11;     NT[i++]=-11; //[283]Mould
H0[i]=71;       PT[i]=+10;     NT[i++]=-10; //[283]Mould
H0[i]=80;       PT[i]=+17;     NT[i++]=-17; //[283]Mould
H0[i]=80;       PT[i]=+17;     NT[i++]=-17; //[284]Nakamura & Suto
H0[i]=58;       PT[i]=+6;      NT[i++]=-6; //[285]Rephaeli
H0[i]=51;       PT[i]=+7;      NT[i++]=-7; //[286]Schaefer
H0[i]=61;       PT[i]=+12;     NT[i++]=-12; //[286]Schaefer
H0[i]=26;       PT[i]=+5;      NT[i++]=-5; //[286]Schaefer
H0[i]=69;       PT[i]=+8;      NT[i++]=-8; //[287]Tanvir et al.
H0[i]=78;       PT[i]=+11;     NT[i++]=-11; //[288]Whitmore & Schweizer
H0[i]=65;       PT[i]=+25;     NT[i++]=-25; //[289]Birkinshaw & Hughes
H0[i]=55;       PT[i]=+17;     NT[i++]=-17; //[289]Birkinshaw & Hughes
H0[i]=80;       PT[i]=+17;     NT[i++]=-17; //[290]Freedman
H0[i]=84;       PT[i]=+5;      NT[i++]=-5; //[291]Lu et al.
H0[i]=73;       PT[i]=+6;      NT[i++]=-6; //[292]Schmidt & Kirshner
H0[i]=90;       PT[i]=+10;     NT[i++]=-10; //[293]Tully
H0[i]=43.5;     PT[i]=+2.7;    NT[i++]=-2.7; //[294]Duemmler
H0[i]=77;       PT[i]=+8;      NT[i++]=-8; //[295]Lauer & Postman
H0[i]=51;       PT[i]=+5;      NT[i++]=-5; //[295]Lauer & Postman
H0[i]=75;       PT[i]=+30;     NT[i++]=-30; //[296]Leibundgut & Pinto
H0[i]=40;       PT[i]=+9;      NT[i++]=-9; //[297]Birkinshaw
H0[i]=45;       PT[i]=+12;     NT[i++]=-12; //[297]Birkinshaw
H0[i]=82;       PT[i]=+7;      NT[i++]=-7; //[298]Tonry
H0[i]=52;       PT[i]=+2;      NT[i++]=-2; //[299]Sandage & Tammann
H0[i]=45;       PT[i]=+3;      NT[i++]=-3; //[299]Sandage & Tammann
H0[i]=73;       PT[i]=+10;     NT[i++]=-10; //[300]Visvanathan
H0[i]=50;       PT[i]=+10;     NT[i++]=-10; //[301]Sandage & Tammann
H0[i]=52;       PT[i]=+2;      NT[i++]=-2; //[301]Sandage & Tammann
H0[i]=50;       PT[i]=+7;      NT[i++]=-7; //[301]Sandage & Tammann
H0[i]=67;       PT[i]=+10;     NT[i++]=-10; //[302]Dressler
H0[i]=74.3;     PT[i]=+11;     NT[i++]=-11; //[304]Visvanathan
H0[i]=74.3;     PT[i]=+11;     NT[i++]=-11; //[305]Hanes
H0[i]=76;       PT[i]=+8;      NT[i++]=-8; //[306]Bottinelli & Gouguenheim
H0[i]=50.3;     PT[i]=+4.3;    NT[i++]=-4.3; //[307]Sandage & Tammann
H0[i]=56.9;     PT[i]=+3.4;    NT[i++]=-3.4; //[308]Sandage & Tammann
H0[i]=57;       PT[i]=+6;      NT[i++]=-6; //[309]Sandage & Tammann
H0[i]=55.5;     PT[i]=+8.7;    NT[i]=-8.7; //[310]Sandage & Tammann
//Creates an H0 array that contains all the extremities of the tolerance ranges
```

```
   for (i=0;i<=nbH0-1;i++) {
      H0[i+nbH0]=H0[i]+PT[i]; Variation[i+nbH0]=PT[i];
      H0[i]=H0[i]+NT[i]; Variation[i]=NT[i]; }
   //Sorts H0 array in ascending order with corresponding Variation of tolerance
   for (j=0;j<=2*nbH0-2;j++) {
      for (i=j+1;i<=2*nbH0-1;i++) {
         if (H0[i]<H0[j]) {
            DH0=H0[j]; DSgn=Variation[j]; H0[j]=H0[i];
            Variation[j]=Variation[i]; H0[i]=DH0; Variation[i]=DSgn; } } }
   for (i=0;i<=2*nbH0-1;i++) {      //Builds the nbCrossings array
      if (i==0) { nbCrossings[i]=1; }
      else {
        if (Variation[i]<0) {nbCrossings[i]=nbCrossings[i-1]+1;}
        if (Variation[i]>0) {nbCrossings[i]=nbCrossings[i-1]-1;}
        if (H0[i]==H0[i-1]) {
           j=i; DeltaCrossings=0;
           do {
              if (Variation[j]<0) {DeltaCrossings=DeltaCrossings+1;}
              if (Variation[j]>0) {DeltaCrossings=DeltaCrossings-1;}
              j=j-1; } while (H0[j]==H0[i]);
           for(k=i;k>j;k--) {nbCrossings[k]=nbCrossings[j]+DeltaCrossings;}
   } } } } //End of CreateTableOfCrossingH0Ranges

//***Function that returns the y coordinate corresponding to x for non
//***centered Gaussian curve
double GaussianCurve(double x, double Mean, double Sigma,
      double Multiplier) {
   double y; //Coordinate y corresponding to x for a non centered Gaussian
   y=(Multiplier/(Sigma*Sqrt(2*Pi)))*exp(-0.5*Sqr((x-Mean)/Sigma));
   return y; }    //End of CreateApproximativeCurve

//***This the best Gaussians to fit the nbCrossing array as a function of H0***
double FindsGaussianCurvesLS(double Mean[5],double Sigma[5],
      double Multiplier[5]) {
   int i,j; /*Counters*/       double LS = 0; //Least square
   double Sum; //Sum of the 5 Gaussien curve for a specific H0 value
   for (j=0;j<=2*nbH0-1;j++) {
      Sum=0;
for (i=0;i<=4;i++) {
   Sum=Sum+GaussianCurve(H0[j],Mean[i],Sigma[i],Multiplier[i]); }
//We give a heavier weight to any error between 69.2 and 72.1 to
// model the gap between these values
      if ((H0[i]>=69.2)&&(H0[i]<=72.1)) {
```

```
            LS=LS+10*(Sqr(nbCrossings[j]-Sum));}
        else { LS=LS+Sqr(nbCrossings[j]-Sum); }
        } return LS; }    //End of FindsGaussianCurvesLS

//***This function finds the best Gaussians to fit the real curve
void FindsBestGaussiansToFitRealCurve(void) {
    int i; //Counter
    double DMean[5],DSigma[5],DMultiplier[5]; //Dummy arrays
    double LS, PLS; //Least Square and Previous Least Square
    double StepMean = 0.1, StepSigma = 0.1, StepMultiplier = 0.1; //Variations
    int nbMeanNotImproved = 0; //Tells how many times not improved
    int nbSigmaNotImproved = 0; //Tells how many times not improved
    int nbMultiplierNotImproved = 0; //Tells how many times not improved
    //Starting values (approximative values only)
    Mean[0]=71;          Sigma[0]=1;    Multiplier[0]=-280;
    Mean[1]=68;          Sigma[1]=17;   Multiplier[1]=3800;
    Mean[2]=Mean[1];     Sigma[2]=3;    Multiplier[2]=880;
    Mean[3]=73;          Sigma[3]=7;    Multiplier[3]=1200;
    Mean[4]=Mean[3];     Sigma[4]=2;    Multiplier[4]=470;
    //Fills the 3 dummy arrays DMean, DSigma and DMultiplier
    //with the same values than the arrays Mean, Sigma and Multiplier
    for(i=0;i<=4;i++) {
        DMean[i]=Mean[i]; DSigma[i]=Sigma[i]; DMultiplier[i]=Multiplier[i]; }
        //Tries to find the 5 best Gaussians to fit the curve
        do {
            for (i=0;i<=4;i++) {
                //We improve Mean[i], but we force
                //Mean[2] = Mean[1] & Mean[4] = Mean[3]
                if ((i!=2)&&(i!=4)) {
                    PLS=FindsGaussianCurvesLS(Mean,Sigma,Multiplier);
                    DMean[i]=Mean[i]+StepMean;
                    if (i==1) {DMean[2]=DMean[i];}
                    if (i==3) {DMean[4]=DMean[i];}
                    LS=FindsGaussianCurvesLS(DMean,DSigma,DMultiplier);
                    if (LS<PLS) {
                        Mean[i]=DMean[i];
                        if (i==1) {Mean[2]=DMean[i];}
                        if (i==3) {Mean[4]=DMean[i];}
                        nbMeanNotImproved=0; }
                    else {
                        DMean[i]=Mean[i]-StepMean;
                        if (i==1) {DMean[2]=DMean[i];}
                        if (i==3) {DMean[4]=DMean[i];}
```

```
        LS=FindsGaussianCurvesLS(DMean,DSigma,DMultiplier);
        if (LS<PLS) {
          Mean[i]=DMean[i];
          if (i==1) {Mean[2]=DMean[i];}
          if (i==3) {Mean[4]=DMean[i];}
          nbMeanNotImproved=0; }
        else {
          DMean[i]=Mean[i];
          if (i==1) {DMean[2]=DMean[i];}
          if (i==3) {DMean[4]=DMean[i];}
          nbMeanNotImproved++;
          if (nbMeanNotImproved>=100) {
            nbMeanNotImproved=0; StepMean=StepMean/10; } } } }
//We try to improve Sigma[i]
PLS=FindsGaussianCurvesLS(Mean,Sigma,Multiplier);
DSigma[i]=Sigma[i]+StepSigma;
LS=FindsGaussianCurvesLS(DMean,DSigma,DMultiplier);
if (LS<PLS) { Sigma[i]=DSigma[i]; nbSigmaNotImproved=0; }
else {
  DSigma[i]=Sigma[i]-StepSigma;
  LS=FindsGaussianCurvesLS(DMean,DSigma,DMultiplier);
  if (LS<PLS) {
    Sigma[i]=DSigma[i]; nbSigmaNotImproved=0; }
  else {
    DSigma[i]=Sigma[i]; nbSigmaNotImproved++;
    if (nbSigmaNotImproved>=100) {
      nbSigmaNotImproved=0; StepSigma=StepSigma/10; } } }
//We try to improve Multiplier[i]
PLS=FindsGaussianCurvesLS(Mean,Sigma,Multiplier);
DMultiplier[i]=Multiplier[i]+StepMultiplier;
LS=FindsGaussianCurvesLS(DMean,DSigma,DMultiplier);
if (LS<PLS) {
  Multiplier[i]=DMultiplier[i]; nbMultiplierNotImproved=0; }
else {
  DMultiplier[i]=Multiplier[i]-StepMultiplier;
  LS=FindsGaussianCurvesLS(DMean,DSigma,DMultiplier);
  if (LS<PLS) {
    Multiplier[i]=DMultiplier[i]; nbMultiplierNotImproved=0; }
  else {
    DMultiplier[i]=Multiplier[i]; nbMultiplierNotImproved++;
    if (nbMultiplierNotImproved>=100) {
      nbMultiplierNotImproved=0;
      StepMultiplier=StepMultiplier/10; } } } }
```

```
        LS=FindsGaussianCurvesLS(DMean,DSigma,DMultiplier);
        } while (LS>=22000); //Sets a stop point
      for(i=0;i<=4;i++) {
    printf("\n Mean[%i]=%10lf    Sigma[%i]=%10lf    Multiplier[%i]=%10lf",
      i,Mean[i],i,Sigma[i],i,Multiplier[i]);
    } } //End of FindsBestGaussiansToFitRealCurve

//***The function begins by shifting Mean[1] and Mean[2] of the two
//***Gaussian curves that are around H0=69.2km/(s*MParsec) to
//***H0=72.1km/(s*MParsec) with a theoretical factor of 1.042516951. Then
//***the function that modifies the global H0 array builds the summation of
//***the 4 positive Gaussian curves.
void CreatesFinalGaussianCurve(void) {
    int i; //Dummy index value
    //We shift Mean[1] and Mean[2] with a theoretical factor of 1.042516951
    Mean[1]=Mean[1]*1.042516951; Mean[2]=Mean[1];
    //We omit i=0 to remove the negative Gaussian curve
    for(i=1;i<=nbH0*2-1;i++) {
      nbCrossings[i]=GaussianCurve(H0[i],Mean[1],Sigma[1],Multiplier[1]);
      nbCrossings[i]=nbCrossings[i]+GaussianCurve(H0[i],Mean[2],Sigma[2],
        Multiplier[2]);
      nbCrossings[i]=nbCrossings[i]+GaussianCurve(H0[i],Mean[3],Sigma[3],
        Multiplier[3]);
      nbCrossings[i]=nbCrossings[i]+GaussianCurve(H0[i],Mean[4],Sigma[4],
        Multiplier[4]); } } //End of CreatesFinalGaussianCurve

//***Returns the Least Mean Square of the equation DA*x^2+DB*x+DC.
double FindsLMS(double DA, double DB, double DC) {
    int i; /*Dummy index value*/      double LMS = 0; //Least Mean Square
    for(i=PosTipIndex-n;i<=PosTipIndex+n;i++){
      LMS=LMS+Sqr(nbCrossings[i]-(DA*H0[i]*H0[i]+DB*H0[i]+DC));
      } return LMS; }    //End of FindsLMS

//***Returns A, B, and C coefficients of the quadratic equation of the tip
void ApproximatesTipEquation(void) {
    double LMSTipMin; //Reminds the lowest value of least mean square
    double PLMSTip, NLMSTip; //LMSTip for a forward and backward step
    double DA,DB,DC; //Dummy values of A, B and C coefficients
    double StepA,StepB,StepC; //Step variation of the coefficients
    double nbCrossingsMax = 0; //Maximum number crossings at the tip
    double xa,xb,xc,ya,yb,yc; /*3 coordinates*/    int i; //Dummy index value
    for(i=0;i<=nbH0*2-1;i++) { //Finds the index of the approximated tip
      if (nbCrossings[i]>nbCrossingsMax) {
```

```
            nbCrossingsMax=nbCrossings[i]; PosTipIndex=i; } }
    i=PosTipIndex; xa=H0[i-n]; xb=H0[i]; xc=H0[i+n];
    ya=nbCrossings[i-n]; yb=nbCrossings[i]; yc=nbCrossings[i+n];
    //Sets coefficients ABC
    A=((yc-ya)/((xc-xa)*(xc-xb)))-((yb-ya)/((xb-xa)*(xc-xb)));
    B=((yb-ya)/(xb-xa))-A*(xb+xa);
    C=ya-A*xa*xa-B*xa; DA=A;DB=B;DC=C;
    }    //End of ApproximatesTipEquation

//***Function that returns the Best estimate of H0
void BestEstimateOfH0(void) {
    CreateTableOfCrossingH0Ranges(); FindsBestGaussiansToFitRealCurve();
    CreatesFinalGaussianCurve(); ApproximatesTipEquation();
    BEH=-B/(2*A); Accuracy_ppm = (BEH-TVH)/(TVH*1E-6);
    LMSTip=FindsLMS(A,B,C); }    //End of BesEstimateOfH0

int main(void) {
    BestEstimateOfH0();
    printf("\n\n Equation of the tip: y = %.10lfx^2+ %.10lfx+ %.10lf",A,B,C);
    printf("\n Best estimate of H0 = %.10lf km/(s*MParsec)",BEH);
    printf("\n Theoretical H0       = %.10lf km/(s*MParsec)",TVH);
    printf("\n Relative accuracy versus theoretical value = %.10lf ppm",
    Accuracy_ppm);
    getchar();    return 0;
    } //End of main
```

Journal of Modern Physics, 2021, 12, 1708-1720
https://www.scirp.org/journal/jmp
ISSN Online: 2153-120X
ISSN Print: 2153-1196

Transport of Relativistic Electrons Scattered by the Coulomb Force and a Thermionic Energy Converter with a Built-in Discharge Tube

Mitsuaki Nagata

Soft Creator Company, Kyoto, Japan
Email: nagata@heian-kogyo.jp

How to cite this paper: Nagata, M. (2021) Transport of Relativistic Electrons Scattered by the Coulomb Force and a Thermionic Energy Converter with a Built-in Discharge Tube. *Journal of Modern Physics*, **12**, 1708-1720.
https://doi.org/10.4236/jmp.2021.1212099

Received: September 16, 2021
Accepted: October 24, 2021
Published: October 27, 2021

Abstract

A transport equation of momentum for relativistic electrons scattered isotropically was previously reported. Here, a momentum-transport equation for relativistic electrons "scattered anisotropically" by the Coulomb force is inquired into. An ideal plasma consisting of electrons and deuterons is treated again. Also, to raise a generation-ability of a thermionic energy converter, a means of introducing external electric and magnetic fields within "a converter in which an emitter plate and a collector plate face simply each other" is proposed.

Keywords

Transport of Relativistic Electrons, Coulomb Force Scattering, Thermionic Energy Converter with Some Supplemental Equipments

1. Introduction

In the classical theory (based on the Boltzmann equation with the Fokker-Planck collision term) with respect to the electron transport in an ideal plasma consisting of electrons and deuterons, as a frictional force to suppress unlimited increase of a drift velocity by an external electric field, only the dynamical frictional force coming from the cumulative effect of small angle deflections ceaselessly occurring is generally taken into consideration. However, considering that rare large angle deflections ought to be the scatterings due to the two-body (an electron and a deuteron) collisions, we reported [1] about the evaluation of an effective radius of the Coulomb force of a deuteron. The unexpected result was that a frictional force coming from the two-body collisions is much stronger than the dynamical frictional one (from Equations (18)-(20) of Ref. [1]). So, for simplifi-

cation of an analysis in this research, we disregard an effect of the many-body collisions on a drift movement of an electron, compared with one of the two-body collisions. Furthermore, assuming that every electron has a mean thermal velocity $\bar{\upsilon}$, we inquire into a transport equation of momentum for relativistic electrons in the ideal plasma.

For changing radiation energy from a huge-sided magnetic mirror reactor into electric energy in future, a thermionic energy converter [2]-[9] is considered to be a promising generator, next to a steam turbine one. We discuss in Section 4 about a way to raise a generation-efficiency of a converter by help of some supplemental equipments.

2. Momentum Transport Equation

This research is discussed under the presupposition that a deuteron has as effective radius $P_{\mathrm{up-r}}$ of the Coulomb force, with respect to the two-body collisions. Then, a mean collision frequency ν_{r} of an electron is $n_{\mathrm{p}}\pi p_{\mathrm{up-r}}^2\bar{\upsilon}$ ($\equiv \bar{\upsilon}/\lambda_{\mathrm{r}}$, n_{p} is a deuteron density which is equal to an electron density n_{e}). A value of $P_{\mathrm{up-r}}$ is estimated in after (24), together with ς_{r} appearing later.

We first consider the case where a small electric field $\mathbf{E}(t)$ and a magnetic field $\mathbf{B}$ are:

$$\begin{cases}\mathbf{E}(t) = -\hat{z}E\cos\omega t \\ \mathbf{B} = \hat{y}B\end{cases} \quad (t \text{ is time, } \omega \text{ is a frequency}) \tag{1}$$

We use four coordinate systems:

$$\begin{cases}\text{the orthogonal coordinates } (x,y,z),(x',y',z') \\ \text{the polar coorinates } (\theta,\phi,z),(\theta',\phi',z')\end{cases}$$

Here, y/y' and the z'-axis is in the direction of an electron drift velocity $\mathbf{u}(t)$ which is both on the x-z plane and on the x'-z' plane. The angles θ and θ' are angles between a velocity variable $\boldsymbol{\upsilon}$ and the z-axis and between $\boldsymbol{\upsilon}$ and the z'-axis, respectively. The angle ϕ and ϕ' are inclinations from the x-axis, the x'-axis on the x-y plane, respectively. We assume that both a temperature distribution and a density distribution, with respect to electrons, are uniform in space and that $|\mathbf{u}(t)| \ll \bar{\upsilon} < 0.1c$ (c: the light speed).

The linearized relativistic equation of motion for an electron having a velocity $\boldsymbol{\upsilon}(t,t_0)$ at time t after having been scattered with a velocity $\boldsymbol{\upsilon}(t_0)$ at past time t_0 by a deuteron is given by (2) of Ref. [10]

$$\frac{m_{\mathrm{e}}}{\left(1-\dfrac{\boldsymbol{\upsilon}(t_0)^2}{c^2}\right)^{1/2}}\frac{\partial\boldsymbol{\upsilon}(t,t_0)}{\partial t} = -\frac{\alpha''}{c^2}\frac{\partial\boldsymbol{\upsilon}_{\mathrm{t}}}{\partial t} - \frac{\boldsymbol{\upsilon}_{\mathrm{t}}}{c^2}\left(-q\mathbf{E}(t)\cdot\boldsymbol{\upsilon}_{\mathrm{t}}\right) - q\mathbf{E}(t) - q\boldsymbol{\upsilon}(t,t_0)\times\mathbf{B} \tag{2}$$

Here, m_{e} is the rest mass of an electron, $-q$ is an electron charge, $\boldsymbol{\upsilon}_{\mathrm{t}} = \boldsymbol{\upsilon}(t,t_0)_{(\mathbf{E}(t)=\mathbf{0})}$, $\alpha'' = \int_{t_0}^{t} -q\mathbf{E}(t)\cdot\boldsymbol{\upsilon}_{\mathrm{t}}\mathrm{d}t$. We note that (2) can be regarded to be the equation of motion for an electron with a constant mass

$m_{\mathrm{e}}\Big/\left(1-\boldsymbol{\upsilon}\left(t_0\right)^2/c^2\right)^{1/2}$.

A momentum transport-equation is written as

$$\sum\left\{\frac{m_{\mathrm{e}}}{\left(1-\dfrac{\boldsymbol{\upsilon}\left(t_0\right)^2}{c^2}\right)^{1/2}}\frac{\partial\boldsymbol{\upsilon}\left(t,t_0\right)}{\partial t}+\frac{\alpha''}{c^2}\frac{\partial\boldsymbol{\upsilon}_{\mathrm{t}}}{\partial t}+\frac{\boldsymbol{\upsilon}_{\mathrm{t}}}{c^2}\left(-q\mathbf{E}\left(t\right)\cdot\boldsymbol{\upsilon}_{\mathrm{t}}\right)\right\} \tag{3}$$
$$=\sum\left\{-q\mathbf{E}\left(t\right)-q\boldsymbol{\upsilon}\left(t,t_0\right)\times\mathbf{B}\right\}+\boldsymbol{P}_{\mathrm{after}}-\boldsymbol{P}_{\mathrm{before}}$$

Here, $\sum$ represents summation of the vector quantity of each term over electrons per unit volume. And with respect to electrons scattered by collisions with deuterons per unit volume and per unit time at time t, $\boldsymbol{P}_{\mathrm{after}}$ and $\boldsymbol{P}_{\mathrm{before}}$ are total momentum of those electrons just after the collisions and just before the collisions, respectively.

1) About $\boldsymbol{P}_{\mathrm{after}}$ in (3)

The number of electrons scattered by deuterons is $n_{\mathrm{e}}\nu_{\mathrm{r}}$ per unit volume and per unit time. For a velocity distribution of those $n_{\mathrm{e}}\nu_{\mathrm{r}}$ electrons just after the collisions, we assume again such a spherical surface as shown in Figure 1 of Ref. [11]:

$$n_{\mathrm{e}}\nu_{\mathrm{r}}\left[\left(\frac{\bar{\upsilon}+2\zeta_{\mathrm{r}}u\left(t\right)\cos\theta'}{\bar{\upsilon}}\right)\frac{\sin\theta\mathrm{d}\phi\mathrm{d}\theta}{4\pi}\right]\delta\left(\upsilon-\upsilon\left(t\right)\right)\mathrm{d}\upsilon=\mathrm{d}\Phi\left(t\right) \tag{4}$$

The quantity in the above bracket is the solid angle element in the direction of $\left(\theta,\phi\right)$, $\boldsymbol{\upsilon}$ is the magnitude of a velocity variable $\boldsymbol{\upsilon}$ of an electron, $u\left(t\right)=\left|\mathbf{u}\left(t\right)\right|$, $\upsilon\left(t\right)=\bar{\upsilon}+\zeta_{\mathrm{r}}u\left(t\right)\cos\theta'$ (ζ_{r} is a remaining ratio of $\mathbf{u}\left(t\right)$ in the relativistic case) and $\delta\left(\cdots\right)$ is a delta-function. $\boldsymbol{P}_{\mathrm{after}}$ is given by

$$P_{\mathrm{after}}=\int_{\theta'=0}^{\pi}\int_{\phi'=0}^{2\pi}\int_{\upsilon=0}^{\infty}n_{\mathrm{e}}\nu_{\mathrm{r}}\left[\left(\frac{\bar{\upsilon}+2\zeta_{\mathrm{r}}u\left(t\right)\cos\theta'}{\bar{\upsilon}}\right)\frac{\sin\theta'\mathrm{d}\phi'\mathrm{d}\theta'}{4\pi}\right]$$
$$\times\delta\left(\upsilon-\upsilon\left(t\right)\right)\mathrm{d}\upsilon\frac{m_{\mathrm{e}}\boldsymbol{\upsilon}'}{\left(1-\dfrac{\left(\boldsymbol{\upsilon}'\right)^2}{c^2}\right)^{1/2}} \tag{5}$$

Here, $\boldsymbol{\upsilon}'=\hat{x}'\upsilon\sin\theta'\cos\phi'+\hat{y}'\upsilon\sin\theta'\sin\phi'+\hat{z}'\upsilon\cos\theta'$. Using the following approximation:

$$\frac{m_{\mathrm{e}}}{\left(1-\dfrac{\left(\bar{\upsilon}+\zeta_{\mathrm{r}}u\left(t\right)\cos\theta'\right)^2}{c^2}\right)^{1/2}}\simeq\frac{m_{\mathrm{e}}}{\left[\left(1-\dfrac{\bar{\upsilon}^2}{c^2}\right)\left(1-\dfrac{2\bar{\upsilon}\zeta_{\mathrm{r}}u\left(t\right)\cos\theta'}{c^2}\right)\right]^{1/2}} \tag{6}$$
$$\simeq\frac{m_{\mathrm{e}}}{\gamma_{\mathrm{r}}}\left(1+\frac{\bar{\upsilon}\zeta_{\mathrm{r}}u\left(t\right)\cos\theta'}{c^2}\right)\left(\text{where},\gamma_{\mathrm{r}}=\left(1-\bar{\upsilon}^2/c^2\right)^{1/2}\right),$$

we have

$$\boldsymbol{P}_{\mathrm{after}}\simeq n_{\mathrm{e}}\nu_{\mathrm{r}}\frac{m_{\mathrm{e}}}{\gamma_{\mathrm{r}}}\hat{z}'\zeta_{\mathrm{r}}\mathbf{u}\left(t\right)\left(1+\frac{\bar{\upsilon}^2}{3c^2}\right)=n_{\mathrm{e}}\nu_{\mathrm{r}}\frac{m_{\mathrm{e}}}{\gamma_{\mathrm{r}}}\zeta_{\mathrm{r}}\mathbf{u}\left(t\right)\left(1+\frac{\bar{\upsilon}^2}{3c^2}\right) \tag{7}$$

The term with products or squares of the drift velocity and the electric field have been neglected in (6) and (7). We will do so also in later calculations.

2) About $\boldsymbol{P}_{\text{before}}$ in (3)

The number of electrons scattered with velocity magnitudes $\upsilon \sim \upsilon + \mathrm{d}\upsilon$ in the direction of (θ, ϕ) during the time interval $t_0 \sim t_0 + \mathrm{d}t_0$ before time t is $\mathrm{d}\Phi(t_0)\mathrm{d}t_0$ per unit volume. Of these electrons, the number of electrons having not collided until time t is $\mathrm{d}\Phi(t_0)\mathrm{d}t_0 \exp\left[-\int_{t_0}^{t} \frac{\upsilon(t,t_0)_{(\upsilon=\upsilon(t_0))}}{\lambda_{\mathrm{r}}}\mathrm{d}t\right]$, where $\upsilon(t,t_0)$ is the magnitude of a velocity $\boldsymbol{\upsilon}(t,t_0)$ at time t after having been scattered with a velocity $\upsilon(t_0) = \overline{\upsilon} + \zeta_{\mathrm{r}} u(t_0)\cos\theta'$. The velocity $\upsilon(t,t_0)$ is given after by (9). These electrons have, at time t, momentum

$$\frac{m_{\mathrm{e}}}{\left(1-\frac{\boldsymbol{\upsilon}(t_0)^2}{c^2}\right)^{1/2}}\boldsymbol{\upsilon}(t,t_0)_{(\upsilon=\upsilon(t_0))},$$

and probability by which these electrons are scattered per unit time at time t is $\upsilon(t,t_0)_{(\upsilon=\upsilon(t_0))}/\lambda_{\mathrm{r}}$. Accordingly, $\boldsymbol{P}_{\text{before}}$ is given by

$$\begin{aligned}\boldsymbol{P}_{\text{before}} = \int_{t_0=-\infty}^{t}\int_{\theta=0}^{\pi}\int_{\phi=0}^{2\pi} n_{\mathrm{e}}\nu_{\mathrm{r}}\mathrm{d}t_0\left[\frac{\overline{\upsilon}+2\zeta_{\mathrm{r}}\mathbf{u}(t)\cos\theta'}{\overline{\upsilon}}\times\frac{\sin\theta\mathrm{d}\phi\mathrm{d}\theta}{4\pi}\right]\\ \times\exp\left[-\int_{t_0}^{t}\frac{\boldsymbol{\upsilon}(t,t_0)_{(\upsilon=\upsilon(t_0))}}{\lambda_{\mathrm{r}}}\mathrm{d}t\right]\frac{\boldsymbol{\upsilon}(t,t_0)_{(\upsilon=\upsilon(t_0))}}{\lambda_{\mathrm{r}}}\\ \times\frac{m_{\mathrm{e}}}{\left(1-\frac{\boldsymbol{\upsilon}(t_0)^2}{c^2}\right)^{1/2}}\boldsymbol{\upsilon}(t,t_0)_{(\upsilon=\upsilon(t_0))}\end{aligned} \tag{8}$$

We substitute the following three relationships into (8).

a) Equation (6) $_{(t\to t_0)}$

b) Equation (9) below:

From the energy relationship

$$\frac{m_{\mathrm{e}}c^2}{\left(1-\frac{\boldsymbol{\upsilon}(t,t_0)^2_{(\upsilon=\upsilon(t_0))}}{c^2}\right)^{1/2}}-\frac{m_{\mathrm{e}}c^2}{\left(1-\frac{\boldsymbol{\upsilon}(t_0)^2}{c^2}\right)^{1/2}}=\int_{t_0}^{t}-q\mathbf{E}(t)\cdot\left(\boldsymbol{\upsilon}(t,t_0)_{(\mathbf{E}(t)=0,\upsilon=\overline{\upsilon})}\right)\mathrm{d}t\equiv\alpha''_{(\upsilon=\overline{\upsilon})},$$

we have

$$\upsilon(t,t_0)_{(\upsilon=\upsilon_0(t))} \simeq \upsilon(t_0)+\frac{\gamma_{\mathrm{r}}^3}{m_{\mathrm{e}}\overline{\upsilon}}\alpha''_{(\upsilon=\overline{\upsilon})} \quad \left(\left|\alpha''_{(\upsilon=\overline{\upsilon})}\right| \ll m_{\mathrm{e}}c^2/\gamma_{\mathrm{r}}\right) \tag{9}$$

where, with $\omega_{\mathrm{cr}} = q|\mathbf{B}|\gamma_{\mathrm{r}}/m_{\mathrm{e}}$ and

$$\begin{aligned}&\boldsymbol{\upsilon}(t,t_0)_{(\mathbf{E}(t)=0,\upsilon=\overline{\upsilon})} = \boldsymbol{\upsilon}_{t_{(\upsilon=\overline{\upsilon})}}\\ &= \hat{x}\left[\overline{\upsilon}\sin\theta\cos\phi\cos\omega_{\mathrm{cr}}(t-t_0)+\overline{\upsilon}\cos\theta\sin\omega_{\mathrm{cr}}(t-t_0)\right]+\hat{y}\left[\overline{\upsilon}\sin\theta\sin\phi\right]\\ &\quad+\hat{z}\left[\overline{\upsilon}\cos\theta\cos\omega_{\mathrm{cr}}(t-t_0)-\overline{\upsilon}\sin\theta\cos\phi\sin\omega_{\mathrm{cr}}(t-t_0)\right],\end{aligned}$$

$$\begin{aligned}\alpha''_{(\upsilon=\bar{\upsilon})} = \frac{q\mathbf{E}}{\omega_{\mathrm{cr}}^2-\omega^2}\Big\{&\bar{\upsilon}\sin\theta\cos\phi\left[\omega_{\mathrm{cr}}\cos\omega t\cos\omega_{\mathrm{cr}}\left(t-t_0\right)+\omega\sin\omega t\sin\omega_{cr}\left(t-t_0\right)\right]\\&+\bar{\upsilon}\cos\theta\left[\omega_{\mathrm{cr}}\cos\omega t\sin\omega_{\mathrm{cr}}\left(t-t_0\right)-\omega\sin\omega t\cos\omega_{\mathrm{cr}}\left(t-t_0\right)\right]\\&-\bar{\upsilon}\sin\theta\cos\phi\left(\omega_{\mathrm{cr}}\cos\omega t_0\right)+\bar{\upsilon}\cos\theta\left(\omega\sin\omega t_0\right)\Big\}\end{aligned} \tag{10}$$

c) An Equation (11) below, for a drift velocity of electrons,

$$\begin{aligned}n_{\mathrm{e}}\mathbf{u}(t) = \int_{t_0}\int_{\theta}\int_{\phi} n_{\mathrm{e}}\nu_{\mathrm{r}}\mathrm{d}t_0\left(1+\frac{2\zeta_{\mathrm{r}}\mathbf{u}\left(t_0\right)\cos\theta'}{\bar{\upsilon}}\right)\frac{\sin\theta\mathrm{d}\phi\mathrm{d}\theta}{4\pi}\\ \times\exp\left[-\int_{t_0}^{t}\frac{\boldsymbol{\upsilon}\left(t,t_0\right)_{(\upsilon=\upsilon(t_0))}}{\lambda_{\mathrm{r}}}\mathrm{d}t\right]\boldsymbol{\upsilon}\left(t,t_0\right)_{(\upsilon=\upsilon(t_0))}\end{aligned} \tag{11}$$

Then, (8) becomes

$$\begin{aligned}\boldsymbol{P}_{\mathrm{before}} = n_{\mathrm{e}}\frac{m_{\mathrm{e}}}{\gamma_{\mathrm{r}}}\nu_{\mathrm{r}}\mathbf{u}(t)+\int_{t_0,\theta,\phi} n_{\mathrm{e}}\nu_{\mathrm{r}}\mathrm{d}t_0\frac{\sin\theta\mathrm{d}\phi\mathrm{d}\theta}{4\pi}\exp\left[-\nu_{\mathrm{r}}\left(t-t_0\right)\right]\frac{m_{\mathrm{e}}}{\gamma_{\mathrm{r}}\lambda_{\mathrm{r}}}\left(1+\frac{\bar{\upsilon}^2}{c^2}\right)\\ \times\varsigma_{\mathrm{r}}u\left(t_0\right)\cos\theta'\boldsymbol{\upsilon}\left(t,t_0\right)_{(\boldsymbol{E}(t)=0,\upsilon=\bar{\upsilon})}+\int_{t_0,\theta,\phi} n_{\mathrm{e}}\nu_{\mathrm{r}}\mathrm{d}t_0\frac{\sin\theta\mathrm{d}\phi\mathrm{d}\theta}{4\pi}\\ \times\exp\left[-\nu_{\mathrm{r}}\left(t-t_0\right)\right]\frac{m_{\mathrm{e}}}{\gamma_{\mathrm{r}}\lambda_{\mathrm{r}}}\cdot\frac{\gamma_{\mathrm{r}}^3}{m_{\mathrm{e}}\bar{\upsilon}}\alpha''_{(\upsilon=\bar{\upsilon})}\boldsymbol{\upsilon}\left(t,t_0\right)_{(\mathbf{E}(t)=0,\upsilon=\bar{\upsilon})}\end{aligned} \tag{12}$$

Furthermore, in order to calculate the second term in the right-hand side (RHS) of (12), we express $\mathbf{u}\left(t_0\right)$ by the following form:

$$\mathbf{u}\left(t_0\right) = \hat{x}u_x\left(t_0\right)+\hat{z}u_z\left(t_0\right)$$

And we use the following relationships

$$\begin{cases}\left|\mathbf{u}\left(t_0\right)\right|\cos\theta' = u\left(t_0\right)\cos\theta' = u_x\left(t_0\right)\sin\theta\cos\phi+u_z\left(t_0\right)\cos\theta\\ u_x\left(t_0\right) = Re\left[\left(u_{xR}+iu_{xI}\right)\mathrm{e}^{\mathrm{i}\omega t_0}\right] = u_{xR}\cos\omega t_0-u_{xI}\sin\omega t_0\\ u_z\left(t_0\right) = Re\left[\left(u_{zR}+iu_{zI}\right)\mathrm{e}^{\mathrm{i}\omega t_0}\right] = u_{zR}\cos\omega t_0-u_{zI}\sin\omega t_0\end{cases}$$

Then, the 2nd term in RHS of (12)

$$\begin{aligned}&= n_{\mathrm{e}}\nu_{\mathrm{r}}^2\frac{m_{\mathrm{e}}}{\gamma_{\mathrm{r}}}\varsigma_{\mathrm{r}}\left(1+\frac{\bar{\upsilon}^2}{c^2}\right)\frac{1}{3}\int_{t_0=-\infty}^{t}\mathrm{d}t_0\exp\left[-\nu_{\mathrm{r}}\left(t-t_0\right)\right]\Big[\hat{x}\left(u_{xR}\cos\omega t_0-u_{xI}\sin\omega t_0\right)\\ &\times\cos\left[\omega_{\mathrm{cr}}\left(t-t_0\right)\right]-\hat{z}\left(u_{xR}\cos\omega t_0-u_{xI}\sin\omega t_0\right)\sin\left[\omega_{\mathrm{cr}}\left(t-t_0\right)\right]+\hat{x}\left(u_{zR}\cos\omega t_0\\ &-u_{zI}\sin\omega t_0\right)\sin\left[\omega_{\mathrm{cr}}\left(t-t_0\right)\right]+\hat{z}\left(u_{zR}\cos\omega t_0-u_{zI}\sin\omega t_0\right)\cos\left[\omega_{\mathrm{cr}}\left(t-t_0\right)\right]\Big]\end{aligned} \tag{13}$$

$$\begin{aligned}&= n_{\mathrm{e}}\nu_{\mathrm{r}}\frac{m_{\mathrm{e}}}{\gamma_{\mathrm{r}}}\varsigma_{\mathrm{r}}\left(1+\frac{\bar{\upsilon}^2}{c^2}\right)\Big[\hat{x}\left(\beta_2+\frac{\beta_2'}{\omega}\frac{\partial}{\partial t}\right)u_x(t)+\hat{z}\left(\beta_1+\frac{\beta_1'}{\omega}\frac{\partial}{\partial t}\right)u_x(t)\\ &+\hat{x}\left(\beta_1+\frac{\beta_1'}{\omega}\frac{\partial}{\partial t}\right)\left(-u_z(t)\right)+\hat{z}\left(\beta_2+\frac{\beta_2'}{\omega}\frac{\partial}{\partial t}\right)u_z(t)\Big]\end{aligned}$$

where, $u_x(t) = u_x\left(t_0\right)_{(t_0\to t)}, u_z(t) = u_z\left(t_0\right)_{(t_0\to t)}$, and $\left(\beta_1,\beta_1',\beta_2,\beta_2'\right)$ together with $\left(\beta_{20},\beta_{20}'\right)$ are shown in after (21). Equation (13) can be generalized as:

The 2nd term in RHS of (12)

$$= n_e \nu_r \frac{m_e}{\gamma_r} \varsigma_r \left(1 + \frac{\overline{\upsilon}^2}{c^2}\right) \times \left[\left(\beta_1 + \frac{\beta_1'}{\omega}\frac{\partial}{\partial t}\right)\left(\mathbf{u}(t) \times \hat{b}\right) + \left(\beta_2 + \frac{\beta_2'}{\omega}\frac{\partial}{\partial t}\right)\hat{b} \times \left(\mathbf{u}(t) \times \hat{b}\right) + \left(\beta_{20} + \frac{\beta_{20}'}{\omega}\frac{\partial}{\partial t}\right)\hat{b}\left(\mathbf{u}(t) \cdot \hat{b}\right)\right] \tag{14}$$

Next, the 3rd term in RHS of (12) becomes $n_e \gamma_r^2 qE\left[\hat{x}\left(-\beta_1 \cos\omega t + \beta_1' \sin\omega t\right) + \hat{z}\left(\beta_2 \cos\omega t - \beta_2' \sin\omega t\right)\right]$. This can be generalized as:

The 3rd term in RHS of (12)

$$= n_e \gamma_r^2 \left[\left(\beta_1 + \frac{\beta_1'}{\omega}\frac{\partial}{\partial t}\right)\left(-q\mathbf{E}(t) \times \hat{b}\right) + \left(\beta_2 + \frac{\beta_2'}{\omega}\frac{\partial}{\partial t}\right)\hat{b} \times \left(-q\mathbf{E}(t) \times \hat{b}\right) + \left(\beta_{20} + \frac{\beta_{20}'}{\omega}\frac{\partial}{\partial t}\right)\hat{b}\left(-q\mathbf{E}(t) \cdot \hat{b}\right)\right] \tag{15}$$

Accordingly, the momentum transfer term in the field of the two-body (electron-deuteron) collisions is given by

$$\boldsymbol{P}_{\text{after}} - \boldsymbol{P}_{\text{before}} = -n_e \nu_r \frac{m_e}{\gamma_r}\mathbf{u}(t)\left[1 - \varsigma_r\left(1 + \frac{\overline{\upsilon}^2}{3c^2}\right)\right] - n_e\left[\left(\beta_1 + \frac{\beta_1'}{\omega}\frac{\partial}{\partial t}\right)\left(\boldsymbol{F}_c \times \hat{b}\right) + \left(\beta_{20} + \frac{\beta_{20}'}{\omega}\frac{\partial}{\partial t}\right)\hat{b}\left(\boldsymbol{F}_c \cdot \hat{b}\right) + \left(\beta_2 + \frac{\beta_2'}{\omega}\frac{\partial}{\partial t}\right)\hat{b} \times \left(\boldsymbol{F}_c \times \hat{b}\right)\right] \tag{16}$$

where,

$$\boldsymbol{F}_c = -q\mathbf{E}(t)\gamma_r^2 + \nu_r \frac{m_e}{\gamma_r}\varsigma_r\left(1 + \frac{\overline{\upsilon}^2}{c^2}\right)\mathbf{u}(t) \tag{17}$$

3) About $\sum \frac{\alpha''}{c^2}\frac{\partial \boldsymbol{\upsilon}_t}{\partial t}$ in (3)

$$\sum \frac{\alpha''}{c^2}\frac{\partial \boldsymbol{\upsilon}_t}{\partial t} = \int_{t_0}\int_\theta\int_\phi \frac{\alpha''_{(\upsilon=\overline{\upsilon})}}{c^2}\frac{\partial \boldsymbol{\upsilon}_{t(\upsilon=\overline{\upsilon})}}{\partial t} n_e \nu_r \mathrm{d}t_0 \frac{\sin\theta \mathrm{d}\phi \mathrm{d}\theta}{4\pi} \exp\left[-\frac{\overline{\upsilon}}{\lambda_r}\left(t - t_0\right)\right] = n_e \frac{\omega_{cr}}{\nu_r}\frac{\overline{\upsilon}^2}{c^2}\left\{-\left(\beta_2 + \frac{\beta_2'}{\omega}\frac{\partial}{\partial t}\right)\left(-q\mathbf{E}(t) \times \hat{b}\right) + \left(\beta_1 + \frac{\beta_1'}{\omega}\frac{\partial}{\partial t}\right)\hat{b} \times \left(-q\mathbf{E}(t) \times \hat{b}\right)\right\} \tag{18}$$

4) About $\sum \frac{\boldsymbol{\upsilon}_t}{c^2}\left[-q\mathbf{E}(t) \cdot \boldsymbol{\upsilon}_t\right]$ in (3)

$$\begin{aligned}
&\sum \frac{\boldsymbol{\upsilon}_t}{c^2}\left[-q\mathbf{E}(t) \cdot \boldsymbol{\upsilon}_t\right] \\
&= \frac{1}{c^2}\int_{t_0}\int_\theta\int_\phi \left\{\hat{x}\left[\overline{\upsilon}\sin\theta\cos\phi\cos\omega_{cr}\left(t - t_0\right) + \overline{\upsilon}\cos\theta\sin\omega_{cr}\left(t - t_0\right)\right]\right. \\
&\quad \left. + \hat{y}\overline{\upsilon}\sin\theta\sin\phi + \hat{z}\left[\overline{\upsilon}\cos\theta\cos\omega_{cr}\left(t - t_0\right) - \overline{\upsilon}\sin\theta\cos\phi\sin\omega_{cr}\left(t - t_0\right)\right]\right\} \\
&\quad \times qE\cos\omega t\left[\overline{\upsilon}\cos\theta\cos\omega_{cr}\left(t - t_0\right) - \overline{\upsilon}\sin\theta\cos\phi\sin\omega_{cr}\left(t - t_0\right)\right] \\
&\quad \times n_e \nu_r \mathrm{d}t_0 \frac{\sin\theta \mathrm{d}\phi \mathrm{d}\theta}{4\pi}\exp\left[-\frac{\overline{\upsilon}}{\lambda_r}\left(t - t_0\right)\right] \\
&= n_e \frac{\overline{\upsilon}^2}{3c^2}\left[-q\mathbf{E}(t)\right]
\end{aligned} \tag{19}$$

5) About $\sum \frac{m_e}{\left(1-\frac{\boldsymbol{\upsilon}(t_0)^2}{c^2}\right)^{1/2}} \frac{\partial \boldsymbol{\upsilon}(t,t_0)}{\partial t}$ in (3)

The above summation is a momentum which n_e electrons gain during unit time through the external fields and the collisions. Here, we assume roughly that a velocity distribution of n_e electrons at time t is isotropic when it is viewed from the velocity point $\mathbf{u}(t)$, similarly in **Figure 1** of Ref. [11]. Then, based on the analysis from (4) to (7), we have, as a momentum summation of n_e electrons at time t,

$$\sum m_e \boldsymbol{\upsilon}(t,t_0)\left(1-\frac{\boldsymbol{\upsilon}(t_0)^2}{c^2}\right)^{-\frac{1}{2}} = n_e \frac{m_e}{\gamma_r}\left(1+\frac{\bar{\upsilon}^2}{3c^2}\right)\mathbf{u}(t) \tag{20}$$

Thus, we obtain the following momentum transport equation for relativistic electrons:

$$\begin{aligned} & n_e \frac{m_e}{\gamma_r}\left(1+\frac{\bar{\upsilon}^2}{3c^2}\right)\frac{\mathrm{d}\mathbf{u}(t)}{\mathrm{d}t} + n_e \omega_{cr}\tau \frac{\bar{\upsilon}^2}{c^2}\left[-\left(\beta_2 + \frac{\beta_2'}{\omega}\frac{\partial}{\partial t}\right)\left(-q\mathbf{E}(t)\times\hat{b}\right)\right. \\ & \left.+\left(\beta_1 + \frac{\beta_1'}{\omega}\frac{\partial}{\partial t}\right)\hat{b}\times\left(-q\mathbf{E}(t)\times\hat{b}\right)\right] + n_e \frac{\bar{\upsilon}^2}{3c^2}\left[-q\mathbf{E}(t)\right] \\ & = n_e\left[-q\mathbf{E}(t) - q\mathbf{E}(t)\times\mathbf{B}\right] + \boldsymbol{P}_{\text{after}} - \boldsymbol{P}_{\text{before}} \end{aligned} \tag{21}$$

Here, with $\kappa = 1/3$ and $\tau = 1/\nu_r$,

$$\beta_1 = \kappa\frac{-\omega_{cr}\tau\left(\omega_{cr}^2\tau^2 - \omega^2\tau^2 + 1\right)}{D},\quad \beta_1' = \kappa\frac{2\omega_{cr}\tau\omega\tau}{D},$$

$$\beta_2 = \kappa\frac{\omega_{cr}^2\tau^2 + \omega^2\tau^2 + 1}{D},\quad \beta_2' = \kappa\frac{\omega\tau\left(\omega_{cr}^2\tau^2 - \omega^2\tau^2 - 1\right)}{D},$$

$$\beta_{20} = \beta_{2(\omega_{cr}=0)} = \frac{\kappa}{1+\omega^2\tau^2},\quad \beta_{20}' = \beta_{20(\omega_{cr}=0)}' = \frac{-\kappa\omega\tau}{1+\omega^2\tau^2},$$

$$D = \left(\omega_{cr}^2\tau^2 - \omega^2\tau^2 + 1\right)^2 + 4\omega^2\tau^2.$$

It is noted that (21) is the transport equation in the case where all electrons have the same velocity $\bar{\upsilon}$ (the mean thermal velocity).

3. ν_r, ς_r and Drift Velocities

We regard, similarly in Equations (21)-(25) of Ref. [11], that a momentum transfer frequency of relativistic electrons scattered anisotropically in the two-body collisions through the Coulomb force is $\nu_r(1-\varsigma_r)$. Based on (A3) $_{(\ell\to\infty)}$ in Appendix of Ref. [1] and the classical procedure, a relativistic collision cross section $\sigma_r(x)$ in the electron-deuteron collisions through the Coulomb force is obtained as

$$\sigma_x(x) = \frac{1}{4}\left(\frac{q^2\gamma_r}{4\pi\varepsilon_0 m_e\bar{\upsilon}^2}\right)^2 \frac{1}{\sin^4\frac{x}{2}} \tag{22}$$

where, x is a deflection angle of an electron with $\bar{\upsilon}$ and ε_0 is the dielectric

constant of vacuum. Then, we obtain

$$\nu_{\mathrm{r}}\left(1-\varsigma_{\mathrm{r}}\right)=n_{\mathrm{p}}\pi p_{\mathrm{up-r}}^{2}\bar{\upsilon}\left[4\left(\frac{p_{\perp\mathrm{r}}}{p_{\mathrm{up-r}}}\right)^{2}\ell n\frac{p_{\mathrm{up-r}}}{p_{\perp\mathrm{r}}}\right] \tag{23}$$

Here, $p_{\mathrm{up-r}}$ is an effective radius of the Coulomb force of a deuteron and $p_{\perp\mathrm{r}}=p_{\perp}\gamma_{\mathrm{r}}\left(p_{\perp}=q^{2}/4\pi\varepsilon_{0}m_{\mathrm{e}}\bar{\upsilon}^{2}\right)$ which is an impact parameter for π/2—deflection in the relativistic electron-deuteron collisions. We presume that $p_{\mathrm{up-r}}$, ν_{r} and ς_{r} are

$$\begin{cases} p_{\mathrm{up-r}}=p_{\mathrm{up}}\gamma_{\mathrm{r}} \\ \nu_{\mathrm{r}}=n_{\mathrm{p}}\pi p_{\mathrm{up-r}}^{2}\bar{\upsilon}=\nu\gamma_{\mathrm{r}}^{2} \\ 1-\varsigma_{\mathrm{r}}=4\left(\dfrac{p_{\perp\mathrm{r}}}{p_{\mathrm{up-r}}}\right)^{2}\ell n\dfrac{p_{\mathrm{up-r}}}{p_{\perp\mathrm{r}}}=1-\varsigma \end{cases} \quad (p_{\mathrm{up}}\text{ is given in (15) of Ref. [10]}) \tag{24}$$

In (24), ν and ς are the quantities for the nonrelativistic case.

Now, when the external force fields are

$$\mathbf{E}=-\hat{z}E,\ \mathbf{B}=\hat{y}B, \tag{25}$$

a solution of the drift velocity $\mathbf{u}=\hat{x}u_{x}+\hat{z}u_{z}$ is given by

$$\frac{u_{z}}{\dfrac{q\mathbf{E}}{m_{\mathrm{e}}\nu}}=\frac{1}{\gamma_{\mathrm{r}}}\cdot\frac{A_{1}A_{2}+A_{3}A_{4}}{A_{1}^{2}+A_{3}^{2}} \tag{26}$$

$$\frac{u_{x}}{\dfrac{q\mathbf{E}}{m_{\mathrm{e}}\nu}}=\frac{1}{\gamma_{\mathrm{r}}}\cdot\frac{-A_{1}A_{4}+A_{2}A_{3}}{A_{1}^{2}+A_{3}^{2}} \tag{27}$$

(note: $q\mathbf{E}/m_{\mathrm{er}}\nu_{\mathrm{r}}=\left(q\mathbf{E}/m_{\mathrm{e}}\nu\right)/\gamma_{\mathrm{r}}$)

$$A_{1}=1-\varsigma_{\mathrm{r}}\left(1+\frac{\alpha}{3}\right)+\beta_{2}\varsigma_{\mathrm{r}}\left(1+\alpha\right)$$

$$A_{2}=1-\frac{\alpha}{3}-\beta_{2}\gamma_{\mathrm{r}}^{2}-\beta_{1}\omega_{\mathrm{cr}}\tau\alpha$$

$$A_{3}=\omega_{\mathrm{cr}}\tau+\beta_{1}\varsigma_{\mathrm{r}}\left(1+\alpha\right)$$

$$A_{4}=\beta_{2}\omega_{\mathrm{cr}}\tau\alpha-\beta_{1}\gamma_{\mathrm{r}}^{2}$$

$$\alpha=\bar{\upsilon}^{2}/c^{2},\ \gamma_{\mathrm{r}}=\left(1-\alpha\right)^{1/2}$$

The value of $\varsigma_{\mathrm{r}}\left(=\varsigma\right)$ can be regarded to be nearly 1.0 from (17) of Ref. [1].

We show in **Figure 1** and **Figure 2** variations of "u_{z} in (26) and u_{x} in (27)" with respect to ω_{c}/ν where ω_{c} is the nonrelativistic cyclotron frequency.

When $\alpha\ll 1.0$ and $\varsigma_{\mathrm{r}}\simeq 1.0$,

$$u_{z}/\left(q\mathbf{E}/m_{\mathrm{e}}\nu\right)\begin{cases}\simeq 2/\gamma_{\mathrm{r}} & \left(\omega_{\mathrm{c}}/\nu=0\right) \\ \simeq\dfrac{1}{3\left(\omega_{\mathrm{c}}^{2}/\nu^{2}\right)} & \left(\omega_{\mathrm{c}}/\nu\to\infty\right)\end{cases}$$

$$u_{x}/\left(q\mathbf{E}/m_{\mathrm{e}}\nu\right)\begin{cases}=0 & \left(\omega_{\mathrm{c}}/\nu=0\right) \\ \simeq\dfrac{1}{\omega_{\mathrm{c}}/\nu} & \left(\omega_{\mathrm{c}}/\nu\to\infty\right)\end{cases}$$

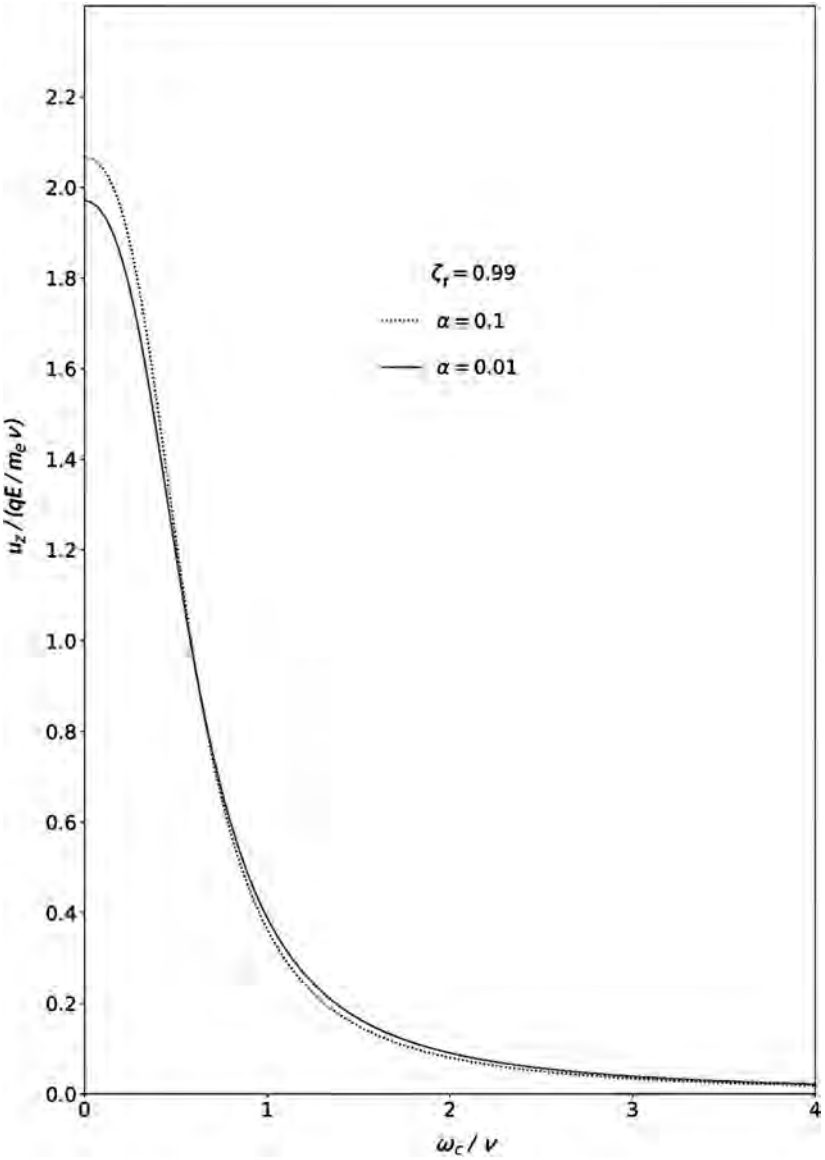

Figure 1. The drift velocity (26) of an electron. The quantities $\nu, m_e, \omega_c \left(= qB/m_e\right)$ are the ones in the nonrelativistic case. $\alpha = \bar{v}^2/c^2$.

4. For Efficiency Increase of a Thermionic Energy Converter

It is presumed that a gas (Cs plasma) within general converters will be a weakly ionized plasma. If the gas is replaced with a fully ionized plasma instead of a weakly ionized one, an internal resistance between an emitter plate and a collector plate extremely decreases, and thermionic electrons can save their thermal energies which have been consumed for ionization of Cs atoms. We consider that this replacement of the internal medium will raise a generation-efficiency. Furthermore, if a force field to convey thermionic electrons from the emitter to the collector is given within the converter, the efficiency will rise more compared with the case where electrons cannot but go to the collector for themselves. Under such a consideration, we propose a means adding some equipments, shown

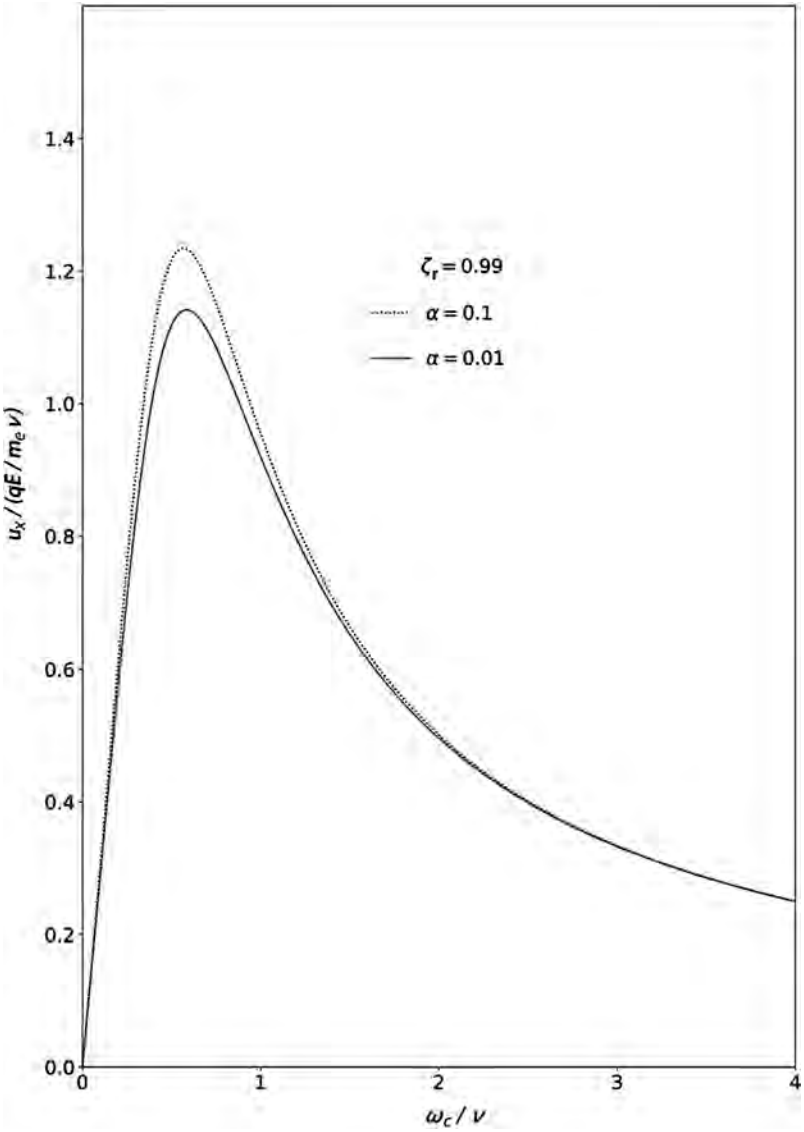

Figure 2. The drift velocity (27) of an electron. The quantities $\nu, m_e, \omega_c \left(= qB/m_e\right)$ are the ones in the nonrelativistic case. $\alpha = \bar{v}^2/c^2$.

in **Figure 3** and **Figure 4**, to the converter. The equipments are connected with Converter by Solenoid. In the inner space, Cs gas is enclosed. Discharge tube (shown in **Figure 4**) is installed as a partner of Converter. Fan makes Cs gas plasma circulate slowly within the closed space. By making a right-circularly polarized wave continue to heat electrons for long time, it is planned that the most part of the closed space is filled with a fully ionized plasma. Even if the electron temperature is not so high, we consider that it is possible to obtain an almost perfectly ionized plasma because the work-function of a Cs atom is very small. Now, let us classify the internal space of Converter into three parts (called space 1, 2, 3), as shown with dotted lines in **Figure 3**. We assume roughly that, in space 2, an electric field due to a space charge is negligible and also that, only in space 2, a magnetic field **B** and an external electric field **E** exist. The magnetic

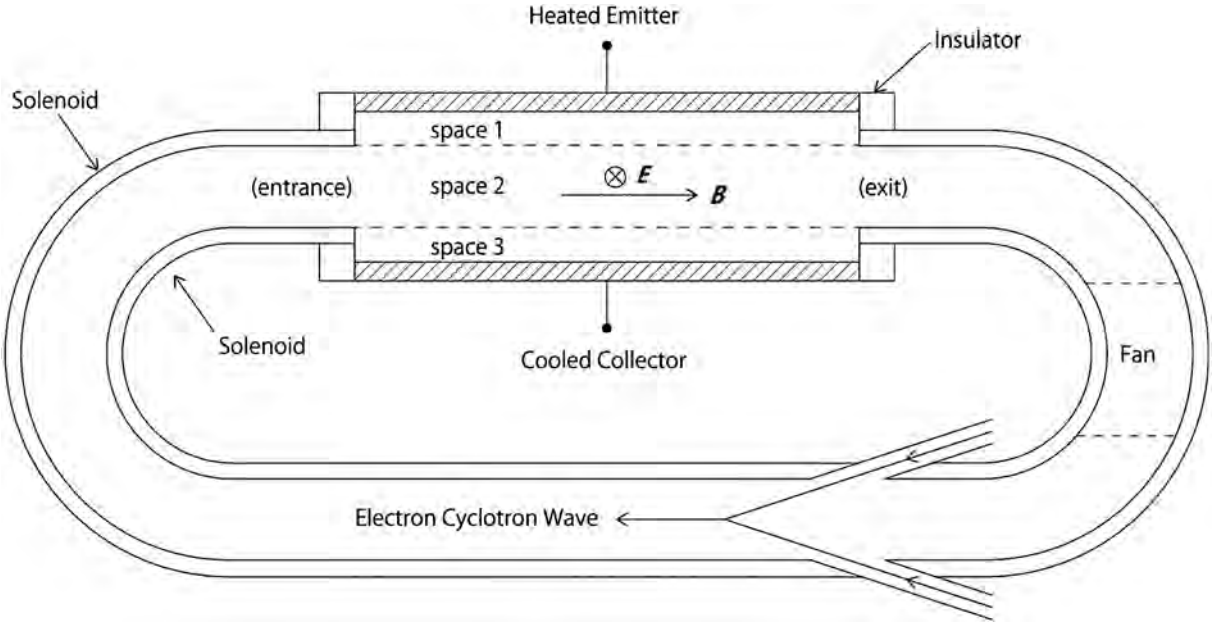

Figure 3. A fundamental structure of a thermionic energy converter which is connected with an Electric Wave Oscillator and a Fan by a rectangular Solenoid.

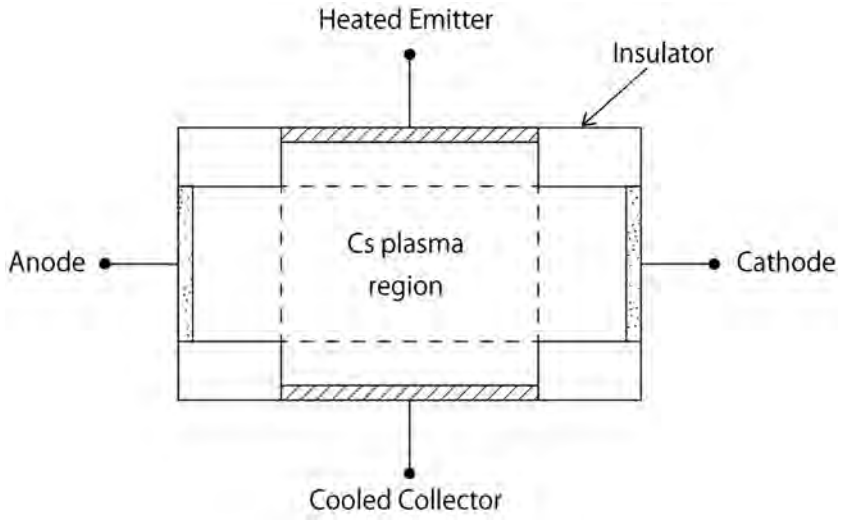

Figure 4. A side view of the converter with a Built-in Dischage Tube.

field **B** is supplied by Solenoid and the electric field **E** is the one in the middle part of the discharge plasma. These external forces convey electrons with the drift velocity u_z (in Figure 1) in the direction of **−E** and with the drift velocity u_x (in Figure 2) in the direction of **E** × **B**. We set the value of ω_c/ν to a larger one than 4.0. Then, a loss in an external circuit between Anode and Cathode is sufficiently suppressed and many electrons will try entering from space 2 into space 3. In this situation, however, the following physical condition must be satisfied: "A total number of electrons which can enter within Collector per unit time is equal to a total number (denoted by N_{tot}) of electrons which jump out of Emitter per unit time." Electrons also combining with ions on Emitter must

be counted for N_{tot} (we suppose that neutral atoms produced near the surface of Emitter are soon ionized within space 1). Accordingly, if we design the converter so that electrons flowing into space 3 per unit time may become much more than N_{tot}, a negative potential barrier to suppress the flow of electrons ought to be produced near Collector surface, which is added to the old barrier. The larger the height of a total negative potential barrier becomes, the larger an output voltage becomes, because a potential of Collector lowers more and more as against a potential of Emitter. The convey of electrons by the force $\mathbf{E} \times \mathbf{B}$ makes it possible to lengthen the distance between Emitter and Collector. When the distance ℓ_{c} from the entrance to the exit in the converter of **Figure 3** is too long, a distribution of $\mathbf{B}$ becomes vague. If it is necessary to lengthen the value of ℓ_{c}, then, we must connect some small-sized converters in series by solenoids.

5. Conclusion

In the field of the Coulomb force scattering, under the premise that the two-body collisions have much more influence than the many-body collisions on the drift movement of an electron, we have inquired into the transport equation of momentum for relativistic electrons. Also, proposing an idea of introducing a fully ionized plasma and an external magnetic field within the combination-apparatus of the converter and the discharge tube, we have discussed about a means to raise a generation-efficiency of a thermionic energy converter.

Acknowledgements

I express my sincere thanks for helpful discussions on this research and also for encouragement and help I have received for many years, to President K. Sawada of Soft Creator Company and Chief C. Adachi of Heian Light Technology Company.

Conflicts of Interest

The author declares no conflicts of interest regarding the publication of this paper.

References

[1] Nagata, M. (2020) *Journal of Modern Physics*, **11**, 1751-1760. https://doi.org/10.4236/jmp.2020.1111108

[2] Rasor, N.S. (1982) *Applied Atomic Collision Physics,* **5**, 169-200. https://doi.org/10.1016/B978-0-12-478805-3.50011-4

[3] Stakhanov, I.P. (1968) *Soviet Physics-Technical Physics*, **12**, 1522.

[4] Miskolczy, G., Wang, C.C. and Lieb, D.P. (1981) *Proceeding of* 16*th Intersociety Energy Conversion Engineering Conference*, **2**, 1956.

[5] Huffman, F., Reagan, P., Miskolczy, G. and Merrill, O. (1982) *Proceeding of* 17*th Intersociety Energy Conversion Engineering Conference,* **3**, 1908.

[6] Huffman, F. (1983) Overview of Terrestrial Thermionics. 18*th Intersociety Energy Conversion Engineering Conference,* Orlando, 21 August 1983, p. 173.

[7] Rasor, N.S. and Warner, C. (1964). *Journal of Applied Physics*, **35**, 2589. https://doi.org/10.1063/1.1713806

[8] Norcross, D.W. and Stone, P.M. (1968) *Journal of Quantitative Spectroscopy and Radiative Transfer*, **8**, 655-684. https://doi.org/10.1016/0022-4073(68)90181-7

[9] Cameron, G.E. and Reynolds, E.L. (1994) 29*th Intersociety Energy Conversion Engineering Conference*, **1**, 389.

[10] Nagata, M. and Sawada, K. (2019) *Journal of Modern Physics*, **10**, 145-156. https://doi.org/10.4236/jmp.2019.102011

[11] Nagata, M. (2011) *The European Physical Journal D*, **65**, 429-440. https://doi.org/10.1140/epjd/e2011-10464-2

Journal of Modern Physics, 2021, 12, 1721-1728
https://www.scirp.org/journal/jmp
ISSN Online: 2153-120X
ISSN Print: 2153-1196

Planck's Oscillators at Low Temperatures and Haken's Perturbation Approach to the Quantum Oscillators Reconsidered

Stanisław Olszewski

Institute of Physical Chemistry, Polish Academy of Sciences, Kasprzaka 44/52, Warsaw, Poland
Email: olsz@ichf.edu.pl

How to cite this paper: Olszewski, S. (2021) Planck's Oscillators at Low Temperatures and Haken's Perturbation Approach to the Quantum Oscillators Reconsidered. *Journal of Modern Physics*, **12**, 1721-1728.
https://doi.org/10.4236/jmp.2021.1212100

Received: September 21, 2021
Accepted: October 25, 2021
Published: October 28, 2021

Abstract

In the first step the extremal values of the vibrational specific heat and entropy represented by the Planck oscillators at the low temperatures could be calculated. The positions of the extrema are defined by the dimensionless ratios between the quanta of the vibrational energy and products of the actual temperature multiplied by the Boltzmann constant. It became evident that position of a local maximum obtained for the Planck's average energy of a vibration mode and position of a local maximum of entropy are the same. In the next step the Haken's time-dependent perturbation approach to the pair of quantum non-degenerate Schrödinger eigenstates of energy is re-examined. An averaging process done on the time variable leads to a very simple formula for the coefficients entering the perturbation terms.

Keywords

Planck's Quantum Oscillators at Low Temperatures, Calculation of the Extremal Specific Heat of the Oscillator Energy and Extremal Entropy, Simplified Haken's Time-Dependent Approach to the Perturbation Energy of a Non-Degenerate Quantum State

1. Introduction

Planck has developed—a time ago—a quantum approach to the oscillator ensembles for which both the vibrational energy and entropy are considered [1]. In the thermal equilibrium these parameters are given respectively by the formula

$$E = N\varepsilon_0 + N\frac{h\nu}{e^{h\nu/kT} - 1} \tag{1}$$

in the energy case, and by

$$S = \frac{1}{T}\frac{Nh\nu}{e^{h\nu/kT}-1} - Nk\log\left(1-e^{-\frac{h\nu}{kT}}\right) \tag{2}$$

in the entropy case. N is the number of the component particles oscillating in the system:

$$N_0 + N_1 + N_2 + \cdots = N \tag{3}$$

and

$$N_0\varepsilon_0 + N_1\varepsilon_1 + N_2\varepsilon_2 + \cdots = E \tag{4}$$

is the energy E given by N. This E is composed by the groups of oscillating particles entering (3), symbols ε_i denote the energy contributed by a single particle belonging to the set N_i.

The parameter T is the absolute temperature, ν —the symbol of frequency of the particle oscillation, h and k are the Planck and Boltzmann constants, respectively. We note that any oscillator has the energy

$$\varepsilon_n = \varepsilon_0 + nh\nu \tag{5}$$

where ε_0 is a common energy component in the system.

Beyond of the general formulae for E and S presented in (1) and (2), Planck examined also a limiting situation when T becomes very high. In this case we obtain

$$e^{h\nu/kT} \cong 1 + \frac{h\nu}{kT}. \tag{6}$$

In effect of (6):

$$e^{h\nu/kT} - 1 \cong \frac{h\nu}{kT} \tag{7}$$

and by neglecting the term having ε_0 —we obtain for energy

$$E \cong Nh\nu\frac{kT}{h\nu} = NkT. \tag{8}$$

A substitution similar to (7) done in the case of S in (2) gives (see [1]):

$$S = Nk\log\left(\frac{ekT}{h\nu}\right). \tag{9}$$

This is an approximate formula in which a small term having

$$T \gg 0 \tag{10}$$

in the denominator in (7) has been neglected.

The low temperatures have not been much examined in [1]. In this case we have for the oscillatory energy

$$E = N\varepsilon_0 + Nh\nu e^{-h\nu/kT} \tag{11}$$

because the first term entering the denominator in the formula (1) highly predominates over the absolute value of the second term of the denominator equal to 1.

The idea of the present paper is to examine the case of very small T more ac-

curately than before. The examination of the energy behaviour is based mainly on the formula (11), a suitable basis of the examination of entropy is also taken from [1]; see Section 2.

The problem of the Planck oscillators for energy and entropy could be connected with the Haken's time-dependent perturbation calculation of a single non-degenerate quantum state. The solutions are shown to become similar to those of an oscillator-like equation having one term fully independent of time. Since an averaging process makes the time-dependent terms equal to zero, the coefficients entering the final solution approach the terms characteristic for the harmonic oscillator.

2. Properties of Planck's *E* and *S* Characteristic for Small Temperature *T*

Very small T give for energy the formula (11), the same T assumed for the entropy S in (2) give (see [1]):

$$S = \frac{Nh\nu}{T} \mathrm{e}^{-h\nu/kT}. \tag{12}$$

On the basis of E in (11) we examine also its derivative with respect to T representing the specific heat

$$\frac{\mathrm{d}E}{\mathrm{d}T} = Nh\nu \frac{\mathrm{d}}{\mathrm{d}T}\left(\mathrm{e}^{-h\nu/kT}\right) = Nh\nu \frac{\mathrm{d}\mathrm{e}^{-x}}{\mathrm{d}x}\frac{\mathrm{d}x}{\mathrm{d}T}. \tag{13}$$

Here we put

$$x = \frac{h\nu}{kT}, \tag{14}$$

so

$$\frac{\mathrm{d}x}{\mathrm{d}T} = -\frac{h\nu}{kT^2}. \tag{15}$$

In effect the term (13) for the specific heat becomes:

$$\frac{\mathrm{d}E}{\mathrm{d}T} = Nh\nu \frac{\mathrm{d}}{\mathrm{d}T}\left(\mathrm{e}^{-h\nu/kT}\right) = Nh\nu(-1)\mathrm{e}^{-x}\left(-\frac{h\nu}{kT^2}\right) = Nkx^2\mathrm{e}^{-x} = Nk\frac{x^2}{\mathrm{e}^x}. \tag{16}$$

In order to examine the external properties of (16) we calculate

$$\frac{\mathrm{d}}{\mathrm{d}x}\left(\frac{x^2}{\mathrm{e}^x}\right) = \frac{\mathrm{d}}{\mathrm{d}x}\left(x^2\mathrm{e}^{-x}\right) = 2x\mathrm{e}^{-x} - x^2\mathrm{e}^{-x} = 0 \tag{17}$$

which gives

$$2x = x^2 \tag{18}$$

or

$$x = 2. \tag{19}$$

The second derivative of the function examined in (17) gives

$$\frac{\mathrm{d}^2}{\mathrm{d}x^2}\left(x^2\mathrm{e}^{-x}\right)\Big|_{x=2} = \mathrm{e}^{-x}\left(2-4x+x^2\right)\Big|_{x=2} = \mathrm{e}^{-2}(-2) < 0, \tag{20}$$

so the result in (20) indicates a local maximum of the function $\mathrm{d}E/\mathrm{d}T$ considered in (16):

$$\left(\frac{\mathrm{d}E}{\mathrm{d}T}\right)_{\max} = Nk\frac{4}{\mathrm{e}^2}. \tag{21}$$

A similar behaviour can be observed for the entropy at low T. This case of S is represented by the formula given in [1] repeated in (12):

$$S = Nkx\mathrm{e}^{-x}. \tag{22}$$

An examination of the derivative of S leads to the result

$$\frac{\mathrm{d}S}{\mathrm{d}x} = Nk\frac{\mathrm{d}}{\mathrm{d}x}\left(x\mathrm{e}^{-x}\right) = Nk\left(\mathrm{e}^{-x} - x\mathrm{e}^{-x}\right) = Nk\mathrm{e}^{-x}\left(1-x\right) \tag{23}$$

from which we obtain the extremum at

$$x = 1. \tag{24}$$

The second derivative of S in (22) gives

$$\frac{\mathrm{d}^2S}{\mathrm{d}x^2} = Nk\left[-\mathrm{e}^{-x} - \mathrm{e}^{-x} - x\left(-\mathrm{e}^{-x}\right)\right] = Nk\left(x-2\right)\mathrm{e}^{-x} \tag{25}$$

which calculated at $x = 1$ becomes:

$$\left.\frac{\mathrm{d}^2S}{\mathrm{d}x^2}\right|_{x=1} = -\frac{Nk}{\mathrm{e}} < 0. \tag{26}$$

The negative result in (26) indicates a maximum value of S in (24). Evidently this extremal value of S becomes:

$$S_{\max} = Nkx\mathrm{e}^{-x}\Big|_{x=1} = \frac{Nk}{\mathrm{e}}. \tag{27}$$

3. Average Energy for the Planck's Vibration Mode and Its Properties

This energy is presented in [2]:

$$E_{av} = \frac{h\nu}{\mathrm{e}^{h\nu/kT} - 1} = \frac{h\nu}{\mathrm{e}^{x} - 1}. \tag{28}$$

The variable x entering (28) [see (14)] taken at small T can make x much larger than 1. Evidently in this case we have

$$\mathrm{e}^{x} = \mathrm{e}^{h\nu/kT} \gg 1 \tag{29}$$

and the term 1 entering the denominator in (28) can be neglected. Because of (14) we have approximately

$$E_{av} = f\left(x\right) \cong \frac{x}{\mathrm{e}^{x}}kT. \tag{30}$$

This gives the energy derivative calculated with respect to x equal to

$$f'\left(x\right) = \left(\frac{1}{\mathrm{e}^{x}} - \frac{x}{\mathrm{e}^{x}}\right)kT = \left(1-x\right)\frac{kT}{\mathrm{e}^{x}}. \tag{31}$$

The requirement that $f'\left(x\right)$ should be equal to zero gives

$$x = 1 \tag{32}$$

which is the result much similar to that obtained in (24). The second derivative of E_{av} in (30) with respect to x gives:

$$f''(x) = kT\left(-2\mathrm{e}^{-x} + x\mathrm{e}^{-x}\right) < 0 \tag{31a}$$

for $x = 1$ indicating a maximum of (30) at that x.

4. Similarities in Behaviour of the Derivatives of E and S Calculated with Respect to the Frequency ν

By taking first the derivative of the energy at low T with respect to ν we obtain from (11):

$$\begin{aligned}\frac{\mathrm{d}E}{\mathrm{d}\nu} &= \frac{\mathrm{d}}{\mathrm{d}\nu}\left(Nh\nu\mathrm{e}^{-h\nu/kT}\right) = NkT\frac{\mathrm{d}}{\mathrm{d}x}\left(x\mathrm{e}^{-x}\right)\frac{\mathrm{d}x}{\mathrm{d}\nu} = NkT\,\mathrm{e}^{-x}\left(1-x\right)\frac{\mathrm{d}x}{\mathrm{d}\nu} \\ &= Nh\mathrm{e}^{-x}\left(1-x\right) = Nh\mathrm{e}^{-h\nu/kT}\left(1-\frac{h\nu}{hT}\right).\end{aligned} \tag{33}$$

A much similar result can be calculated from the derivative of S taken at low T [see (12)]:

$$\begin{aligned}\frac{\mathrm{d}S}{\mathrm{d}\nu} &= \frac{\mathrm{d}S}{\mathrm{d}x}\frac{\mathrm{d}x}{\mathrm{d}\nu} = \left[Nk\mathrm{e}^{-x} + Nkx\left(-1\right)\mathrm{e}^{-x}\right]\frac{\mathrm{d}x}{\mathrm{d}\nu} \\ &= Nk\mathrm{e}^{-x}\left(1-x\right)\frac{h}{kT} = \frac{Nh}{T}\mathrm{e}^{-h\nu/kT}\left(1-\frac{h\nu}{kT}\right).\end{aligned} \tag{34}$$

Both derivatives in (33) and (34) vanish at

$$h\nu/kT = 1. \tag{35}$$

The second derivatives of E and S calculated with respect to ν at $x = 1$ give negative values which indicate positions of the maxima of E and S at the variable $x = 1$:

$$E_{\max} = \frac{Nh\nu}{\mathrm{e}}, \tag{36}$$

$$S_{\max} = \frac{Nh\nu}{T\mathrm{e}}, \tag{36a}$$

valid at low T.

5. Oscillator Properties Representing the Haken's Time-Dependent Perturbation Approach to the Schrödinger's Quantum State

This approach is rather special because it refers us directly to the time variable which, in general, is rather avoided by the quantum physicists.

Let us assume that only two separate quantum levels, say 1 and 2, of the unperturbed Hamilton eigenequation

$$\hat{H}_0\varphi_n = W_n\varphi_n \tag{37}$$

are for us of interest [3]. This implies that the solution of the time-dependent Schrödinger equation

$$i\hbar\frac{\mathrm{d}\psi}{\mathrm{d}t}=\hat{H}\psi, \tag{38}$$

where

$$\hat{H}=\hat{H}_0+\hat{H}_p \tag{39}$$

and $\hat{H}_p$ is the perturbation potential, is constructed with the aid of the combination of φ_1 and φ_2 entering (37):

$$\psi=c_1(t)\varphi_1+c_2(t)\varphi_2. \tag{40}$$

The $c_1(t)$ and $c_2(t)$ should be found. The equations defining the coefficients are:

$$i\hbar\frac{\mathrm{d}c_1}{\mathrm{d}t}=c_1W_1+c_1H_{11}^p+c_2H_{12}^p, \tag{41}$$

$$i\hbar\frac{\mathrm{d}c_2}{\mathrm{d}t}=c_2W_2+c_2H_{22}^p+c_1H_{21}^p. \tag{42}$$

If we assume that the diagonal matrix elements of $\hat{H}_p$ vanish, *i.e.*

$$H_{11}^p=H_{22}^p=0, \tag{43}$$

a substitution can be done [3]:

$$c_1(t)=d_1\exp(-iW_1t/\hbar), \tag{44}$$

$$c_2(t)=d_2\exp(-iW_2t/\hbar). \tag{45}$$

This leads to the pair of equations for d_1 and d_2 equal respectively to [3]

$$i\hbar\frac{\mathrm{d}}{\mathrm{d}t}d_1=d_2H_{12}^p\exp(-i\tilde{\omega}t), \tag{46}$$

$$i\hbar\frac{\mathrm{d}}{\mathrm{d}t}d_2=d_1H_{21}^p\exp(i\tilde{\omega}t) \tag{47}$$

where

$$\tilde{\omega}=\omega_{21}=(W_2-W_1)\frac{1}{\hbar}. \tag{48}$$

Our idea is to calculate the second derivatives of d_1 and d_2 entering (46) and (47) with respect to t each multiplied by $i\hbar$:

$$\begin{aligned}-\hbar^2\frac{\mathrm{d}^2}{\mathrm{d}t^2}d_1&=i\hbar\frac{\mathrm{d}}{\mathrm{d}t}(d_2)H_{12}^p\exp(-i\tilde{\omega}t)+i\hbar d_2H_{12}^p(-i\tilde{\omega})\exp(-i\tilde{\omega}t)\\&=d_1H_{21}^p\exp(i\tilde{\omega}t)H_{12}^p\exp(-i\tilde{\omega}t)+d_2\hbar H_{12}^p\tilde{\omega}\exp(-i\tilde{\omega}t)\\&=d_1H_{21}^pH_{12}^p+\hbar d_2H_{12}^p\tilde{\omega}\exp(-i\tilde{\omega}t)\end{aligned} \tag{49}$$

and

$$\begin{aligned}-\hbar^2\frac{\mathrm{d}^2}{\mathrm{d}t^2}d_2&=i\hbar\frac{\mathrm{d}}{\mathrm{d}t}(d_1)H_{21}^p\exp(i\tilde{\omega}t)+i\hbar d_1H_{21}^pi\tilde{\omega}\exp(i\tilde{\omega}t)\\&=d_2H_{12}^p\exp(-i\tilde{\omega}t)H_{21}^p\exp(i\tilde{\omega}t)-d_1\hbar H_{21}^p\tilde{\omega}\exp(i\tilde{\omega}t)\\&=d_2H_{12}^pH_{21}^p-\hbar d_1H_{21}^p\tilde{\omega}\exp(i\tilde{\omega}t).\end{aligned} \tag{50}$$

The results indicate that a part of the second derivative of both d_1 and d_2 is

fully independent of t, being a multiple of d_1 and d_2 respectively. On the other side, the next part of each second derivative is very rapidly oscillating with t, because usually we have

$$\tilde{\omega} \gg 1; \tag{48a}$$

see (48). This means that the average obtained for the time dependent part on the right of (49) and (50) is a very small number tending to zero. In effect we obtain the equations:

$$-\hbar^2 \frac{\mathrm{d}^2}{\mathrm{d}t^2}(d_1) \cong d_1 H_{21}^p H_{12}^p \tag{51}$$

and

$$-\hbar^2 \frac{\mathrm{d}^2}{\mathrm{d}t^2}(d_2) \cong d_2 H_{12}^p H_{21}^p. \tag{52}$$

Because the coefficients on the right of (51) and (52) are the same, this imples that d_1 and d_2 can be represented respectively by the same function of time, say

$$d_1 \cong d_2 = \cos \nu t. \tag{53}$$

Since we have

$$\frac{\mathrm{d}^2}{\mathrm{d}t^2}(d_1) \cong \frac{\mathrm{d}^2}{\mathrm{d}t^2}(d_2) = -\nu^2 \cos(\nu t) \tag{54}$$

the frequency square ν^2 in (54) becomes

$$\nu^2 = \frac{H_{12}^p H_{21}^p}{\hbar^2} \sim \sec^{-2} \tag{55}$$

if we note that $H_{12}^p \sim H_{21}^p \sim \mathrm{erg}$ and $\hbar \sim \mathrm{erg} \cdot \sec$

We expect ν to be a large frequency because of a very small size of $\hbar$.

6. Summary

In the first step of the paper the extremal values of the specific heat of the Planck oscillator and the oscillator entropy are calculated. The results are attained by considering the well-established Planck's expressions for the oscillator energy and entropy in [1] taken for the limit of the low temperature T. As a variable x suitable to the extrema calculations the dimensionless energy ratio (14) has been chosen.

It is found that the specific heat as well as entropy of the oscillators attains their maximal values given by the formulae (21)-(27), respectively, at $x = 2$ and $x = 1$. Both results, being proportional to the Boltzmann constant k, are small for $N = 1$ but independent of T.

The limits of $\mathrm{d}E/\mathrm{d}T$ and S obtained at very small T become equal to zero for both specific heat and entropy:

$$\lim_{T \to 0} \frac{\mathrm{d}E}{\mathrm{d}T} = \lim_{x \to \infty} Nk \frac{x^2}{\mathrm{e}^x} = 0, \tag{56}$$

$$\lim_{T\to 0} S = \lim_{x\to\infty} Nk\frac{x}{e^x} = 0. \tag{57}$$

In the next step the Haken's time-dependent perturbation method is discussed [3]. It is shown that the time-dependent perturbation coefficients representing this method can be obtained very easily on the basis of the harmonic oscillations having the frequency defined by the non-diagonal matrix element of the perturbation potential and the Planck constant h.

It should be noted that more recently the classical and quantum behaviour of the oscillations was examined with the aid of the linear canonical transformations in [4].

Conflicts of Interest

The author declares no conflicts of interest regarding the publication of this paper.

References

[1] Planck, M. (1932) Einführung in die Theorie der Wärme. 2nd Edition, S. Hirzel, Leipzig.

[2] Jauncey, G.E.M. (1948) Modern Physics. 3rd Edition, Van Nostrand, New York.

[3] Haken, H. (1986) Light Waves, Photons, Atom. Elsevier, Amsterdam.

[4] Ogura, A. (2016) *Journal of Modern Physics*, **7**, 2205-2218. https://doi.org/10.4236/jmp.2016.715191

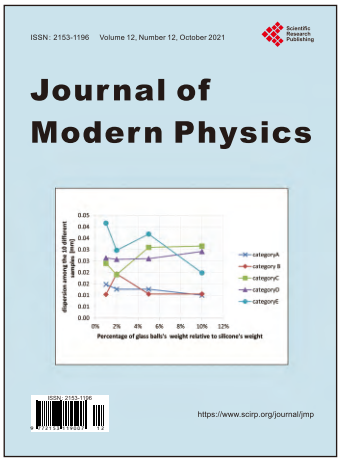

Call for Papers

Journal of Modern Physics

ISSN: 2153-1196 (Print) ISSN: 2153-120X (Online)
https://www.scirp.org/journal/jmp

Journal of Modern Physics **(JMP)** is an international journal dedicated to the latest advancement of modern physics. The goal of this journal is to provide a platform for scientists and academicians all over the world to promote, share, and discuss various new issues and developments in different areas of modern physics.

Editor-in-Chief

Prof. Yang-Hui He City University, UK

Subject Coverage

Journal of Modern Physics publishes original papers including but not limited to the following fields:

Biophysics and Medical Physics
Complex Systems Physics
Computational Physics
Condensed Matter Physics
Cosmology and Early Universe
Earth and Planetary Sciences
General Relativity
High Energy Astrophysics
High Energy/Accelerator Physics
Instrumentation and Measurement
Interdisciplinary Physics
Materials Sciences and Technology
Mathematical Physics
Mechanical Response of Solids and Structures
New Materials: Micro and Nano-Mechanics and Homogeneization
Non-Equilibrium Thermodynamics and Statistical Mechanics
Nuclear Science and Engineering
Optics
Physics of Nanostructures
Plasma Physics
Quantum Mechanical Developments
Quantum Theory
Relativistic Astrophysics
String Theory
Superconducting Physics
Theoretical High Energy Physics
Thermology

We are also interested in: 1) Short Reports—2-5 page papers where an author can either present an idea with theoretical background but has not yet completed the research needed for a complete paper or preliminary data; 2) Book Reviews—Comments and critiques.

Notes for Intending Authors

Submitted papers should not have been previously published nor be currently under consideration for publication elsewhere. Paper submission will be handled electronically through the website. All papers are refereed through a peer review process. For more details about the submissions, please access the website.

Website and E-Mail

https://www.scirp.org/journal/jmp **E-mail: jmp@scirp.org**

What is SCIRP?

Scientific Research Publishing (SCIRP) is one of the largest Open Access journal publishers. It is currently publishing more than 200 open access, online, peer-reviewed journals covering a wide range of academic disciplines. SCIRP serves the worldwide academic communities and contributes to the progress and application of science with its publication.

What is Open Access?

All original research papers published by SCIRP are made freely and permanently accessible online immediately upon publication. To be able to provide open access journals, SCIRP defrays operation costs from authors and subscription charges only for its printed version. Open access publishing allows an immediate, worldwide, barrier-free, open access to the full text of research papers, which is in the best interests of the scientific community.

- High visibility for maximum global exposure with open access publishing model
- Rigorous peer review of research papers
- Prompt faster publication with less cost
- Guaranteed targeted, multidisciplinary audience

Scientific Research Publishing

Website: https://www.scirp.org

Subscription: sub@scirp.org

Advertisement: service@scirp.org